

Model-Centric Approach to Discrete-Time Signal Processing for Dense Wavelength-Division
Multiplexing Systems

A Dissertation

Presented to
the faculty of the School of Engineering and Applied Science
University of Virginia

in partial fulfillment
of the requirements for the degree

Doctor of Philosophy

by

Houbing Song

August

2012

©Copyright by

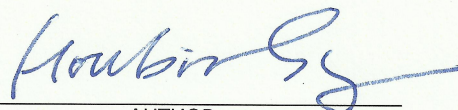
Houbing Song

All rights reserved

August 2012

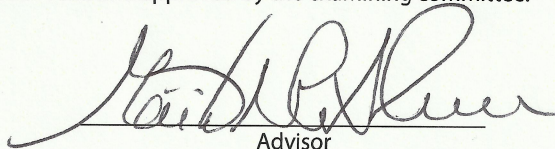
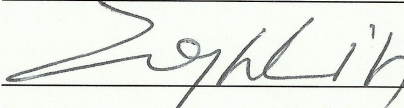
APPROVAL SHEET

The dissertation
is submitted in partial fulfillment of the requirements
for the degree of
Doctor of Philosophy

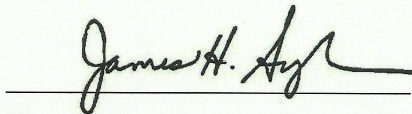


AUTHOR

The dissertation has been read and approved by the examining committee:


Advisor

Accepted for the School of Engineering and Applied Science:



Dean, School of Engineering and Applied Science

August

2012

Abstract

Dense wavelength-division multiplexing (DWDM) is the solution of choice for high-capacity optical backbone networks. However, in long-haul DWDM systems with periodic dispersion compensation and amplification, all optical communications give rise to severe physical impairments, due to fiber dispersion and nonlinearity, together with noise due to amplified spontaneous emission (ASE), that adversely degrade system performance. To mitigate these physical impairments and exploit system capacity of long-haul DWDM systems, a mathematical model that describes the input-output relationship of these systems and characterizes various physical impairments is required to serve as the foundation of discrete-time signal processing for fiber-optic communication systems.

This dissertation develops a model-centric approach for discrete-time signal processing for long-haul DWDM systems and addresses the development, validation and applications of a 2D discrete-time model of physical impairments in long-haul DWDM systems with periodic dispersion compensation and amplification.

The model development is based on the third-order Volterra series transfer function (VSTF) method. The model overcomes the well-known triple integral problem inherent in the original VSTF method and simplifies it to a simple integral that is easy to evaluate. The model takes into account multichannel effects, fiber losses, frequency chirp, optical filtering, and photodetection, which are ignored in the current literature. The model is in discrete-time and facilitates its applications in discrete-time signal processing to improve the system performance of long-haul DWDM systems. The model characterizes each individual

physical impairment by introducing the corresponding impairment coefficient. The model offers obvious advantages over the third-order VSTF method and the split-step Fourier (SSF) method. The model is in excellent agreement with results obtained from the SSF method.

The 2D discrete-time model is applied in system analysis and system performance improvement of long-haul DWDM systems. In system analysis, two applications are developed. Using the 2D discrete-time model, the effects of varying system parameters (symbol rate and channel spacing) and pulse shape on individual physical impairments in long-haul DWDM systems are analyzed. The concept of range of influence (RoI) of physical impairments is proposed and the RoI of each individual physical impairment is determined to guide the development of discrete-time signal processing. In system performance improvement, two applications are developed. Using the 2D discrete-time model, a novel constrained code based on the Total Impairment Extent Rank (TIER) is proposed to mitigate nonlinear physical impairments in long-haul fiber-optic communication systems; a TIER-LDPC concatenation scheme is proposed to combine the strength of the TIER code in effectively suppressing severe nonlinear physical impairments and that of the LDPC code in correcting memoryless errors due to ASE noise. A nonlinear equalizer based on the third-order inverse Volterra theory is also proposed. Different from backpropagation which is hard to implement in hardware, this equalizer features the most basic discrete-time signal processing device. The nonlinear equalizer is effective in suppressing linear and nonlinear physical impairments in a long-haul fiber-optic communication systems, particularly for high launched power levels where fiber nonlinearity dominates.

To the memory of my beloved mother, Peilan Zhao

Acknowledgments

First and foremost, I would like to express my sincerest gratitude to my advisor, Prof. Maité Brandt-Pearce, for her inspiring mentorship via freedom to explore and create, encouragement, patience, confidence-building, and her financial support via the National Science Foundation under Grant CCF-0916880. The years with her effective mentoring since August 2009 are the most enjoyable and productive time of my academic journey so far. She always has been and always will be my role model in my pursuit of academic excellence.

I would like to thank my dissertation advisory committee members, Prof. Stephen G. Wilson, Prof. Toby Berger, Prof. Zongli Lin and Prof. Irena Lasiecka, for their invaluable time and helpful suggestions. My special thanks go to Prof. Lin for rescheduling his important meeting to accommodate my dissertation defense. I am greatly indebted to Prof. Wilson, Prof. Berger, and Prof. Lin for writing reference letters on my behalf.

I would like to acknowledge Dr. Bo Xu for his help in the numerical integration of the third-order VSTF method and Mr. Tingjun Xie for his help in the implementation of the TIER-LDPC code. Without their help, I would need more time to finish my dissertation. I also thank the members of the Optical Multiuser/Multichannel Communications Group, for their friendship.

Finally, I would like to thank my wife, Huihui Wang, for her tireless support and unconditional love, and my father, Gaozhong Song, my sisters, Xuelian Song and Xueru Song, for their encouragement. This dissertation is impossible without the understanding of my parents-in-law, Lifu Wang and Yanqin Liu, and my aunt, Yanping Liu.

Contents

Contents	v
List of Tables	vii
List of Figures	viii
1 Introduction	1
1.1 Long-Haul DWDM Systems	3
1.1.1 Long-Haul Systems	3
1.1.2 High-Capacity Systems	4
1.1.3 Long-Haul DWDM Components	5
1.2 Motivation	9
1.3 Research Methodology	12
1.4 Significance	12
1.5 Dissertation Organization	13
2 Background	16
2.1 Nonlinear Schrödinger (NLS) Equation	16
2.2 Solution to the NLS Equation	22
2.2.1 Analytical methods	23
2.2.2 Numerical methods	24
2.3 Physical Impairments	26
2.3.1 Linear Impairments	26
2.3.2 Nonlinear Impairments	27
2.4 ASE Noise	28
2.5 Demodulation and Performance Measure	29
2.6 Signal Processing	34
2.6.1 Forward Error Correction	34
2.6.2 Constrained Coding	35
2.6.3 Predistortion/equalization	37
2.7 Summary	38
3 Model Development and Validation	40
3.1 Model Development	41
3.2 Model Validation	53
3.2.1 Model Accuracy	54
3.2.2 Computational Complexity	55

3.3	Summary	57
4	Model Applications in System Analysis	58
4.1	Effect of System Parameters and Pulse Shape	58
4.1.1	Effect of Symbol Rate	59
4.1.2	Effect of Channel Spacing	59
4.1.3	Effect of Pulse Shape	62
4.2	Range of Influence of Physical Impairments	63
4.2.1	RoI of ISI	70
4.2.2	RoI of Intrachannel Nonlinear Impairments	71
4.2.3	RoI of Interchannel Nonlinear Impairments	73
4.3	Summary	74
5	Model Applications in System Performance Improvement	76
5.1	TIER-LDPC Concatenation Scheme	76
5.1.1	TIER-LDPC Concatenation Scheme	78
5.1.2	Performance Evaluation	80
5.2	Nonlinear Equalization	84
5.2.1	Nonlinear Equalizer	85
5.2.2	Performance Evaluation	88
5.3	Summary	89
6	Conclusions and Future Work	92
A	Derivation of 2-D Discrete-Time Model	95
A.1	Simplification of Triple Integral	95
A.2	Simplifying Functions Used in Frequency Domain Output	98
A.3	Simplifying Functions Used in Time Domain Output	99
A.4	Simplifying Functions and Coefficients Used in PD Output for DBPSK	101
A.5	Simplifying Functions and Coefficients Used in PD Quadrature Output of DQPSK	101
	Bibliography	103

List of Tables

3.1	The Photodetector Output for OOK	51
3.2	The Photodetector Output for DBPSK	51
3.3	The Photodetector Output for Quadrature Channel of DQPSK	52
3.4	Typical Parameter Values	54
4.1	Index Triplets [lmn] for a Triple Pulse Case	67
4.2	Intrachannel Coefficients for a Triple Pulse Case	68
4.3	Index Triplets [uvw] for a Triple Channel Case	68
4.4	Interchannel Coefficients for a Triple Channel Case	69
4.5	RoIs of Intrachannel Nonlinear Impairments at 40 Gs/s	73
4.6	RoIs of Intrachannel Nonlinear Impairments at 100 Gs/s	73

List of Figures

1.1	A Typical DWDM System. Separate transmitter-receiver pairs are used to send and receive the signal at different wavelengths [1]	5
2.1	Symmetrized split-step Fourier method used for numerical simulations. Fiber length is divided into a large number of segments of width h . The effect of nonlinearity is included at the middle of the segment. [2]	25
2.2	Fluctuating signal generated at the receiver for OOK [1]	30
2.3	Gaussian probability densities of 1 and 0 bits	31
2.4	BER versus Q factor	33
3.1	Schematic of a typical long-haul DWDM system with periodic dispersion compensation and amplification	41
3.2	Normalized squared deviation of the output fields obtained by our proposed model and the SSF simulation	56
4.1	Effect of symbol rate on individual physical impairments for OOK ($F=3, K=7$)	60
4.2	Effect of symbol rate on individual physical impairments for DBPSK ($F=3, K=7$)	60
4.3	Effect of channel spacing on individual physical impairments for OOK ($F=7, K=3$)	61
4.4	Effect of channel spacing on individual physical impairments for DBPSK ($F=7, K=3$)	61
4.5	Effect of pulse shape on individual physical impairments for OOK ($F=7, K=7, R_s=10$ Gsps, $\Delta=100$ GHz, m is the edge sharpness parameter of the super-Gaussian pulses [2])	63
4.6	Concept of RoI	69
4.7	Computation of cumulative degradation due to ISI for SMF fiber operating at $1.55 \mu m$ for various symbol rates	71
4.8	Computation of cumulative degradation due to IXPM for SMF fiber operating at $1.55 \mu m$ for various symbol rates	72
4.9	Computation of cumulative degradation due to IFWM for SMF fiber operating at $1.55 \mu m$ for various symbol rates	73
4.10	Computation of cumulative degradation due to XPM for SMF fiber operating at $1.55 \mu m$ for various channel spacings	74

4.11	Computation of cumulative degradation due to FWM for SMF fiber operating at $1.55 \mu m$ for various channel spacings	75
5.1	Schematic of TIER-LDPC Concatenation Scheme	78
5.2	Histograms obtained from split-step Fourier simulation ($P_0=2$ mW)	82
5.3	Performance evaluation of the TIER-LDPC concatenation scheme, the TIER-only scheme, and the LDPC-only scheme (40 spans)	83
5.4	Performance evaluation of the TIER-LDPC concatenation scheme, the TIER-only scheme, and the LDPC-only scheme (50 spans)	83
5.5	Performance evaluation of the TIER-LDPC concatenation scheme, the TIER-only scheme, and the LDPC-only scheme (60 spans)	84
5.6	Nonlinear Equalization	85
5.7	BER Performance of the nonlinear equalizer (40 spans)	89
5.8	BER Performance of the nonlinear equalizer (50 spans)	90
5.9	BER Performance of the nonlinear equalizer (60 spans)	90

Chapter 1

Introduction

People in modern society are surrounded by mobile and ambient wireless communications, such as cellular telephony and Wi-Fi. However, we cannot live without wireline communications, particularly fiber-optic communications. An optical fiber is a dielectric wave guide that transports light signals from one place to another [3]. Since optical fibers were suggested by Charles Kuen Kao (2009 Nobel laureate in physics) to be the best choice for an increase of several orders of magnitude in the bit rate-distance product (BL , where B is the bit rate and L is the repeater spacing, is a commonly used figure of merit for communication systems) [4], optical fibers have remained the communications medium of choice for telephone networks, internet backbone networks, cell phone networks, CATV (Cable television), LAN (Local Area Network) backbones, security cameras, industrial networks, utility networks, and military platforms. Fiber-optic communication systems are optical communication systems (also referred to as lightwave systems) that employ optical fibers for information transmission and use high carrier frequencies (200 THz) in the visible or near-infrared region of the electromagnetic spectrum [1]. Since 1975, fiber-optic communication systems have revolutionized the industry of telecommunications and have played a major role in the advent of the “information age” during the 1990s [1]. This is due to the unique advantages offered by optical fibers: enormous potential bandwidth (as large as 2×10^{13} Hz theoretically); low

transmission losses (as low as 0.1 dB/km); immunity to electromagnetic interference; small size and weight; ruggedness and flexibility [3].

The research and development of fiber-optic communication systems started around 1975. There has been enormous progress made since 1975, which can be grouped into five distinct generations [1]. Each successive generation symbolizes a fundamental change in the improvement of the system performance, operating at higher bit rates and over longer distances.

The first generation of fiber-optic communication systems in the 1970s operated near 0.8 μm and used GaAs semiconductor lasers [1]. These systems allowed a bit rate of 45 Mb/s and repeater spacings of up to 10 km.

The second generation of fiber-optic communication systems in the early 1980s operated near 1.3 μm where fiber losses are below 1 dB/km and dispersion is minimum, and used InGaAsP semiconductor lasers [1]. With the use of single-mode fibers, the bit rate increased to 2 Gb/s from below 100 Mb/s due to dispersion in multimode fibers. However, the repeater spacing was only 50 km, which was limited by fiber losses (typically 0.5 dB/km) at an operating wavelength of 1.3 μm .

The third generation of fiber-optic communication systems in the late 1980s operated near 1.55 μm where fiber losses are minimum (0.2 dB/km) and the fiber dispersion is large [1]. By using dispersion-shifted fibers in combination with lasers oscillating in a single longitudinal mode, the bit rate increased to 10 Gb/s, but the spacing of electronic repeaters was only 60-70 km. The repeater spacing could be increased by making use of coherent detection.

The fourth generation of fiber-optic communication systems in the 1990s featured the use of optical amplification introduced in 1989 for increasing the repeater spacing, and the use of wavelength-division multiplexing (WDM) introduced in 1992 for increasing the bit rate [1]. Fiber losses were compensated periodically using Erbium-doped fiber amplifiers (EDFAs) spaced 60-80 km apart, and amplifier-based all optical fiber-optic communication systems became feasible. A large number of submarine systems have been deployed worldwide, such

as the 27,000-km fiber-optic link around the globe (FLAG) [5] and the 35,000-km Africa One network [6]. In WDM systems, with the increase in the number of the channels, it is impossible to amplify all channels using a single amplifier. New amplification schemes, such as distributed Raman amplification, have been developed to cover the spectral region extending from 1.45 μm to 1.62 μm . With the use of Raman amplification, a capacity of 3.2 Tb/s was achieved in 2003 with 80 channels, each transmitting 40 Gb/s.

The fifth generation of fiber-optic communication systems, after 2001, extends the wavelength range over which a WDM system can operate simultaneously from the conventional C band, which covers the wavelength range 1.53-1.57 μm , to the L and S bands [1]. Raman amplification has been applied successfully on all three wavelength bands. The dry fiber with the property that fiber losses are small over the entire wavelength region from 1.30 to 1.65 μm has been developed. Compared with the focus of the fourth generation of fiber-optic communication systems on increasing system capacity by increasing the number of channels in WDM systems, the focus of current fifth-generation systems shifts to increasing the spectral efficiency of WDM systems by using advanced modulation formats in which information is encoded using both the amplitude and phase of the optical carrier. The spectral efficiency has increased to > 8 b/s/Hz from below 0.8 b/s/Hz for fourth generation systems [1].

1.1 Long-Haul DWDM Systems

Modern society calls for sustainable development. One part of sustainable development is sustainable optical backbone networks, which are characterized by long-haul and high-capacity. Long-haul high-capacity fiber-optic communication systems are the focus of this dissertation.

1.1.1 Long-Haul Systems

Fiber-optic communication systems have been developed mostly for telecommunication applications, which can be broadly classified into two categories: long-haul and short-haul,

depending on whether the transmission distance is larger or smaller than the typical intercity distance (100 km) [1]. Most long-haul systems are implemented as multispan systems, for which periodic dispersion compensation and amplification is required at the end of each span. The span length is identical to the amplifier spacing. Fiber-optic communication systems are very attractive for long-haul applications due to considerable increase in both the bit rate and the repeater spacing.

1.1.2 High-Capacity Systems

High-capacity optical backbone networks are needed to support dramatically increasing demand for internet data traffic. A promising solution is dense wavelength-division multiplexing (DWDM), in which data is first time-division multiplexed (TDM) to form a channel centered at a given wavelength and many channels at different wavelengths are then wavelength-division multiplexed (WDM) together for transmitting high-throughput data on a single optical fiber [7]. A total capacity of 69.1 Tb/s with 432 channels and 171 Gb/s per channel has been demonstrated experimentally [8].

For long-haul fiber-optic communication systems serving as the backbone of telecommunication networks, the role of DWDM is simply to increase the total bit rate [9]. Fig. 1.1 shows a typical DWDM system schematically. The output of a set of transmitters, each operating at its own carrier wavelength, is multiplexed together. The multiplexed signal is launched into the optical fiber for transmission to the other end, where a demultiplexer sends each channel to its own receiver. When F channels at bit rates B_1, B_2, \dots, B_F are transmitted simultaneously over a fiber of length L , the total bit rate-distance product, BL , becomes $BL = (B_1 + B_2 + \dots + B_F)L$. For equal bit rates, the system capacity is enhanced by a factor of F .

The ultimate capacity of a DWDM system is dependent on the channel spacing, i.e., how closely channels are packed in the wavelength domain. The minimum channel spacing is limited by interchannel crosstalk. It is helpful to introduce a measure of the spectral efficiency

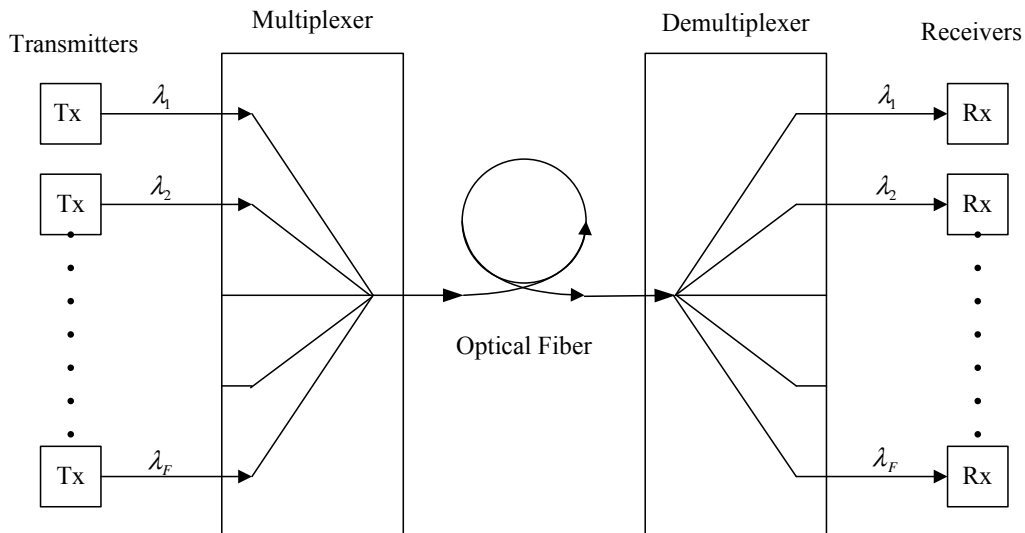


Figure 1.1: A Typical DWDM System. Separate transmitter-receiver pairs are used to send and receive the signal at different wavelengths [1]

of a DWDM system as

$$\eta_s = B_i / \Delta\nu_{ch} \quad (1.1)$$

where B_i is the bit rate of the i th channel and $\Delta\nu_{ch}$ is the channel spacing in frequency unit. A value of η_s as large as possible is desired. For direct detection systems, $\eta_s < 1$ b/s/Hz, i.e., channel spacing must be larger than the bit rate B . For coherent detection systems, $\eta_s > 1$ b/s/Hz is possible. The International Telecommunication Union (ITU) has specified DWDM channels with a channel spacing of either 100 GHz or 50 GHz.

1.1.3 Long-Haul DWDM Components

A typical long-haul DWDM system consists of the following major components: optical fibers as a communication channel, loss management component, dispersion management component, and WDM components. Further, WDM components include WDM transmitters and receivers, multiplexers and demultiplexers. This section introduces these long-haul DWDM components.

Optical Fibers

The optical signals propagate over optical fibers. In long-haul systems with optical fibers serving as the communication channel, fiber losses, dispersion and nonlinearities, collectively called physical impairments, are introduced during transmission of optical signals.

Fiber losses are due to material absorption, Rayleigh scattering, bending, and scattering of light at the core-cladding interface [2]. If P_0 is the launched power at the input of a fiber of length L , the received power P_R is given by

$$P_R = P_0 \exp(-\alpha L) \quad (1.2)$$

where α is the attenuation constant, a measure of total fiber losses from all sources. α is usually expressed in units of dB/km using the relationship $\alpha_{dB} = 4.343\alpha$ [2]. Although fiber losses are as small as 0.2 dB/km near 1.55 μm , the optical power reduces to only 1% of the launched power after 100 km. Fiber losses affect the repeater or amplifier spacing.

Most fiber-optic communication systems use single mode fibers due to the absence of intermodal dispersion inherent in multimode fibers. However, fiber dispersion still accompanies single mode fibers. Fiber dispersion, also referred to as group-velocity dispersion (GVD), or intramodal dispersion, is due to material dispersion and waveguide dispersion. Fiber dispersion comes from different spectral components of the pulse traveling at slightly different group velocities. Fiber dispersion is measured by the GVD parameter, β_2 . At 1.55 μm , $\beta_2 \approx -20 \text{ ps}^2/\text{km}$ for standard silica fibers. Fiber dispersion leads to pulse broadening.

The response of any dielectric to light becomes nonlinear for intense electromagnetic fields. The response of optical fibers to light introduces fiber nonlinearities due to the intensity dependence of the refractive index and stimulated inelastic scattering. The Kerr effect, due to nonlinear refraction, is the dominating fiber nonlinearity for long-haul DWDM systems with periodic dispersion compensation and amplification. The Kerr effect is measured by the nonlinear parameter γ . At 1.55 μm , $\gamma \approx 2 \text{ W}^{-1}\text{km}^{-1}$ for standard silica fibers. The Kerr effect is responsible for various nonlinear physical impairments. The control of nonlinear

physical impairments is a difficult task.

Loss Management and Dispersion Management

Loss management and dispersion management have been developed to compensate fiber losses and fiber dispersion for long-haul systems. Fiber Losses are countered using EDFAs or Raman amplification. Dispersion is controlled using a dispersion compensator [1]. In this way, fiber losses and dispersion cease to be limiting factors for fiber-optic communication systems. The performance of modern long-haul systems is typically limited by the nonlinear physical impairments [1]. The mitigation of nonlinear physical impairments is the focus of this dissertation.

Multiplexers and Demultiplexers

Multiplexers combine the signals from WDM transmitters and launch it into an optical fiber. Demultiplexers separate the received signals into individual channels associated with different WDM receivers. Demultiplexers require a wavelength-selective mechanism. Demultiplexers can be classified into two broad categories: diffraction-based and interference-based. Diffraction-based demultiplexers use an angularly dispersive element, such as a diffraction grating, to disperse incident light spatially into various wavelength components. Interference-based demultiplexers use optical filters and directional couplers. Depending on the propagation direction, a device can be used as a multiplexer or a demultiplexer.

WDM Transmitters and Receivers

WDM transmitters convert the electrical signals into optical signals. A WDM transmitter consists of an optical source, a modulator, and a channel coupler. The optical source, usually a semiconductor laser or a lighting-emitting diode (LED), provides stable light within a specific, narrow bandwidth that carries the digital data. The modulator imprints the data onto the light. Most fiber-optic communication systems use a simple digital modulation scheme called on-off keying (OOK) in which an electrical binary bit stream modulates the peak amplitude (or intensity) of an optical carrier inside an optical transmitter. Advanced modulation formats employ both the amplitude and the phase of an optical carrier. The coupler focuses the

optical signal on the single-mode fiber. The launched power is an important parameter of an optical transmitter. For LEDs, the launched power is less than -10 dBm; for semiconductor lasers, the launched power can be up to 10 dBm. A large launched power results in various severe nonlinear physical impairments.

WDM receivers convert the demultiplexed optical signals back into the original electrical signals. A WDM receiver consists of a coupler, a photodetector, and a demodulator. The coupler focuses the received demultiplexed optical signal onto the photodetector. The photodetector generates an electrical signal from the demultiplexed signal. The demodulator is dependent on the modulation format used by the fiber-optic communication system. Most fiber-optic communication systems use a scheme referred to as “intensity modulation with direct detection” (IM/DD), in which a decision circuit identifies bits as 1 or 0, depending on the amplitude of the electrical signal.

To improve the spectral efficiency of DWDM systems, advanced modulation schemes which modulate both the amplitude and the phase of a carrier wave have been developed. In this case, direct detection cannot be used for demodulation because all phase information is lost during the detection. Advanced modulation schemes require advanced demodulation schemes that convert phase information into intensity variations. Depending on the receive design, these demodulation schemes can be classified into two categories: coherent demodulation schemes and delay demodulation schemes [1]. In coherent demodulation schemes, the received signal is detected using homodyne or heterodyne detection, which requires mixing with a local oscillator [10]. In the case of differential phase-shift keying (DPSK), delay demodulation schemes can be used. In delay demodulation schemes, the received signal is first processed optically to transfer phase information into intensity modulations and then sent to a direct-detection receiver [11]. To improve receiver performance, a balanced detection scheme, which employs the difference between the outputs of two photodetectors, is used.

The performance measure of a fiber-optic communication system is the bit-error rate (BER), which is defined as the average probability of incorrect bit identification [1]. The BER

depends on the signal-to-noise ratio (SNR), which in turn depends on various noise sources and physical impairments that corrupt the received signal. In addition to shot noise (or quantum noise) and thermal noise, in long-haul systems with periodic dispersion compensation and amplification, the use of optical amplifiers introduces amplified spontaneous emission (ASE) noise. The ASE noise added by each amplifier is the dominating noise source for long-haul systems with periodic dispersion compensation and amplification.

1.2 Motivation

All-optical communications eliminate the bottleneck of optical-to-electrical-to-optical (OEO) conversion over long-haul DWDM systems. However, with periodic dispersion management and amplification, the long lightpaths that result inevitably give rise to severe physical impairments, which in turn adversely affect system performance [1]. These physical impairments include not only linear physical impairments due to dispersion, but also nonlinear physical impairments due to fiber nonlinearities, which further consist of both intrachannel impairments and interchannel impairments. The performance of long haul DWDM systems is fundamentally limited by dispersion, fiber nonlinearity, and noise [12][13][14].

Sophisticated signal processing techniques are needed to mitigate the physical impairments and fully exploit the system capacity [15]. These techniques cannot be developed without a mathematical model which describes the input-output relationship of long-haul DWDM systems and characterizes the physical impairments experienced. To better explore the digital communications potential of these systems, this model should be a discrete-time model so that various mature digital signal processing (DSP) techniques can be applied. This model should also consider the two dimensions (2D: time and wavelength) so that both intrachannel and interchannel effects can be simultaneously mitigated.

The basic equation that describes the propagation of optical pulses inside single-mode fibers (SMF) is the nonlinear Schrödinger (NLS) equation [2]. The NLS equation is a

nonlinear partial differential equation (PDE) whose exact analytic solutions generally are difficult to obtain except for some specific cases, such as soliton solutions in which the inverse scattering method can be employed [16][17][18]. It is an implicit and continuous time expression, both of which limit its usefulness for signal processing applications. A large number of approximate analytical and numerical methods have been developed to solve the NLS equation. Linearization is a widely used approximate analytical approach. Most linearization methods can be classified into two categories: the Volterra series transfer function (VSTF) method [19] and the regular perturbation (RP) method [20].

The Volterra series is a polynomial expansion that represents the input-output relationship of a nonlinear system with memory [21]. The VSTF method expresses the NLS equation as a polynomial expansion in the frequency domain and retains the most significant terms (Volterra kernels) in the resulting transfer function. Since the NLS equation was first formulated as the Volterra series expansion form in 1997 [19], the VSTF method has been applied to investigate system design issues [22], fiber nonlinearities [23][24][25][26], channel capacity [27][28][29][30], dispersion compensation [31], pulse broadening [32], and filtering [33]. The convergence of the VSTF method was also investigated in [34]. The RP method is applicable to differential equations when the nonlinearity is weak [35]. Since 1998 the RP method has been used to solve the NLS equation [20][36][37], investigate the channel capacity [38] and fiber nonlinearities [39][40][41]. It has been shown that when the nonlinearities are due to the Kerr effect alone, the n -order RP solution coincides with the $2n + 1$ -order Volterra series solution [37]. Both the third-order VSTF method and the first-order RP method result in the same triple integral.

An alternative is to use a purely numerical method. Numerical methods can be classified into two categories: finite-difference methods and pseudospectral methods [2]. The split-step Fourier method (SSF) is one pseudospectral method that has been used extensively to solve the NLS equation. This method runs much faster than most finite-difference methods due in part to the use of the fast-Fourier-transform (FFT) algorithm [42]. The SSF method is usually

taken as the standard of accuracy for validating other methods in the absence of experimental data due to its well-established ability to accurately simulate the pulse propagation in fibers. However, the SSF method has three important drawbacks: (1) it is unable to display the effects of varying parameters on system output analytically; (2) it is unable to isolate what impairment is causing the most degradation; and (3) it is computationally expensive.

Both the VSTF method and the RP method have the same complexity and computational efficiency. However, the triple integral involves massive numerical evaluation of iterated integration. We must reduce the triple integral to a much simpler form; otherwise, there is little computational advantage in using either the VSTF method or the RP method over the SSF method.

Many researchers have attempted to solve the triple integral problem. However, most attempts have failed to reach a much simpler form with the exception of a simple integral for a simplified single-channel single-span case in which both fiber losses and pulse chirp are ignored [7][31][32]. A common scheme that deals with the triple integral problem is to introduce the concept of the nonlinear transfer function [43] (called the DM (dispersion-managed) kernel in [44]) and approximate it by asymptotic approximations [45][46][47]. In this way, the triple integral can be simplified to a double integral but at the cost of accuracy. Three improvements of the RP method have been proposed but they apply to the single-channel single-span case only. The first is the enhanced RP (ERP) method [37], whose solution contains a simple integral involving a complicated Fourier transform. The second is the multiplicative approximation method [48], whose solution includes a simple integral of a complicated convolution. The third is a recursive method [49], which asymptotically approaches the exact solution of the NLS equation but whose computational complexity remains an issue.

1.3 Research Methodology

This dissertation proposes a model-centric approach for discrete-time signal processing for fiber-optic communications and addresses the development, validation and applications of a general deterministic analytical model of physical impairments in long-haul DWDM systems, specifically multichannel multipulse multispans systems with periodic dispersion management and amplification. It is assumed that chirped Gaussian pulses are used at the transmitter and Gaussian optical filters are used at the receiver. In this research, we extend the VSTF method further to the general multichannel multipulse multispans case and reduce the triple integral to a simple integral, gaining computational efficiency advantage over the SSF method with comparable accuracy. The resulting model is a polynomial model that takes into account fiber losses, dispersion, fiber nonlinearities, multiple channel effects, pulse chirp, and multiple spans.

1.4 Significance

The development of a 2D discrete-time model of physical impairments in long-haul DWDM systems is of significance to both the field of fiber-optic communication systems and modern society.

The model has the potential to serve as the foundation of discrete-time signal processing for fiber-optic communication systems. Compared with both the SSF method and the original third-order VSTF model, this model offers three significant advantages. First, the model provides significant computational savings. Second, this model has strong analytic capacity. It can isolate the importance of any individual physical impairment while the SSF method can report only on the total level of all physical impairments combined, and cannot provide this valuable break-down information. Moreover, with this model, the insight into what impact varying various parameters has on the system output analytically can be gained easily. Third, the model has the potential to serve as the foundation of discrete-time signal

processing for optical communications and be applied in multichannel signal processing for intersymbol and interchannel interference mitigation, constrained coding for WDM systems, multiuser coding, multichannel detection and path-diversity for all-optical networks. This is the biggest benefit of this model which could not be offered by either the SSF method or the original third-order VSTF model.

With the help of discrete-time signal processing due to the model, the performance of fiber-optic communication systems could be improved so that sustainable optical backbone networks become realities. People in modern society will experience faster data transmission, lower latency, and less interference.

The previous solutions to the NLS equation could not meet the needs required by discrete-time signal processing for fiber-optic communication systems. With the strong analytic capacity of the model, it is possible for us to analyze the long-haul DWDM systems. The discrete-time property of the model makes it the natural candidate for discrete-time signal processing for fiber-optic communication systems to improve system performance. The potentials of discrete-time signal processing and digital communications could be exploited fully due to the model. This may lead to fiber-optic communication system throughput and performance near its theoretical capacity limits. Applications in system analysis and system performance improvement could not be developed before the 2D discrete-time model is developed.

The model opens the way for signal processing experts to contribute to the improvement of fiber-optic communication systems. They have shied away from this in the past due to the daunting physical description of these systems.

1.5 Dissertation Organization

The dissertation is organized as follows.

The nonlinear Schrödinger (NLS) equation is the basic equation that governs propagation of optical pulses in single-mode fibers. In Chapter 2, background work and a literature review for the field are given. After an introduction of the NLS equation, including its history and derivation, existing solution methods to the NLS equation (Volterra series transfer function method and split-step Fourier method) are presented and their drawbacks are pointed out, justifying the need for a new solution to the NLS equation. Then various physical impairments and ASE noise in long-haul DWDM systems that limit system performance and performance measures used in fiber-optic communication systems are introduced. Lastly, existing signal processing techniques, including forward error correction, predistortion/equalization, and constrained coding, to improve system performance are reviewed.

Chapter 3 describes the development and validation of a 2D discrete-time model of physical impairments in long-haul DWDM systems. The model development is based on the Volterra series transfer function (VSTF) method. There are three main contributions made in model development: (1) the model is a simple integral, compared with the triple integral associated with the original VSTF method; (2) the model takes into account multichannel effect, fiber losses, frequency chirp, optical filtering, and photodetection, which are ignored in the current literature; (3) the model is a discrete-time model that characterizes various individual physical impairments, and is easy to use to develop discrete-time signal processing techniques to mitigate physical impairments in long-haul DWDM systems. This chapter also discusses the complexity of the model.

In Chapter 4, the 2D discrete-time model is applied in two different ways to analyze the system. The first application is to analyze the effects of varying two most important system parameters (symbol rate and channel spacing) and pulse shape on the individual physical impairments in a long-haul DWDM system. The second application is to determine the ranges of influence (RoI) of various individual physical impairments in long-haul DWDM systems.

In Chapter 5, the 2D discrete-time model is used to develop two signal processing

applications to improve the system performance. The first application is to implement a novel constrained coding scheme based on total impairment extent rank (TIER), or a TIER-LDPC concatenation scheme. The TIER-LDPC concatenation scheme combines the strength of the TIER code in avoiding errors due to physical impairment and that of the LDPC code in correcting memoryless errors due to ASE noise. The TIER-LDPC concatenation scheme is effective over the entire range of transmitter power levels and link length in suppressing both the physical impairments and the ASE noise in long-haul fiber-optic communication systems. The second application is to propose a nonlinear equalizer based on the inverse Volterra theory. The nonlinear equalizer improves the system performance significantly, particularly for high power levels where nonlinearity dominates.

Chapter 6 concludes the dissertation and proposes future avenues for research.

Chapter 2

Background

The objective of this chapter is to present the necessary background knowledge relevant to this dissertation. Section 2.1 introduces the nonlinear Schrödinger (NLS) equation, which is the basic equation that governs propagation of optical pulses in single-mode fibers. Section 2.2 reviews the approximate analytical methods and numerical methods used to solve the NLS equation. The two most important factors that limit system performance of long-haul DWDM systems, i.e., physical impairments and ASE noise, are introduced in Sections 2.3 and 2.4, respectively. Section 2.5 presents the performance measures used in fiber-optic communication system analysis. Section 2.6 reviews various signal processing techniques that can improve system performance of long-haul DWDM systems, including forward error correction, constrained coding, and predistortion/equalization. Section 2.7 concludes this chapter with a summary.

2.1 Nonlinear Schrödinger (NLS) Equation

When short optical pulses with widths ranging from a few nanoseconds down to 10 femtoseconds propagate inside a fiber, their shapes and spectra are influenced by both dispersive and nonlinear effects. A basic equation that governs propagation of optical pulses in nonlinear dispersive fibers is the nonlinear Schrödinger (NLS) equation.

The NLS equation is a nonlinear version of the Schrödinger equation that was formulated in 1925 and for which Erwin Schrödinger received the Nobel Prize in Physics in 1933. In quantum mechanics, the Schrödinger equation is a linear partial differential equation that describes how the quantum state of a physical system changes with time. In theoretical physics, the NLS equation is a nonlinear partial differential equation that describes wave propagation in a nonlinear medium [50].

Historically, the essence of the NLS equation appeared in the work of Vitaly L. Ginzburg (2003 Nobel laureate in Physics) in his study of the theory of superconductors and superfluids in the 1950s [51][52][53]. After the NLS equation was applied successfully to the phenomenon of self-focusing and the conditions under which an electromagnetic beam can propagate without spreading in nonlinear media in the 1960s [54][55], the wider physical significance of the NLS equation became well-recognized by the scientific community. The recent additional interest in the NLS equation is mainly due to its applications in nonlinear fiber optics [56][57] and soft-condensed matter physics [58].

The general form of the NLS equation is [59]

$$i\frac{\partial\psi}{\partial t} + \frac{\partial^2\psi}{\partial x^2} + f(|\psi|)\psi = 0 \quad (2.1)$$

where x and t are the propagation variables, $\psi(x, t)$ is the slowly varying complex envelope of the complex field, $f(u)$ is a real function of a real variable u .

The significance of the NLS equation in the physics community lies in its universal character [60]. The NLS equation is applicable to most weakly-nonlinear, dispersive, energy-preserving systems. It has been used to describe the nonlinear propagation of wave packets in many physical fields, such as fluid dynamics[61], nonlinear fiber optics [2], magnetic spin waves [62][63], and plasma physics[59]. The NLS equation provides a canonical description of the envelope dynamics of a quasi-monochromatic plane wave propagating in a weakly nonlinear dispersive medium [50].

The significance of the NLS equation in the mathematics community lies in its integrability in one transverse dimension via the inverse scattering transform, a nonlinear Fourier transform which admits multisoliton solutions and possesses many interesting properties [50].

The NLS equation in nonlinear fiber optics was first derived by Akira Hasegawa and Fred Tappert in 1973 [64][65]. Detailed derivations can be found in [66] and [2]. The following description is a simplified derivation based on [2].

Starting from Maxwell's equations and assuming the optical field to be quasi-monochromatic and maintain its polarization along the fiber, the electric field $E(r, t)$ can be expressed as

$$E(r, t) = \frac{1}{2} \hat{x} \{ F(x, y) A(z, t) \exp[i(\beta_0 z - \omega_0 t)] + c.c. \}, \quad (2.2)$$

where $E(r, t)$ is a slowly varying function of time t relative to the optical field and position r , \hat{x} is the polarization unit vector, for a single-mode fiber $F(x, y)$ is the modal distribution of the fundamental fiber mode (linearly polarized in either the x or y direction) given by the Gaussian approximation

$$F(x, y) \approx \exp\left[-\frac{x^2 + y^2}{w^2}\right], \quad (2.3)$$

where the width parameter w is determined by curve fitting or by following a variational procedure. $A(z, t)$ is the slowly varying pulse envelope, which depends on the propagation distance z and the propagation time t , β_0 is the wave number, ω_0 is the center frequency of the pulse spectrum, and the abbreviation c.c. stands for complex conjugate.

The Fourier transform $\tilde{A} \doteq \tilde{A}(z, \omega - \omega_0)$ of $A(z, t)$ satisfies

$$\frac{\partial \tilde{A}}{\partial z} = i[\tilde{\beta}(\omega) - \beta_0] \tilde{A}, \quad (2.4)$$

where $\tilde{\beta}(\omega)$ is the eigenvalue of the Helmholtz equation satisfied by the Fourier transform of $E(r, t)$, depending on the frequency ω .

Using the first-order perturbation theory, Eq. (2.4) becomes

$$\frac{\partial \tilde{A}}{\partial z} = i[\beta(\omega) + \Delta\beta(\omega) - \beta_0]\tilde{A}, \quad (2.5)$$

where $\beta(\omega)$ is the wave number, and $\Delta\beta(\omega)$ is a small perturbation of $\beta(\omega)$. The meaning of Eq. (2.5) is that each spectral component within the pulse envelope acquires a phase shift whose magnitude is both frequency and intensity dependent, as it propagates down the fiber. Because an exact functional form of $\beta(\omega)$ is unknown, it is necessary to expand $\beta(\omega)$ in a Taylor series around the carrier frequency ω_0 as

$$\beta(\omega) = \beta_0 + (\omega - \omega_0)\beta_1 + \frac{1}{2}(\omega - \omega_0)^2\beta_2 + \frac{1}{6}(\omega - \omega_0)^3\beta_3 + \dots, \quad (2.6)$$

where $\beta_0 = \beta(\omega_0)$ and other parameters are defined as

$$\beta_m = \left(\frac{d^m \beta}{d\omega^m} \right)_{\omega=\omega_0}, m = 1, 2, \dots \quad (2.7)$$

Similarly, $\Delta\beta(\omega)$ is expanded as

$$\Delta\beta(\omega) = \Delta\beta_0 + (\omega - \omega_0)\Delta\beta_1 + \frac{1}{2}(\omega - \omega_0)^2\Delta\beta_2 + \frac{1}{6}(\omega - \omega_0)^3\Delta\beta_3 + \dots \quad (2.8)$$

If the spectral width of the pulse satisfies the condition $\Delta\omega \ll \omega_0$, the third and higher-order terms in the expansion (2.6) are negligible; the first and higher-order terms in the expansion (2.8) are negligible. These two approximations are consistent with the quasi-monochromatic assumption.

By taking the inverse Fourier transform of Eq. (2.5) with the above two approximations using

$$A(z, t) = \frac{1}{2\pi} \int_{-\infty}^{+\infty} \tilde{A}(z, \omega - \omega_0) \exp[-i(\omega - \omega_0)t] d\omega, \quad (2.9)$$

one can obtain the following propagation equation for $A(z, t)$

$$\frac{\partial A}{\partial z} + \beta_1 \frac{\partial A}{\partial t} + \frac{i\beta_2}{2} \frac{\partial^2 A}{\partial t^2} = i\Delta\beta_0 A. \quad (2.10)$$

By including both the effects of fiber losses and nonlinearity in the $\Delta\beta_0$ term on the right hand side of Eq. (2.10), Eq. (2.10) becomes

$$\frac{\partial A}{\partial z} + \beta_1 \frac{\partial A}{\partial t} + \frac{i\beta_2}{2} \frac{\partial^2 A}{\partial t^2} + \frac{\alpha}{2} A = i\gamma|A|^2 A, \quad (2.11)$$

where γ is the nonlinear parameter.

Eq. (2.11) describes propagation of picosecond optical pulses in single-mode fibers and includes the effects of fiber losses through α , of group velocity through β_1 , of chromatic dispersion through β_2 , and of fiber nonlinearity through γ . The pulse envelope moves at the group velocity $v_g \equiv \frac{1}{\beta_1}$, while the effects of group-velocity dispersion (GVD) are governed by β_2 and the nonlinear effects due to the Kerr effect are governed by γ .

By making the transformation

$$t' = t - \frac{z}{v_g} = t - \beta_1 z, \quad (2.12)$$

a frame of reference moving with the pulse at the group velocity v_g (the so-called retarded frame) is used and Eq. (2.11) becomes

$$\frac{\partial A}{\partial z} = -\frac{\alpha}{2} A - \frac{i\beta_2}{2} \frac{\partial^2 A}{\partial t'^2} + i\gamma|A|^2 A. \quad (2.13)$$

Eq. (2.13) is referred to as the NLS equation due to its resemblance to the Schrödinger equation with a nonlinear term and a loss term. The NLS equation holds for pulses of width $T_0 > 5$ ps. The NLS equation is a fundamental equation of nonlinear fiber optic propagation, which is the simplest nonlinear equation for studying the third-order nonlinear effects in

optical fibers. If the peak power of an optical pulse is large enough, the NLS equation needs to be modified to include the fifth and higher-order terms. Hereinafter we drop the prime over t for notational simplicity. The three terms on the right hand side (RHS) describe, respectively, the effects of fiber losses, dispersion, and nonlinearity on the pulses propagating inside optical fibers.

Either dispersive or nonlinear effects dominate along the fiber, depending on the initial width T_0 and the peak power P_0 of the incident pulse. It is helpful to introduce two length scales: the dispersion length L_D and the nonlinear length L_{NL} .

Define a time scale normalized to the input pulse width T_0 as [2]

$$\tau = \frac{t}{T_0}, \quad (2.14)$$

and a normalized amplitude U as

$$U(z, \tau) = \frac{A(z, \tau)}{\sqrt{P_0} \exp(-\frac{\alpha z}{2})}. \quad (2.15)$$

Also define the dispersion length L_D as [2]

$$L_D = \frac{T_0^2}{|\beta_2|}, \quad (2.16)$$

and the nonlinear length L_{NL} as

$$L_{NL} = \frac{1}{\gamma P_0}. \quad (2.17)$$

The NLS equation then becomes [2]

$$i \frac{\partial U}{\partial z} = \frac{\text{sgn}(\beta_2)}{2L_D} \frac{\partial^2 U}{\partial \tau^2} - \frac{\exp(-\alpha z)}{L_{NL}} |U|^2 U, \quad (2.18)$$

where $\text{sgn}(\beta_2) = \pm 1$ depends on the sign of the GVD parameter β_2 . Depending on the relative magnitude of L_D , L_{NL} , and the fiber length L , there are four different propagation

regimes.

When the fiber length L satisfies both $L \ll L_D$ and $L \ll L_{NL}$, neither dispersive nor nonlinear effects are significant during pulse propagation.

When the fiber length L satisfies both $L \sim L_D$ and $L \ll L_{NL}$, the nonlinear term is negligible compared with the dispersion term. The pulse evolution is governed by GVD and the dispersion-dominant regime is applicable if the fiber parameters and pulse parameters satisfy [2]

$$\frac{L_D}{L_{NL}} = \frac{\gamma P_0 T_0^2}{|\beta_2|} \ll 1. \quad (2.19)$$

When the fiber length L satisfies both $L \ll L_D$ and $L \sim L_{NL}$, the dispersion term is negligible compared with the nonlinear term. The pulse evolution is governed by SPM and the nonlinearity-dominant regime is applicable if the fiber parameters and pulse parameters satisfy [2]

$$\frac{L_D}{L_{NL}} = \frac{\gamma P_0 T_0^2}{|\beta_2|} \gg 1. \quad (2.20)$$

When the fiber length L is longer or comparable to both L_D and L_{NL} , dispersion and nonlinearity act together during pulse propagation. In the anomalous-dispersion regime ($\beta_2 < 0$), the interplay of the GVD and SPM effects results in solitons. In the normal-dispersion regime ($\beta_2 > 0$), the combined effects of GVD and SPM leads to pulse compression.

2.2 Solution to the NLS Equation

The NLS equation is a nonlinear PDE whose exact analytic solutions are difficult to obtain [2] except for some specific cases, such as soliton solutions in which the inverse scattering method can be employed [16][17][18]. A large number of approximate analytical and numerical methods have been developed to solve the NLS equation. This section summarizes some methods that have been used extensively to solve the NLS equation.

2.2.1 Analytical methods

Most approximate analytical methods can be classified into two categories: the Volterra series transfer function (VSTF) method [19] and the regular perturbation (RP) method [20].

The Volterra series is a polynomial expansion that represents the input-output relationship of a nonlinear system, similar to the Taylor series but with the ability to capture memory effects [21]. The VSTF method expresses the NLS equation as a polynomial expansion in the frequency domain. Retaining only the first-order and the third-order Volterra kernels (the second-order kernel is zero due to the absence of even-order nonlinearities in an optical fiber), the frequency-domain output of the fiber at length L is given as [19]

$$\begin{aligned} \tilde{A}(L, \omega) \approx H_1(L, \omega)\tilde{A}(0, \omega) + \int_{-\infty}^{+\infty} \int_{-\infty}^{+\infty} H_3(L, \omega_1, \omega_2, \omega - \omega_1 + \omega_2)\tilde{A}(0, \omega_1)\tilde{A}^*(0, \omega_2) \\ \tilde{A}(0, \omega - \omega_1 + \omega_2)d\omega_1d\omega_2, \end{aligned} \quad (2.21)$$

where

$$H_1(L, \omega) = \exp\left(-\frac{\alpha}{2}L + i\frac{\beta_2}{2}\omega^2L\right), \quad (2.22)$$

$$H_3(L, \omega_1, \omega_2, \omega - \omega_1 + \omega_2) = \frac{i\gamma}{4\pi^2}H_1(L, \omega) \int_0^L \exp[-\alpha z + i\beta_2 z(\omega_1 - \omega)(\omega_1 - \omega_2)]dz, \quad (2.23)$$

$\tilde{A}(z, \omega)$ is the Fourier transform of $A(z, t)$, and $H_1(L, \omega)$ and $H_3(L, \omega_1, \omega_2, \omega - \omega_1 + \omega_2)$ are the first-order and third-order Volterra kernels, which are the linear and nonlinear transfer functions of an optical fiber of length L , respectively. Substituting (2.22) and (2.23) into (2.21) yields the well-known triple integral. Returning to the time domain can result in yet another integral.

The idea behind the RP method is that when an equation is changed by only a small amount, the solution will often only change by a small amount. This method is applicable to differential equations with a small nonlinear parameter and yields a series of terms of

decreasing magnitude that approximate the solution of the original differential equation [35]. With this method, the first-order RP approximation to the output optical field has been obtained with the result being the same triple integral as above [37][38]. Further, it is found that the n -order RP solution coincides with the $2n + 1$ VSTF solution for any integer n [37].

In this dissertation, the development of the 2D discrete-time model of physical impairments in long-haul DWDM systems is based on the above third-order VSTF model. The triple integral problem is overcome and simplified to a simple integral form, which has the potential to be applied in signal processing for fiber-optic communication systems.

2.2.2 Numerical methods

The split-step Fourier (SSF) method was developed for electromagnetic and ocean acoustic propagation by Fred Tappert in 1973 [67].

The NLS equation can be written in the form [2]

$$\frac{\partial A}{\partial z} = (\hat{D} + \hat{N})A, \quad (2.24)$$

where \hat{D} is a differential operator that takes into account fiber losses and dispersion on pulse propagation and is given by [2]

$$\hat{D} = -\frac{\alpha}{2} - \frac{i\beta_2}{2} \frac{\partial^2}{\partial t^2}, \quad (2.25)$$

and \hat{N} is a nonlinear operator that takes into account fiber nonlinearity on pulse propagation and is given by [2]

$$\hat{N} = i\gamma|A|^2. \quad (2.26)$$

Generally both dispersion and nonlinearity act together during fiber propagation. The SSF method obtains an approximate solution by assuming that the dispersive and nonlinear effects act independently during the propagation of the optical field over a small segment of distance h . More specifically, propagation from z to $z + h$ is carried out in two steps: in the

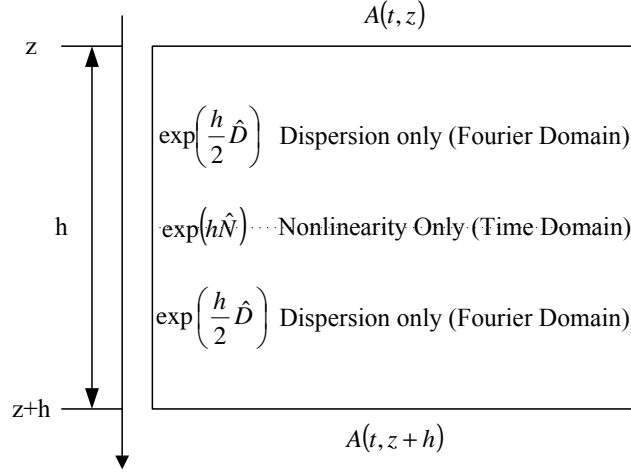


Figure 2.1: Symmetrized split-step Fourier method used for numerical simulations. Fiber length is divided into a large number of segments of width h . The effect of nonlinearity is included at the middle of the segment. [2]

first step, $\hat{D} = 0$, $\hat{N} \neq 0$, i.e., the nonlinearity acts alone; in the second step, $\hat{N} = 0$, $\hat{D} \neq 0$ i.e., the dispersion acts alone. Mathematically,

$$A(t, z + h) \approx \exp(h\hat{D}) \exp(h\hat{N}) A(t, z). \quad (2.27)$$

The exponential operator $\exp(h\hat{D})$ can be evaluated in the Fourier domain and the exponential operator $\exp(h\hat{N})$ can be evaluated in the time domain.

A common improvement in the accuracy of the generic split-step Fourier method is a scheme called the symmetrized split-step Fourier method [2], in which the effect of nonlinearity is included in the middle of the segment, rather than at the segment boundary. Mathematically,

$$A(t, z + h) \approx \exp\left(\frac{h}{2}\hat{D}\right) \exp(h\hat{N}) \exp\left(\frac{h}{2}\hat{D}\right) A(t, z). \quad (2.28)$$

The symmetrized split-step Fourier method is schematically shown in Fig. 2.1.

The SSF method is usually taken as the standard of accuracy for validating other methods in the absence of experimental data due to its well-established ability to accurately simulate the pulse propagation in fibers. In this dissertation, the SSF simulation is used to validate the accuracy of the 2D discrete-time model.

2.3 Physical Impairments

In long-haul DWDM systems with periodic dispersion management and amplification, the elimination of optical-to-electrical-to-optical (OEO) conversion inevitably gives rise to severe physical impairments, which in turn adversely affect system performance [1]. These physical impairments include not only linear impairments due to dispersion, but also nonlinear impairments due to fiber nonlinearity, which further consist of both intrachannel impairments and interchannel impairments. The performance of long haul DWDM systems is fundamentally limited by dispersion, fiber nonlinearity, and ASE noise [12][13][14].

2.3.1 Linear Impairments

The main effect of GVD is to broaden an optical pulse as it propagates through the fiber. In the multipulse case, temporal spreads of neighboring bits overlap, leading to intersymbol interference (ISI); further, in the multichannel multipulse case, GVD, coupled with nonlinearity, also leads to interchannel interference (ICI). In addition to GVD-induced pulse broadening, polarization-mode dispersion (PMD) leads to distortion of optical pulses due to fiber birefringence. However, PMD is important for long-haul high-speed communication systems near the zero-dispersion wavelength of the fiber, i.e., $1.27 \mu\text{m}$. For standard silica fibers at $1.55 \mu\text{m}$, PMD-induced pulse broadening is relatively small compared with GVD effect [2].

In long-haul systems, the problem of fiber losses can be solved by periodic optical amplifiers. Similarly, the problem of GVD can be managed by periodic dispersion compensation. With the use of periodic dispersion and amplification, both fiber losses and dispersion cease to be limiting factors for long-haul fiber-optic communication systems.

2.3.2 Nonlinear Impairments

Fiber nonlinearity can be classified into two types: Kerr effect and stimulated scattering [68]. Stimulated scattering leads to intensity-dependent gain or loss, the most detrimental of which is stimulated Raman scattering (SRS). The Kerr effect is due to the intensity dependence of the refractive index and causes an intensity-dependent phase shift experienced by an optical field during propagation in optical fibers [2]. Stimulated scattering is relatively small compared with the Kerr effect and is ignored in this dissertation. In the case of successive transmissions of pulses in a DWDM system, the Kerr effect leads to the nonlinear interaction among optical pulses on the same channel (intrachannel effects), and among pulses on neighboring channels in a DWDM system (interchannel effects). Intrachannel effects can be further divided into three types: self-phase modulation (SPM), intrachannel cross-phase modulation (IXPM), and intrachannel four-wave mixing (IFWM); interchannel effects can also be further separated into two types: cross-phase modulation (XPM), and four-wave mixing (FWM).

The field of a multipulse DWDM system can be represented as a double summation of the fields of all individual pulses in all individual channels, $A = \sum_{f=0}^{F-1} \sum_{k=0}^{K-1} A_{fk}$, where $A_{fk} = A_{fk}(z, t)$ is the field representing the k th of K pulses centered at kT_s located in the f th of F channels centered at $f\Delta$ in our baseband representation, where T_s is the symbol duration and Δ is the channel spacing. By substituting this summation into (2.13) we obtain

$$\sum_{f=0}^{F-1} \sum_{k=0}^{K-1} \left(\frac{\partial A_{fk}}{\partial z} + \frac{\alpha}{2} A_{fk} + i \frac{\beta_2}{2} \frac{\partial^2 A_{fk}}{\partial t^2} \right) = i\gamma \sum_{u,v,w=0}^{F-1} \sum_{l,m,n=0}^{K-1} A_{ul} A_{vm}^* A_{wn}. \quad (2.29)$$

The nonlinear terms on the RHS of (2.29) can be identified as follows: when $u = v = w$ and $l = m = n$, we have SPM; when $u = v \neq w$ or $u \neq v = w$ and $l = m = n$, it is XPM; when $u \neq v \neq w$ or $u = w \neq v$ and $l = m = n$, it is FWM; when $l = m \neq n$ or $l \neq m = n$ and $u = v = w$, it is IXPM; when $l \neq m \neq n$ or $l = n \neq m$ and $u = v = w$, it is IFWM. For interchannel effects, i.e., XPM and FWM, the frequency location of the nonlinear interaction

is given approximately by the phase-matching condition: $(u - v + w)\Delta$; for intrachannel effects, i.e., IXPM and IFWM, the time location of the nonlinear interaction is given approximately by $(l - m + n)T_s$, which is analogous to the phase-matching condition used to determine the frequency location of interchannel effects. SPM leads to spectral broadening of optical pulses. XPM leads to a phase distortion of one wave as a reaction to the intensity of another and causes a frequency broadening [69]. FWM generates new waves at the phase-matching frequencies. In the case of equally spaced frequency channels, new frequencies coincide with existing frequencies and produce in-band crosstalk [2]. IXPM results in timing jitter. IFWM is responsible for two effects that degrade the system performance: amplitude jitter and ghost pulse generation [69].

In this dissertation, the 2D discrete-time model characterizes the above individual linear and nonlinear impairments. Such a model can be used to develop signal processing applications to mitigate physical impairments to improve system performance of long-haul DWDM systems.

2.4 ASE Noise

In long-haul fiber-optic communication systems, fiber losses must be compensated using a chain of amplifiers that boosts the signal power periodically back to its original value. Periodic amplification schemes can be classified into two categories: lumped amplification and distributed amplification (or Raman amplification). Most current long-haul fiber-optic communication systems usually use EDFAs for lumped amplification.

With lumped periodic amplification, amplified spontaneous emission (ASE) adds noise to the signal during its amplification. Compared with the impact of dispersion and nonlinearity, which is deterministic, the impact of ASE noise is inherently random. In long-haul fiber-optic communication systems with lumped periodic amplification that use a chain of cascaded lumped amplifiers, ASE accumulates to high levels with the increase in the number of amplifiers (or spans). For low nonlinearity, this is equivalent to simply adding the ASE

powers of all amplifiers at the end of a fiber. For strong nonlinearity, the interaction of the ASE noise with the signal must be considered. This effect is not modelled in this dissertation and is left for future work.

The spectral density of ASE noise is nearly constant (white noise) and can be expressed by [1]

$$S_{ASE}(v_0) = n_{sp} h v_0 (G - 1), \quad (2.30)$$

where n_{sp} is the spontaneous emission factor, h is the Planck constant, and v_0 is the optical carrier frequency of the signal being amplified.

Consider a long-haul fiber-optic communication system that consists of N spans with each span of length L , which is the amplifier spacing. Assuming that all amplifiers are operated with the same gain $G = \exp(\alpha L)$, the total ASE power is given by [1]

$$P_{ASE}^{tot} = 2N S_{ASE} \Delta v_0, \quad (2.31)$$

where the factor of 2 takes into account the unpolarized nature of ASE noise and Δv_0 is the bandwidth of the optical filter.

In this dissertation, although ASE noise is not included in the 2D discrete-time model, it is considered in system performance evaluation.

2.5 Demodulation and Performance Measure

The performance of a fiber-optic communication system is measured by the bit-error rate (BER), which is defined as the average probability of incorrect bit identification by the decision circuit of the receiver. Most fiber-optic communication systems require a BER of $10^{-9} - 10^{-15}$.

To calculate the BER, we need to know the input of the decision circuit, i.e., the sampled output of the photodetector (normally photocurrent I). Depending on the demodulation

scheme and the receiver design, the output of the photodetector varies. Let $r_f(t)$ be the output of the WDM demultiplexer. For OOK, I is directly proportional to the incident optical power of the photodetector. Assuming the responsivity of the photodetector to be 1, $I = |r_f(t)|^2$. For DBPSK with optical delay demodulation with balanced detection, $I = \left| \frac{r_f(t) + r_f(t-T_s)}{2} \right|^2 - \left| \frac{r_f(t) - r_f(t-T_s)}{2} \right|^2$. For DQPSK with optical delay demodulation with balanced detection, there are two photocurrents corresponding to the in-phase and quadrature components of the received optical field. The in-phase photocurrent is identical to the photocurrent in the case of DBPSK. Due to the introduction of a relative phase shift of $\pi/2$, the quadrature photocurrent $I_Q = \left| \frac{r_f(t) \exp(i\frac{\pi}{2}) + r_f(t-T_s)}{2} \right|^2 - \left| \frac{r_f(t) \exp(i\frac{\pi}{2}) - r_f(t-T_s)}{2} \right|^2$.

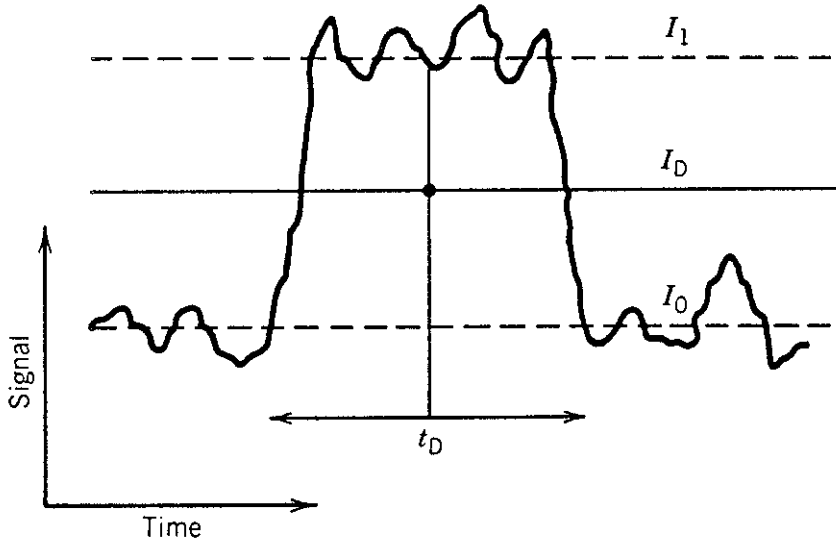


Figure 2.2: Fluctuating signal generated at the receiver for OOK [1]

Fig. 2.2 shows schematically the fluctuating signal received by the decision circuit for OOK, which is sampled at the decision instant t_D determined through clock recovery [1]. Generally, the sampled value I of each bit (1 or 0) fluctuates around an average value I_1 or I_0 . The decision circuit compares the sampled value with a threshold value I_D and identify it as bit 1 if $I > I_D$ or bit 0 if $I < I_D$. Due to various physical impairments and noises, there are two types of errors: $I > I_D$ for bit 0 and $I < I_D$ for bit 1. To include these two sources

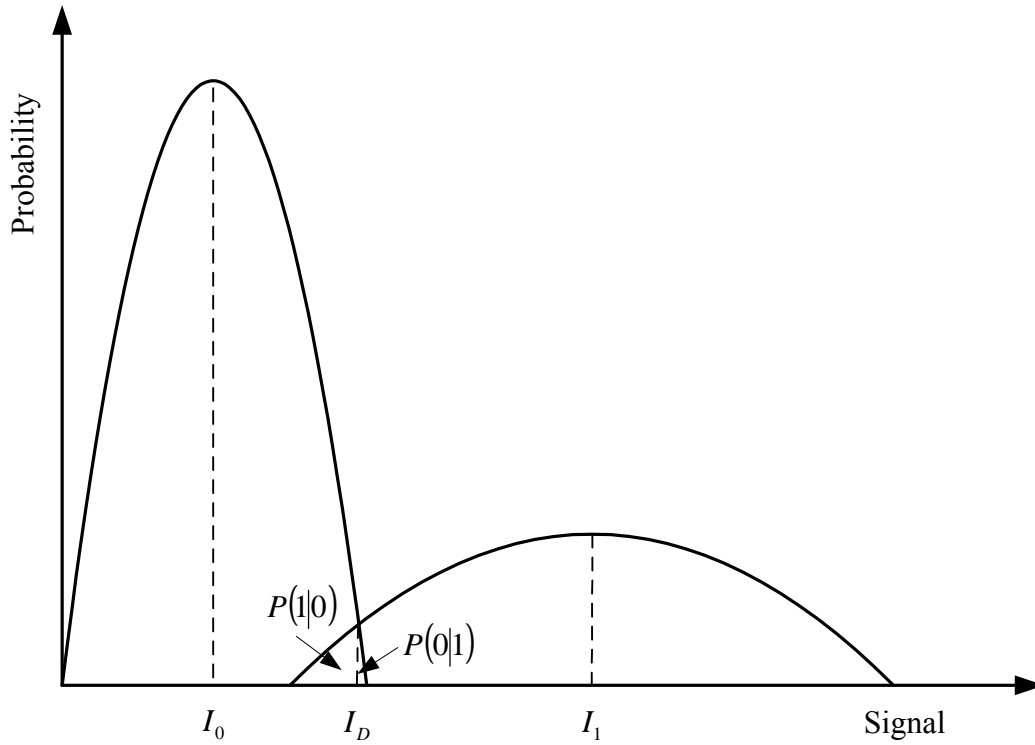


Figure 2.3: Gaussian probability densities of 1 and 0 bits

of error, the BER is defined as

$$BER = p(1)P(0|1) + p(0)P(1|0) \quad (2.32)$$

where $p(1)$ and $p(0)$ are the probabilities of transmitting bits 1 and 0, respectively, $P(0|1)$ is the probability of deciding 0 when 1 is transmitted, and $P(1|0)$ is the probability of deciding 1 when 0 is transmitted. If 1 and 0 bits are equally likely to occur, i.e., $p(1) = p(0) = \frac{1}{2}$, the BER becomes

$$BER = \frac{1}{2}[P(0|1) + P(1|0)] \quad (2.33)$$

Fig. 2.3 shows how $P(0|1)$ and $P(1|0)$ depend on the conditional probability density functions $P(I|b)$ of the sampled value I for $b = 1$ or 0. The functional form of $P(I|b)$ depends on the statistics of noise sources, including thermal noise and shot noise, which result in signal fluctuations. The noise plus the many impairments that contribute to the photo current is

often modeled as being Gaussian distributed. So the sampled value I under each transmitted pulse can be modelled as having a Gaussian probability density function. If the mean and the variance of the sampled value I for bit 1 are denoted as I_1 and σ_1^2 , and the mean and the variance of the sampled value I for bit 0 are I_0 and σ_0^2 , respectively, the conditional probabilities are given by [1]

$$P(0|1) = \frac{1}{\sigma_1\sqrt{2\pi}} \int_{-\infty}^{I_D} \exp\left(-\frac{(I - I_1)^2}{2\sigma_1^2}\right) dI = \frac{1}{2} \operatorname{erfc}\left(\frac{I_1 - I_D}{\sigma_1\sqrt{2}}\right) \quad (2.34)$$

and

$$P(1|0) = \frac{1}{\sigma_0\sqrt{2\pi}} \int_{I_D}^{\infty} \exp\left(-\frac{(I - I_0)^2}{2\sigma_0^2}\right) dI = \frac{1}{2} \operatorname{erfc}\left(\frac{I_D - I_0}{\sigma_0\sqrt{2}}\right) \quad (2.35)$$

where erfc stands for the complementary error function defined as

$$\operatorname{erfc}(x) = \frac{2}{\sqrt{\pi}} \int_x^{\infty} \exp(-y^2) dy. \quad (2.36)$$

Substituting Eqs. (2.34) and (2.35) in Eq. (2.33) yields

$$BER = \frac{1}{4} \left[\operatorname{erfc}\left(\frac{I_1 - I_D}{\sigma_1\sqrt{2}}\right) + \operatorname{erfc}\left(\frac{I_D - I_0}{\sigma_0\sqrt{2}}\right) \right]. \quad (2.37)$$

It is obvious that the BER depends on the decision threshold I_D . The minimum BER occurs when I_D satisfies

$$\frac{(I_D - I_0)^2}{2\sigma_0^2} = \frac{(I_1 - I_D)^2}{2\sigma_1^2} + \ln\left(\frac{\sigma_1}{\sigma_0}\right) \quad (2.38)$$

The term $\ln\left(\frac{\sigma_1}{\sigma_0}\right)$ is usually negligible. So the optimal I_D is obtained as

$$I_D = \frac{\sigma_0 I_1 + \sigma_1 I_0}{\sigma_0 + \sigma_1}. \quad (2.39)$$

Substituting Eq. (2.39) into Eq. (2.37) yields the BER with the optimal decision threshold

$$BER = \frac{1}{2} \operatorname{erfc}\left(\frac{Q}{\sqrt{2}}\right) \approx \frac{\exp\left(-\frac{Q^2}{2}\right)}{Q\sqrt{2\pi}}, \quad (2.40)$$

where the parameter Q , called the “ Q factor”, is given by

$$Q = \frac{I_1 - I_0}{\sigma_1 + \sigma_0}. \quad (2.41)$$

There is a one-to-one correspondence between the BER and the Q factor, as shown in Fig. 2.4. For example, a BER of 10^{-9} corresponds to $Q = 6$. With the increase of the Q factor, the BER decreases. A higher Q factor is of course desirable.

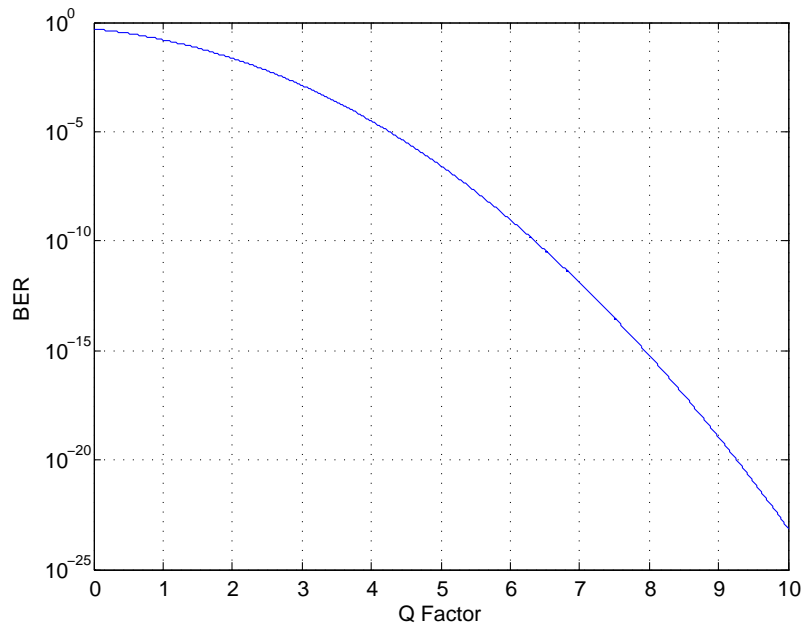


Figure 2.4: BER versus Q factor

The above derivation is based on the assumption that the dominating noise sources are ASE noise, thermal noise and shot noise. In high-data-rate DWDM systems, fiber nonlinearity becomes important and the calculation of I_0 , I_1 , σ_0^2 , and σ_1^2 is hard. Further, in long-haul DWDM systems, the nonlinear interaction between the ASE noise and the signal also becomes important but its statistics is an open problem and will be addressed in future work.

2.6 Signal Processing

Many signal processing techniques have been developed to mitigate the physical impairments and the ASE noise. These techniques can be classified into two categories: optical techniques and electrical techniques. Optical techniques rely on device development, whose complexity and cost limits their use. Electrical techniques can be applied on existing optical backbone infrastructures without any hardware change and are attracting wide attention. The main limitation of these techniques is their implementation speeds. The signal processing techniques of interest to us can be classified further into three categories: forward error correction (FEC), constrained coding, and predistortion/equalization.

2.6.1 Forward Error Correction

FEC is a technique used for controlling errors in data transmission over noisy communication channels. Its central idea is the transmitter encodes its message in a redundant way by using an error-correcting code (ECC) [3]. The improvement in system performance due to the use of FEC is measured by the coding gain [70]

$$G_c = 20 \log_{10} \left(\frac{Q_c}{Q} \right), \quad (2.42)$$

where Q_c and Q are the Q factor with and without FEC. Alternatively, the correction capability of the FEC can be evaluated in terms of the net coding gain (NCG), which is the sum of the code rate R (the ratio of bit rate without FEC to bit rate with FEC) and the coding gain G_c , as defined as [71]

$$NCG = G_c + 10 \log_{10} R \quad (2.43)$$

Although FEC appeared at the end of 1940s, FEC was first applied in fiber-optic communication systems in 1987 [71]. Three generations of FEC codes have been developed for

fiber-optic communication systems since 1987 [71].

The first generation FEC, which appeared between 1987 and 1993, is based on hard-decision decoding (a single quantization level in bit sampling) and the representative RS(255,239), where 239 is the size of a packet of bytes that is converted through coding into a larger packet with 255 bytes, yields an NCG of 5.8 dB with a code rate R of 0.93.

The second-generation FEC, which were developed between 2000 and 2004, is a class of concatenated code with hard-decision decoding. The concatenated code with the best performance achieved an NCG of 9.4 dB with R of 0.8.

The third generation is based on soft-decision decoding. Turbo codes and low-density parity check (LDPC) codes belong to the third generation FEC.

However, the performance of the current FEC schemes is very vulnerable to nonlinear physical impairments in optical communications. In Section 5.1, we propose the use of LDPC code, in conjunction with our novel constrained code, to combat both ASE noise and nonlinearity.

2.6.2 Constrained Coding

Constrained coding, which involves the use of a code to avoid patterns (waveforms) in the transmitted signal that will most likely be detected incorrectly, has been proved to be an effective approach to suppress some physical impairments [72, 73, 74, 75, 76, 77, 78, 79, 80]. A communication system is said to be constrained if there are some constraints on the input sequences that the transmitter allows. The most common constraints can be classified into two categories: (d, k) or runlength-limited (RLL) constraint and DC-free constraint [81]. The (d, k) constraint allows only sequences with runs of 0 having length at least d and no more than k . The DC-free constraint allows all sequences $s = \dots, s_{-1}, s_0, s_1, \dots, s_i \in \{-1, +1\}$ for all i , such that for all k

$$\left| \sum_{-\infty}^k s_i \right| < D \quad (2.44)$$

where D is an appropriately chosen positive number.

Generally constrained coding requires the use of a finite state transition diagram (FSTD) that describes the time-dependent behavior of a system and consists of allowable states and transitions between the states. By traversing the states along the edges and reading the labels off the edges traversed, all valid sequences can be drawn from the FSTD and represented as paths in the FSTD. The set of all paths constitute the constrained system.

FSTD is an excellent tool to design finite-state encoders and decoders [81]. A finite-state encoder can be constructed using the state-splitting algorithm. The decoders for constrained codes can be classified into two categories: state-dependent decoders and sliding-block decoders. In addition to FSTD, there are constrained codes based on table lookup, whose encoder establishes a mapping between the input and the codewords to be used at the decoder. This mapping satisfies the desired constraints [81].

The applications of constrained coding in fiber-optic communication systems involve the use of three constraints [81]. In the first constraint, the resonant sequences “1101”, “1011”, and “11011” are identified as the most troublesome sequences and forbidden. In the second constraint, the zero symbol in “resonant positions” is converted into a one-symbol to make the time matching conditions for generating ghost pulses unsatisfied. Consider a sequence of length L , $c_i c_{i+1} \dots c_{i+L-1}$; if for $l, m, n \in [i, i+1)$ and $l+m-n \in [i, i+1)$, $c_l = c_m = c_n = 1$, then $c_{l+m-n} \neq 0$. In the third constraint, one can deliberately add a single pulse on the left or right side of an “asymmetric sequence” to completely cancel out different ghost-pulse contributors at a zero-bit “resonant position”. For example, modify the sequence 1101 to 11011.

Constrained codes for fiber-optic communication systems [73, 74, 75, 76, 77, 78, 79, 80] share two common drawbacks: (1) they are limited to the suppression of IFWM only; (2) their performance evaluation is performed in the absence of the ASE noise. In Section 5.1, we propose a constrained code based on our 2D discrete-time model, and evaluate it in the presence of ASE noise.

2.6.3 Predistortion/equalization

Predistortion/equalization belong to a class of electronic techniques to compensate for the physical impairments in fiber-optic communication channel [82]. This is often accomplished by applying an inverse transfer function to the signal. When this is implemented at the transmitter side, i.e., predistorting the signal to invert the channel, and then transmitting the predistorted waveform, it is a predistorter; when this is implemented at the receiver side, i.e., equalizing the received signal to invert the channel, it is an equalizer. In the absence of ASE noise, they are equivalent in the mitigation of physical impairments, including fiber nonlinearity.

Electronic equalizers can be classified into four categories: feed-forward equalizer (FFE), decision-feedback equalizer (DFE), maximum likelihood sequence estimation (MLSE) equalizer [82], and backpropagation.

An FFE is a finite-impulse-response (FIR) filter, which has several stages, each consisting of a delay element, a multiplier and an adder [82]. After every delay element, the delayed input is multiplied with a coefficient h_i and added to the signal.

A DFE is an FFE with a second FIR filter and decision device added to form a feedback loop [82]. There are two modes of operation for a DFE: a training mode and a decision mode. During the training mode, the tap weights h_i of the equalizer are adjusted in accordance with some adaptation rule, such as the least-mean-square (LMS) algorithm. During the decision mode, small variations in the taps allow for compensation of time varying effects of the channel.

An MLSE equalizer compares a segment of the noisy received signal with all the possible noiseless waveforms of the same length that could be received and chooses the one that is most likely to have been sent. An MLSE equalizer requires a Viterbi decoder and a channel estimator [82]. It also requires soft decisions for decoding.

Backpropagation is an emerging approach to mitigate both linear impairments and nonlinear impairments [83][84][85]. It is based on a simple idea: the original optical field at

the transmitter can be recovered fully by numerical backpropagation of the received signal through an inverse nonlinear channel. In the absence of ASE noise, the transmitted signal can be exactly recovered by “backpropagating” the received signal through the inverse NLS equation given by [83]:

$$\frac{\partial A}{\partial z} = \frac{\alpha}{2}A + \frac{i\beta_2}{2} \frac{\partial^2 A}{\partial t'^2} - i\gamma|A|^2A, \quad (2.45)$$

This operation is equivalent to passing the received signal through a fictitious fiber having opposite-signed parameters. It is also possible to perform backpropagation at the transmitter side by pre-distorting the signal to invert the channel, and then transmitting the pre-distorted waveform. In the absence of ASE noise, both approaches are equivalent.

Both FFE and DFE can only mitigate efficiently the linear impairments, such as those caused by GVD and PMD only. They are not sufficiently powerful to remove nonlinear impairments, or combined effects of linear and nonlinear impairments. An MLSE equalizer has been implemented to compensate for the linear impairments and the intrachannel nonlinear impairments only [82]. Backpropagation is infeasible in practice due to hardware implementation of the negative nonlinear coefficient with optical devices using DSP. It is too computationally complex to be practical.

In Section 5.2, a nonlinear equalizer that is easy to implement has been developed to mitigate the linear and nonlinear physical impairments in long-haul DWDM systems.

2.7 Summary

The nonlinear Schrödinger (NLS) equation is the basic equation that governs propagation of optical pulses in single-mode fibers. This chapter first introduces the NLS equation and the solution methods used to solve the NLS equation, including approximate analytical methods and numerical methods. Then the two most important factors that limit system performance of long-haul DWDM systems, i.e., physical impairments and ASE noise, are introduced. Next performance measures of fiber-optic communication systems, namely, the BER and

the Q factor, are presented. Last various signal processing techniques to improve system performance of long-haul DWDM systems, including forward error correction, constrained coding, and predistortion/equalization, are reviewed.

Chapter 3

Model Development and Validation

This dissertation proposes a model-centric approach for discrete-time signal processing for optical communications and addresses the development, validation, and applications of a 2-D discrete-time model of physical impairments in long-haul DWDM systems. This chapter focuses on the development and validation of the model. The applications of the model in system analysis and system performance improvement are presented in Chapter 4 and Chapter 5, respectively. In Section 3.1, the third-order VSTF model is extended from a single-span case to a multichannel multipulse multispan case with periodic dispersion compensation and periodic amplification. By assuming chirped Gaussian pulses at the transmitter and a Gaussian optical filter at the receiver, a 2D discrete-time model that features a simple integral and characterizes each individual physical impairment in long-haul DWDM systems is derived. The model is then extended to include photodetection for three popular modulation formats: on-off keying (OOK), differential binary phase-shift keying (DBPSK) and differential quadrature phase-shift keying (DQPSK). Section 3.2 presents validation results comparing our model with SSF simulation. Section 3.3 concludes this chapter with a summary.

3.1 Model Development

This section describes the development of our 2D discrete-time model of physical impairments in long-haul DWDM systems [86]. In this dissertation, a typical long-haul DWDM system with periodic dispersion compensation and amplification, as shown in Fig. 3.1, is considered. The model development methodology proposed in this dissertation can easily be extended to other fiber-optic communication systems.

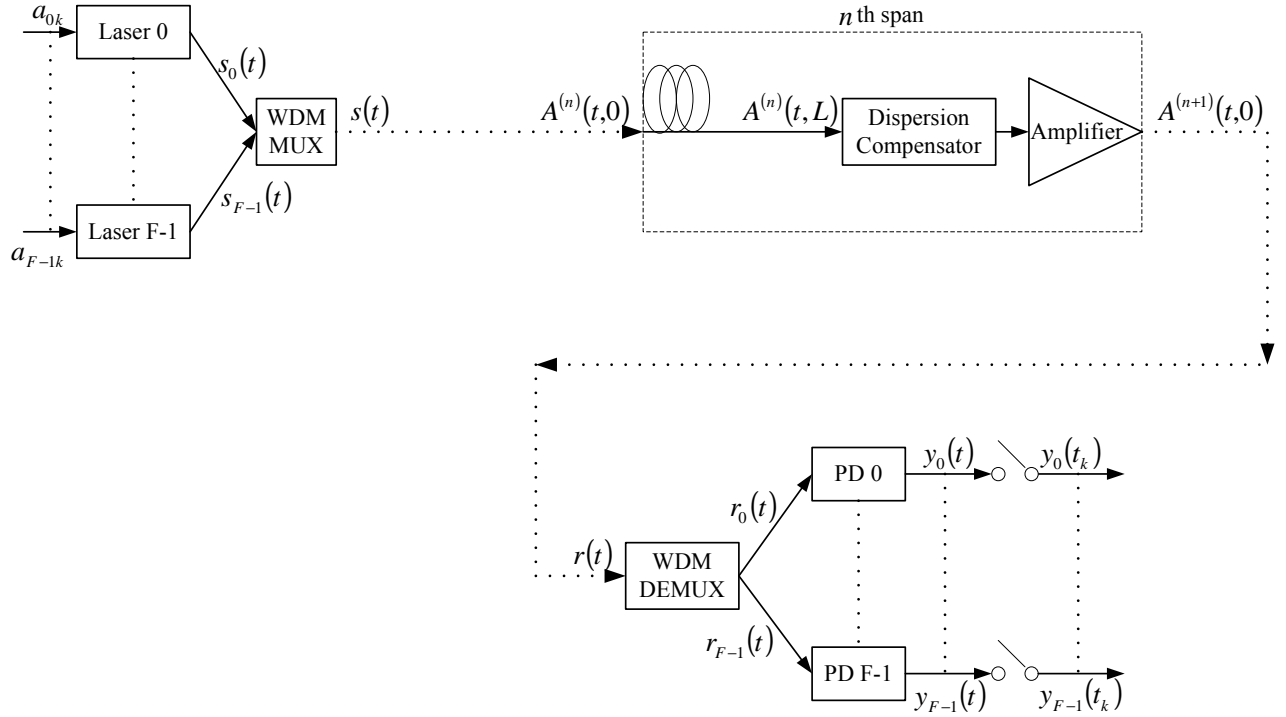


Figure 3.1: Schematic of a typical long-haul DWDM system with periodic dispersion compensation and amplification

Consider a F -channel DWDM system. At the optical transmitter, a bank of laser diodes and a WDM multiplexer convert the data of the f th channel and k th pulse to be transmitted $\{a_{fk}\} \in \{0, 1\}$ into the corresponding transmitted optical signal $s(t) = \sum_{f=0}^{F-1} s_f(t)$ and then launches it into the optical fiber serving as the communication channel. With proper carrier and modulation selection, $s_f(t)$ can be an amplitude-shift keyed (ASK), frequency-shift keyed (FSK), or phase-shift keyed (PSK) signal instead. On-off keying (OOK) and differential phase-shift keying (DPSK) are two commonly used modulation formats for DWDM systems.

$s(t)$ is transmitted through the fiber span by span and becomes the receiver input signal $r(t)$. The signal $r(t)$ is then passed through a bank of optical filters serving as a WDM demultiplexer, a bank of photodetectors to convert back into the electrical form $y_f(t)$, and decision devices.

In model development, we assume that chirped Gaussian pulses are used at the transmitter and Gaussian optical filters are used at the receiver. The ASE noise from the optical amplifiers and the postdetection electrical filter are not considered in the model development portion of this dissertation as we focus on nonlinear physical impairments. ASE noise is later included in simulation results.

The model development is based on the third-order VSTF model proposed by [19]. In this dissertation, a 7-step model development methodology is used:

Step 1: Extend the third-order VSTF model to the multispan case with periodic dispersion compensation and amplification

Step 2: Further extend the model to the multichannel multipulse case to yield the fiber output $R(\omega)$

Step 3: Multiply $R(\omega)$ with the optical fiber for channel f , $H_f(\omega)$, to yield $R_f(\omega)$

Step 4: Simplify $R_f(\omega)$ from a triple integral to a simple integral form

Step 5: Take the inverse Fourier transform of $R_f(\omega)$ to yield $r_f(t)$, the input to the photodetector for channel f

Step 6: Derive the output of the photodetector, $y_f(t)$, depending on modulation format

Step 7: Sample $y_f(t)$ at $t_k = kT_s, k = 0, \dots, K - 1$ to yield $y_f(t_k)$, corresponding to the data $\{a_{fk}\}$

Suppose the system under consideration consists of N spans, with each span of length L . The output of each span after dispersion compensation and lumped amplification becomes

the input of the next span. In the frequency domain, the combined effects of dispersion compensation and amplification can be represented by

$$H_1^{-1}(L, \omega) = \exp\left(\frac{\alpha}{2}L - i\frac{\beta_2}{2}\omega^2L\right). \quad (3.1)$$

Applying Eq. (2.21) followed by Eq. (3.1) span by span yields the multispan VSTF model of a long-haul system with periodic dispersion compensation and amplification

$$\begin{aligned} \tilde{A}^{(N+1)}(0, \omega) \approx & \tilde{A}^{(1)}(0, \omega) + \frac{iN\gamma}{4\pi^2} \int_0^L \int_{-\infty}^{+\infty} \int_{-\infty}^{+\infty} \exp[-\alpha z + i\beta_2 z(\omega_1 - \omega)(\omega_1 - \omega_2)] \\ & \tilde{A}(0, \omega_1) \tilde{A}^*(0, \omega_2) \tilde{A}(0, \omega - \omega_1 + \omega_2) d\omega_1 d\omega_2, \end{aligned} \quad (3.2)$$

where $\tilde{A}^{(n)}(z, \omega)$ is the Fourier transform of $A^{(n)}(z, t)$, which is the slowly varying complex envelope of the optical field at length z of the n th span. $\tilde{A}^{(1)}(0, \omega)$ and $\tilde{A}^{(N+1)}(0, \omega)$ correspond to the input field and the output field of the N -span system, respectively.

To extend further the multispan VSTF model to the multichannel multipulse case, $S(\omega)$ and $R(\omega)$ are defined as the input of the fiber and the input to the WDM demultiplexer in the frequency domain, which correspond to $s(t)$ and $r(t)$ in the time domain. $S(\omega) = \tilde{A}^{(1)}(0, \omega)$ and $R(\omega) = \tilde{A}^{(N+1)}(0, \omega)$. We model the pulse shape at the transmitter as a Gaussian function with a chirp parameter on the pulse in the f th channel, C_f , which governs the frequency chirp imposed on the pulse, and the half-width of the pulse in the f th channel at the $1/e$ intensity point, T_{0f} . For notational simplicity, the effective width of the pulse in the f th channel is defined as $\tilde{T}_f^2 = \frac{T_{0f}^2}{1+iC_f}$. In the case of K successive independent modulated chirped Gaussian input pulses and F equally frequency-spaced channels, the input field to the fiber is given as

$$s(t) = \sum_{f=0}^{F-1} \sum_{k=0}^{K-1} a_{fk} A_f \exp \left[-\frac{(t - kT_s)^2}{2\tilde{T}_f^2} + if\Delta t + i\Phi_{fk} \right], \quad (3.3)$$

and its Fourier transform is given as

$$S(\omega) = \sqrt{2\pi} \sum_{f=0}^{F-1} \sum_{k=0}^{K-1} a_{fk} A_f \tilde{T}_f \exp \left[-\frac{(\omega - f\Delta)^2 \tilde{T}_f^2}{2} - i(\omega - f\Delta)kT_s + i\Phi_{fk} \right], \quad (3.4)$$

where a_{fk} is the modulating symbol of the f th channel and the k th pulse; $A_f = \sqrt{P_f}$ is the peak amplitude of the Gaussian pulse in the f th channel, where P_f is the launched peak power; Δ is the channel spacing in rads/sec; $T_s = \frac{1}{R_s}$ is the symbol period, where R_s is the symbol rate; and Φ_{fk} is the input phase of the k th pulse in the f th channel.

Substituting Eq. (3.4) into the multispan VSTF model (Eq. (3.2)) yields the output of the fiber $R(\omega)$ as follows

$$\begin{aligned} R(\omega) = & \sqrt{2\pi} \sum_{f=0}^{F-1} \sum_{k=0}^{K-1} a_{fk} A_f \tilde{T}_f \exp \left[-i(\omega - f\Delta)kT_s - \frac{(\omega - f\Delta)^2 \tilde{T}_f^2}{2} + i\Phi_{fk} \right] \\ & + \frac{iN\gamma}{\sqrt{2\pi}} \sum_{u=0}^{F-1} \sum_{v=0}^{F-1} \sum_{w=0}^{F-1} \sum_{l=0}^{K-1} \sum_{m=0}^{K-1} \sum_{n=0}^{K-1} a_{ul} a_{vm} a_{wn} A_u A_v A_w \tilde{T}_u \tilde{T}_v \tilde{T}_w \exp [i(\Phi_{ul} - \Phi_{vm} + \Phi_{wn})] \\ & \times \exp [i\Delta T_s (ul - vm + wn) - i\omega(l - m + n)T_s] \\ & \times \exp \left[-\frac{(\omega - u\Delta)^2 \tilde{T}_u^2}{2} - \frac{(\omega - v\Delta)^2 \tilde{T}_v^2}{2} - \frac{(\omega - w\Delta)^2 \tilde{T}_w^2}{2} \right] \\ & \times \int_0^L \exp(-\alpha z) \int_{-\infty}^{+\infty} \int_{-\infty}^{+\infty} \exp(-i\omega_1 \omega_2 \beta_2 z) \exp \left(-\frac{\omega_1^2 \tilde{T}_u^2}{2} - \frac{\omega_1^2 \tilde{T}_v^2}{2} - \frac{\omega_2^2 \tilde{T}_v^2}{2} - \frac{\omega_2^2 \tilde{T}_w^2}{2} \right) \\ & \times \exp[-\omega\omega_1(\tilde{T}_u^2 + \tilde{T}_v^2) - \omega\omega_2(\tilde{T}_v^2 + \tilde{T}_w^2) - \omega_1\omega_2\tilde{T}_v^2] \\ & \times \exp(\omega_1 u \Delta \tilde{T}_u^2 + \omega_1 v \Delta \tilde{T}_v^2 + \omega_2 v \Delta \tilde{T}_v^2 + \omega_2 w \Delta \tilde{T}_w^2) \\ & \times \exp[-i\omega_1(l - m)T_s - i\omega_2(n - m)T_s] d\omega_1 d\omega_2 dz. \end{aligned} \quad (3.5)$$

In this dissertation, the WDM demultiplexer is modeled as a bank of optical Gaussian filters that can either be matched to the input signal or to the channel spacing, where the

frequency response of the f th demultiplexing filter is given by

$$H_f(\omega) = A_{df}(2\pi T_{df}^2)^{\frac{1}{2}} \exp \left[-\frac{(\omega - f\Delta)^2 T_{df}^2}{2} \right]. \quad (3.6)$$

A_{df} is the peak amplitude of the f th filter impulse response, and T_{df} is the half-width of the impulse response of the f th filter at the $1/e$ intensity point. If the filter is matched to the input pulse shape, then $T_{df} = T_0^*$ and $A_{df} = \frac{(1+C_f^2)^{\frac{1}{4}}}{(2\pi T_0^{*2})^{\frac{1}{2}}}$; if the filter is matched to the channel spacing, $T_{df} = 2\pi/\Delta$ and $A_{df} = \frac{\Delta}{(2\pi)^{\frac{3}{2}}}$.

To extend the model to include the WDM multiplexer, $R(\omega)$ is multiplied with $H_f(\omega)$ (i.e., convolve $r(t)$ with $h_f(t)$ in the time domain) to yield the output of the WDM demultiplexer $R_f(\omega)$. Computing $R_f(\omega)$ requires a triple integral. By simplifying the triple integral to a simple integral, as shown in the Appendix, the output field of the WDM demultiplexer in the frequency domain is obtained as

$$\begin{aligned} R_f(\omega) = & 2\pi \sum_{\hat{f}=0}^{F-1} \sum_{\hat{k}=0}^{K-1} a_{\hat{f}\hat{k}} A_{\hat{f}} A_{df} \tilde{T}_{\hat{f}} T_{df} \exp \left[-\frac{(\omega - \hat{f}\Delta)^2 \tilde{T}_{\hat{f}}^2}{2} - \frac{(\omega - f\Delta)^2 T_{df}^2}{2} \right] \\ & \times \exp \left[-i(\omega - \hat{f}\Delta) \hat{k} T_s + i\Phi_{\hat{f}\hat{k}} \right] \\ & + i2\pi N \gamma \sum_{u=0}^{F-1} \sum_{v=0}^{F-1} \sum_{w=0}^{F-1} \sum_{l=0}^{K-1} \sum_{m=0}^{K-1} \sum_{n=0}^{K-1} a_{ul} a_{vm} a_{wn} A_u A_v A_w A_{df} \tilde{T}_u \tilde{T}_v \tilde{T}_w T_{df} \\ & \times \exp[i(\Phi_{ul} - \Phi_{vm} + \Phi_{wn})] \exp \left[-\frac{(\omega - f\Delta)^2 T_{df}^2}{2} \right] E_{u,v,w,l,m,n}(\omega) \\ & \times \int_0^L \exp(-\alpha z) I_{u,v,w,l,m,n}(\omega, z) dz, \end{aligned} \quad (3.7)$$

where

$$\begin{aligned} E_{u,v,w,l,m,n}(\omega) = & \exp [i\Delta T_s (ul - vm + wn) - i\omega(l - m + n)T_s] \\ & \times \exp \left[-\frac{(\omega - u\Delta)^2 \tilde{T}_u^2}{2} - \frac{(\omega - v\Delta)^2 \tilde{T}_v^2}{2} - \frac{(\omega - w\Delta)^2 \tilde{T}_w^2}{2} \right], \end{aligned} \quad (3.8)$$

and

$$I_{u,v,w,l,m,n}(\omega, z) = \frac{\exp(A + B + C)}{\sqrt{(\tilde{T}_u^2 + \tilde{T}_v^2)(\tilde{T}_v^2 + \tilde{T}_w^2) - (\tilde{T}_v^2 + i\beta_2 z)^2}}. \quad (3.9)$$

The simplifying functions A, B, and C are defined in the Appendix.

Taking the inverse Fourier transform of (3.7) yields the output field of the WDM demultiplexer in the time domain $r_f(t)$ as

$$\begin{aligned} r_f(t) = & \sqrt{2\pi} \sum_{\hat{f}=0}^{F-1} \sum_{\hat{k}=0}^{K-1} a_{\hat{f}\hat{k}} A_{\hat{f}} A_{df} \exp(i\Phi_{\hat{f}\hat{k}}) \frac{1}{\sqrt{\frac{1}{\tilde{T}_{\hat{f}}^2} + \frac{1}{T_{df}^2}}} \\ & \times \exp \left\{ \frac{\left[\frac{\hat{k}T_s}{\tilde{T}_{\hat{f}}^2} + \frac{t}{T_{df}^2} + i(\hat{f} - f)\Delta \right]^2}{2 \left(\frac{1}{\tilde{T}_{\hat{f}}^2} + \frac{1}{T_{df}^2} \right)} - \frac{\hat{k}^2 T_s^2}{2\tilde{T}_{\hat{f}}^2} - \frac{t^2}{2T_{df}^2} + if\Delta t \right\} \\ & + iN\gamma \sqrt{2\pi} \sum_{u=0}^{F-1} \sum_{v=0}^{F-1} \sum_{w=0}^{F-1} \sum_{l=0}^{K-1} \sum_{m=0}^{K-1} \sum_{n=0}^{K-1} a_{ul} a_{vm} a_{wn} A_u A_v A_w A_{df} \tilde{T}_u \tilde{T}_v \tilde{T}_w \\ & \times \exp[i(\Phi_{ul} - \Phi_{vm} + \Phi_{wn})] E_{u,v,w,l,m,n}(t) \int_0^L \exp(-\alpha z) J_{u,v,w,l,m,n}(t, z) dz. \quad (3.10) \end{aligned}$$

where

$$\begin{aligned} E_{u,v,w,l,m,n}(t) = & \exp \left[i\Delta T_s (ul - vm + wn) - \frac{(u\Delta)^2 \tilde{T}_u^2}{2} - \frac{(v\Delta)^2 \tilde{T}_v^2}{2} - \frac{(w\Delta)^2 \tilde{T}_w^2}{2} \right] \\ & \times \exp \left[-\frac{t^2}{2T_{df}^2} + if\Delta t \right], \quad (3.11) \end{aligned}$$

$$\begin{aligned} J_{u,v,w,l,m,n}(t, z) = & \frac{\exp \left\{ \frac{\left[\frac{(l-m+n)T_s + i(u\Delta \tilde{T}_u^2 + v\Delta \tilde{T}_v^2 + w\Delta \tilde{T}_w^2 + A_1 + B_1)}{\tilde{T}_u^2 + \tilde{T}_v^2 + \tilde{T}_w^2 + 2A_2} + \frac{t}{T_{df}^2} - if\Delta \right]^2}{\frac{2}{\tilde{T}_u^2 + \tilde{T}_v^2 + \tilde{T}_w^2 + 2A_2} + \frac{2}{T_{df}^2}} + A_0 + B_0 + C \right\}}{\sqrt{\left[(\tilde{T}_u^2 + \tilde{T}_v^2)(\tilde{T}_v^2 + \tilde{T}_w^2) - (\tilde{T}_v^2 + i\beta_2 z)^2 \right] \left[1 + \frac{1}{T_{df}^2} (\tilde{T}_u^2 + \tilde{T}_v^2 + \tilde{T}_w^2 + 2A_2) \right]}} \\ & \times \exp \left\{ \frac{\left[u\Delta \tilde{T}_u^2 + v\Delta \tilde{T}_v^2 + w\Delta \tilde{T}_w^2 + A_1 + B_1 - i(l-m+n)T_s \right]^2}{2(\tilde{T}_u^2 + \tilde{T}_v^2 + \tilde{T}_w^2 + 2A_2)} \right\}. \quad (3.12) \end{aligned}$$

The simplifying functions A_0 , A_1 , A_2 , B_0 , B_1 , and C are defined in the Appendix.

For these expressions to hold, the system must use chirped Gaussian pulses at the transmitter and Gaussian optical filters at the receiver. With these assumptions, the methodology can apply to any WDM system, including advanced demodulation schemes such as those using heterodyne detection.

Although these expressions are obtained under the assumption of chirped Gaussian pulses at the transmitter and the results will change when non-Gaussian pulse shapes are used, they can serve as a powerful analytical tool to get an insight into the relative comparison of the intensities among all physical impairments for non-Gaussian pulse shapes for which it is difficult to obtain simple integrals similar to Eqs. (3.7) and (3.10). The assumption of Gaussian optical filters at the receiver can be easily relaxed. For any form of optical filters $H_f(\omega)$, the output of the fiber $R(\omega)$ (in the frequency domain) can be multiplied by $H_f(\omega)$ before the square-law operation of the photodetector. In this way, the expressions of the output of the WDM demultiplexer specific to the given optical filters can be obtained using a simple integral similar to Eq. (3.7) plus an integral needed to return to the time domain.

To convert the received signal $r_f(t)$ back into electrical form and recover the data transmitted through the system, $r_f(t)$ is passed through a photodetector and sampled at discrete times $t_k = kT_s$, $k = 0, \dots, K-1$. The photodetector output function varies for different modulation schemes: for OOK, the sampled output is simply $y_f(t_k) = |r_f(t_k)|^2$, $f = 0, \dots, F-1$; for DBPSK, if a balanced photodetector is used, $y_f(t_k) = \left| \frac{r_f(t_k) + r_f(t_{k-1})}{2} \right|^2 - \left| \frac{r_f(t_k) - r_f(t_{k-1})}{2} \right|^2$; for DQPSK, if a balanced photodetector is used, the in-phase output $y_f(t_k)|_I$ is the same as the output of DBPSK and the quadrature output is $y_f(t_k)|_Q = \left| \frac{r_f(t_k) \exp(i\frac{\pi}{2}) + r_f(t_{k-1})}{2} \right|^2 - \left| \frac{r_f(t_k) \exp(i\frac{\pi}{2}) - r_f(t_{k-1})}{2} \right|^2$ ¹.

To characterize each individual physical impairment, we define the impairment characteristic coefficients, including $\rho_{f,k}^{Sig}$, $\rho_{f,k}^{ISI}$, $\rho_{f,k}^{ICI}$, $\rho_{f,k}^{SPM}$, $\rho_{f,k}^{IXPM}$, $\rho_{f,k}^{IFWM}$, $\rho_{f,k}^{XPM}$, and $\rho_{f,k}^{FWM}$, used in

¹Without loss of generality, the responsivity of the photodetector is taken to be unity.

the DEMUX output, as follows

$$\rho_{f,k}^{Sig} = \rho_{\hat{f},\hat{k}}^L \mid_{(\hat{f}=f) \cap (\hat{k}=k)} . \quad (3.13)$$

$$\rho_{f,k}^{ISI} = \rho_{\hat{f},\hat{k}}^L \mid_{(\hat{f}=f) \cap (\hat{k} \neq k)} . \quad (3.14)$$

$$\rho_{f,k}^{ICI} = \rho_{\hat{f},\hat{k}}^L \mid_{\hat{f} \neq f} . \quad (3.15)$$

$$\rho_{f,k}^{SPM} = \rho_{f,k}^{NL} \mid_{(u=v=w=f) \cap (l=m=n=k)} . \quad (3.16)$$

$$\rho_{f,k}^{IXPM} = \rho_{f,k}^{NL} \mid_{(u=v=w=f) \cap (l-m+n=k) \cap ((l=m \neq n) \cup (l \neq m = n))} . \quad (3.17)$$

$$\rho_{f,k}^{IFWM} = \rho_{f,k}^{NL} \mid_{(u=v=w=f) \cap (l-m+n=k) \cap ((l \neq m \neq n) \cup (l = n \neq m))} . \quad (3.18)$$

$$\rho_{f,k}^{XPM} = \rho_{f,k}^{NL} \mid_{(l=m=n=k) \cap (u-v+w=f) \cap ((u=v \neq w) \cup (u \neq v = w))} . \quad (3.19)$$

$$\rho_{f,k}^{FWM} = \rho_{f,k}^{NL} \mid_{(l=m=n=k) \cap (u-v+w=f) \cap ((u \neq v \neq w) \cup (u = w \neq v))} . \quad (3.20)$$

where

$$\begin{aligned} \rho_{\hat{f},\hat{k}}^L = & \sqrt{\frac{2\pi}{\frac{1}{\tilde{T}_f^2} + \frac{1}{T_{df}^2}}} \exp \left\{ \frac{\left[\frac{\hat{k}T_s}{\tilde{T}_f} + \frac{kT_s}{T_{df}} + i(\hat{f} - f)\Delta \right]^2}{2 \left(\frac{1}{\tilde{T}_f^2} + \frac{1}{T_{df}^2} \right)} \right\} \\ & \times \exp \left(-\frac{\hat{k}^2 T_s^2}{2\tilde{T}_f^2} - \frac{k^2 T_s^2}{2T_{df}^2} + if\Delta kT_s \right), \end{aligned} \quad (3.21)$$

and

$$\rho_{f,k}^{NL} = i\gamma\sqrt{2\pi} E_{u,v,w,l,m,n}(kT_s) \int_0^L \exp(-\alpha z) J_{u,v,w,l,m,n}(kT_s, z) dz. \quad (3.22)$$

The demultiplexer output $r_f(t_k)$ from Eq. (3.10), required for all three modulation formats, is rewritten in Eq. (3.23) in terms of impairment coefficients. This forms a part of our 2D discrete-time model of physical impairments in long-haul DWDM systems.

$$\begin{aligned}
r_f(t_k) = & a_{fk}A_fA_{df} \exp(i\Phi_{fk})\rho_{f,k}^{Sig} + \sum_{\hat{k}=0; \hat{k} \neq k}^{K-1} a_{f\hat{k}}A_fA_{df} \exp(i\Phi_{f\hat{k}})\rho_{f,k}^{ISI} \\
& + \sum_{\hat{f}=0; \hat{f} \neq f}^{F-1} \sum_{\hat{k}=0}^{K-1} a_{f\hat{k}}A_{\hat{f}}A_{d\hat{f}} \exp(i\Phi_{f\hat{k}})\rho_{f,k}^{ICI} + a_{fk}^3A_f^3A_{df}\tilde{T}_f^3 \exp(i\Phi_{ul})\rho_{f,k}^{SPM} \\
& + \sum_{l=0}^{K-1} \sum_{m=0}^{K-1} \sum_{n=0}^{K-1} a_{fl}a_{fm}a_{fn}A_f^3A_{df}\tilde{T}_f^3 \exp[i(\Phi_{fl} - \Phi_{fm} + \Phi_{fn})] (\rho_{f,k}^{IXPM} + \rho_{f,k}^{IFWM}) \\
& + \sum_{u=0}^{F-1} \sum_{v=0}^{F-1} \sum_{w=0}^{F-1} a_{uk}a_{vk}a_{wk}A_uA_vA_wA_{df}\tilde{T}_u\tilde{T}_v\tilde{T}_w \exp[i(\Phi_{uk} - \Phi_{vk} + \Phi_{wk})] (\rho_{f,k}^{XPM} + \rho_{f,k}^{FWM}).
\end{aligned} \tag{3.23}$$

where the impairment coefficients, $\rho_{f,k}^{Sig}$, $\rho_{f,k}^{ISI}$, $\rho_{f,k}^{ICI}$, $\rho_{f,k}^{IXPM}$, $\rho_{f,k}^{IFWM}$, $\rho_{f,k}^{XPM}$, and $\rho_{f,k}^{FWM}$, are defined in the Appendix.

The sampled photodetector outputs for OOK, DBPSK and DQPSK are summarized in Tables 3.1, 3.2 and 3.3. The definitions of the simplifying functions, including $r^{Sig}(f, k)$, $r^{ISI}(f, k)$, $r^{ICI}(f, k)$, and $r^{NL}(f, k)$, used in the photodetector output for OOK modulation, are defined as follows

$$r^{Sig}(f, k) = a_{fk}A_fA_{df} \exp(i\Phi_{fk})\rho_{f,k}^{Sig}. \tag{3.24}$$

$$r^{ISI}(f, k) = \sum_{\hat{k}=0; \hat{k} \neq k}^{K-1} a_{f\hat{k}}A_fA_{df} \exp(i\Phi_{f\hat{k}})\rho_{f,k}^{ISI}. \tag{3.25}$$

$$r^{ICI}(f, k) = \sum_{\hat{f}=0; \hat{f} \neq f}^{F-1} \sum_{\hat{k}=0}^{K-1} a_{f\hat{k}}A_{\hat{f}}A_{d\hat{f}} \exp(i\Phi_{f\hat{k}})\rho_{f,k}^{ICI}. \tag{3.26}$$

$$r^{NL}(f, k) = \sum_{u,v,w=0}^{F-1} \sum_{l,m,n=0}^{K-1} a_{ul}a_{vm}a_{wn}A_uA_vA_wA_{df} \tag{3.27}$$

$$\times \tilde{T}_u\tilde{T}_v\tilde{T}_w \exp[i(\Phi_{ul} - \Phi_{vm} + \Phi_{wn})]\rho_{f,k}^{NLsum}. \tag{3.28}$$

where

$$\rho_{f,k}^{NLsum} = I^{SPM} \rho_{f,k}^{SPM} + I^{IXPM} \rho_{f,k}^{IXPM} + I^{IFWM} \rho_{f,k}^{IFWM} + I^{XPM} \rho_{f,k}^{XPM} + I^{FWM} \rho_{f,k}^{FWM}. \quad (3.29)$$

The indicator functions I^{SPM} , I^{IXPM} , I^{IFWM} , I^{XPM} , and I^{FWM} are defined as

$$I^{SPM} = \begin{cases} 1, & \text{if } u, v, w, l, m, n \text{ satisfy } (u = v = w = f) \text{ and } (l = m = n = k); \\ 0, & \text{otherwise.} \end{cases}$$

$$I^{IXPM} = \begin{cases} 1, & \text{if } l, m, n \text{ satisfy } (u = v = w = f) \text{ and } (l - m + n = k) \text{ and } (l = m \neq n \mid l \neq m = n); \\ 0, & \text{otherwise.} \end{cases}$$

$$I^{IFWM} = \begin{cases} 1, & \text{if } l, m, n \text{ satisfy } (u = v = w = f) \text{ and } (l - m + n = k) \text{ and } (l \neq m \neq n \mid l = n \neq m); \\ 0, & \text{otherwise.} \end{cases}$$

$$I^{XPM} = \begin{cases} 1, & \text{if } u, v, w \text{ satisfy } (l = m = n = k) \text{ and } (u - v + w = f) \text{ and } (u = v \neq w \mid u \neq v = w); \\ 0, & \text{otherwise.} \end{cases}$$

$$I^{FWM} = \begin{cases} 1, & \text{if } u, v, w \text{ satisfy } (l = m = n = k) \text{ and } (u - v + w = f) \text{ and } (u \neq v \neq w \mid u = w \neq v); \\ 0, & \text{otherwise.} \end{cases}$$

The Appendix contains the definitions of the simplifying functions used in Tables 3.2 and 3.3, including $r^{Sig\pm}(f, k)$, $r^{ISI\pm}(f, k)$, $r^{ICI\pm}(f, k)$, $r^{NL\pm}(f, k)$, $r_Q^{Sig\pm}(f, k)$, $r_Q^{ISI\pm}(f, k)$, $r_Q^{ICI\pm}(f, k)$, and $r_Q^{NL\pm}(f, k)$. One common aspect of these three modulation formats is that the sampled photodetector output consists of seven terms: the contribution of the original transmitted bit, followed by ISI, ICI, the interaction between the targeted bit and the ISI, the interaction between the targeted bit and the ICI, the interaction between the ISI and the ICI, and, lastly, the nonlinear effects. The latter can be further separated into five different effects: SPM, IXPM, IFWM, XPM, and FWM.

Table 3.1: The Photodetector Output for OOK

Type	$OOK : y_f^{OOK}(t_k) \approx$
<i>Signal</i>	$ r^{Sig}(f, k) ^2$
<i>ISI</i>	$+ r^{ISI}(f, k) ^2$
<i>ICI</i>	$+ r^{ICI}(f, k) ^2$
<i>Signal</i> \times <i>ISI</i>	$+2Re \{r^{Sig}(f, k)[r^{ISI}(f, k)]^*\}$
<i>Signal</i> \times <i>ICI</i>	$+2Re \{r^{Sig}(f, k)[r^{ICI}(f, k)]^*\}$
<i>ISI</i> \times <i>ICI</i>	$+2Re \{r^{ISI}(f, k)[r^{ICI}(f, k)]^*\}$
<i>Nonlinear</i>	$+2NRe \{r^{Sig}(f, k)[r^{NL}(f, k)]^*\} + N^2 r^{NL}(f, k) ^2$

Table 3.2: The Photodetector Output for DBPSK

Type	$DBPSK : y_f^{DBPSK}(t_k) \approx$
<i>Signal</i>	$\frac{1}{4} (r^{Sig+}(f, k) ^2 - r^{Sig-}(f, k) ^2)$
<i>ISI</i>	$+\frac{1}{4} (r^{ISI+}(f, k) ^2 - r^{ISI-}(f, k) ^2)$
<i>ICI</i>	$+\frac{1}{4} (r^{ICI+}(f, k) ^2 - r^{ICI-}(f, k) ^2)$
<i>Signal</i> \times <i>ISI</i>	$+\frac{1}{2}Re \{r^{Sig+}(f, k)[r^{ISI+}(f, k)]^*\} - \frac{1}{2}Re \{r^{Sig-}(f, k)[r^{ISI-}(f, k)]^*\}$
<i>Signal</i> \times <i>ICI</i>	$+\frac{1}{2}Re \{r^{Sig+}(f, k)[r^{ICI+}(f, k)]^*\} - \frac{1}{2}Re \{r^{Sig-}(f, k)[r^{ICI-}(f, k)]^*\}$
<i>ISI</i> \times <i>ICI</i>	$+\frac{1}{2}Re \{r^{ISI+}(f, k)[r^{ICI+}(f, k)]^*\} - \frac{1}{2}Re \{r^{ISI-}(f, k)[r^{ICI-}(f, k)]^*\}$
<i>Nonlinear</i>	$+\frac{1}{2}NRe \{r^{Sig+}(f, k)[r^{NL+}(f, k)]^*\} - \frac{1}{2}NRe \{r^{Sig-}(f, k)[r^{NL-}(f, k)]^*\}$

In this way, we establish a mapping from the input $\{a_{fk}\}$ to the sampled photodetector output $\{y_f(t_k)\}$ via the impairment characteristic coefficients: ρ_{ISI} , ρ_{ICI} , ρ_{SPM} , ρ_{IXPM} , ρ_{IFWM} , ρ_{XPM} , and ρ_{FWM} defined in the Appendix. For a certain modulation format and a set of system parameters (F, Δ, T_s, L) , these coefficients are uniquely determined by fiber parameters $(\alpha, \beta_2, \gamma)$, and pulse parameters $(K, T_{0f}, C_f, \Phi_{fk})$ and can be precomputed. With these impairment characteristic coefficients, given an input matrix $[a_{fk}]_{F \times K}$, we only need

Table 3.3: The Photodetector Output for Quadrature Channel of DQPSK

Type	$Q - channel : y_f^Q(t_k) \approx$
<i>Signal</i>	$\frac{1}{4} \left(r_Q^{Sig+}(f, k) ^2 - r_Q^{Sig-}(f, k) ^2 \right)$
<i>ISI</i>	$+\frac{1}{4} \left(r_Q^{ISI+}(f, k) ^2 - r_Q^{ISI-}(f, k) ^2 \right)$
<i>ICI</i>	$+\frac{1}{4} \left(r_Q^{ICI+}(f, k) ^2 - r_Q^{ICI-}(f, k) ^2 \right)$
<i>Signal</i> \times <i>ISI</i>	$+\frac{1}{2} Re \left\{ r_Q^{Sig+}(f, k) [r_Q^{ISI+}(f, k)]^* \right\} - \frac{1}{2} Re \left\{ r_Q^{Sig-}(f, k) [r_Q^{ISI-}(f, k)]^* \right\}$
<i>Signal</i> \times <i>ICI</i>	$+\frac{1}{2} Re \left\{ r_Q^{Sig+}(f, k) [r_Q^{ICI+}(f, k)]^* \right\} - \frac{1}{2} Re \left\{ r_Q^{Sig-}(f, k) [r_Q^{ICI-}(f, k)]^* \right\}$
<i>ISI</i> \times <i>ICI</i>	$+\frac{1}{2} Re \left\{ r_Q^{ISI+}(f, k) [r_Q^{ICI+}(f, k)]^* \right\} - \frac{1}{2} Re \left\{ r_Q^{ISI-}(f, k) [r_Q^{ICI-}(f, k)]^* \right\}$
<i>Nonlinear</i>	$+\frac{1}{2} N Re \left\{ r_Q^{Sig+}(f, k) [r_Q^{NL+}(f, k)]^* \right\} - \frac{1}{2} N Re \left\{ r_Q^{Sig-}(f, k) [r_Q^{NL-}(f, k)]^* \right\}$

to know the launched power in channel f , P_f , and the number of spans, N , to calculate the corresponding sampled photodetector output, without the need for time-consuming SSF simulation.

The above model can be easily extended to a coherent receiver. For a balanced coherent BPSK receiver, if a local oscillator (LO) is given by $E_{LO} = A_{LO} \exp[-i(\omega_{LO}t + \phi_{LO})]$, where A_{LO} , ω_{LO} , and ϕ_{LO} represent the amplitude, frequency, and phase of the local oscillator, respectively, the photodetector output $y_f(t_k) = \left| \frac{r_f(t_k) + E_{LO}}{2} \right|^2 - \left| \frac{r_f(t_k) - E_{LO}}{2} \right|^2$. Similar expressions as in Table 3.2 can be derived.

The VSTF method can be extended to polarization-division multiplexing (PDM) systems in which the frequency-domain output of the fiber for each polarization is expressed as the sum of one linear term and two triple integrals. These four triple integrals in PDM systems are of the same form as the triple integral in this dissertation. With the technique of simplifying the triple integral to a simple integral in this dissertation, we can easily simplify each triple integral to a simple integral. Analysis of the resulting physical impairments in PDM systems is left for future work.

There are three major contributions unified within our 2D discrete-time model. First, the model features a simple integral that is easy to evaluate, rather than the triple integral, which is difficult to evaluate. Second, the model takes into account multichannel effects, fiber losses, frequency chirp, optical filtering, and photodetection, which are ignored in the current literature. Third, the model is in discrete-time and thus facilitates the application of discrete-time signal processing to improve the system performance of long-haul DWDM systems, such as nonlinear equalization, constrained coding, multiuser coding and path-diversity for all-optical networks.

The 2D discrete-time model offers obvious advantages over the third-order VSTF method and the SSF method in the following aspects. First, compared with the third-order VSTF method and the SSF method, the model provides significant computational savings, which is discussed further in Section 3.2.2. Second, compared with the SSF method, the model can isolate the importance of any individual physical impairment while the SSF method can report only on the total level of all physical impairments combined, and cannot provide this valuable break-down information. Third, compared with the third-order VSTF method and the SSF method, the model has strong analytical capability. Insight into what impact varying the different parameters has on the sampled photodetector output can be gained from the model analytically. These parameters include fiber parameters $(\alpha, \beta_2, \gamma)$, pulse parameters $(K, A_f, T_{0f}, C_f, \Phi_{fk})$, and system parameters (F, Δ, T_s, L, N) .

3.2 Model Validation

This sections presents validation results of our model compared with SSF simulation and discusses the computational complexity of the model compared with the third-order VSTF model and the SSF method.

3.2.1 Model Accuracy

To validate the accuracy of our model, consider the transmission of 40-Gb/s OOK signals over a 16-span standard single-mode fiber for the following two scenarios: a 5-channel 5-pulse case and a 31-channel 31-pulse case. The parameters used are given in Table 3.4.

Table 3.4: Typical Parameter Values

Symbols	Typical Value	Description
α	0.2 dB/km	attenuation constant, a measure of total power loss during transmission of optical signals inside the fiber
β_2	-20 ps ² /km	group-velocity dispersion (GVD) parameter, a measure of chromatic dispersion
γ	2 W ⁻¹ km ⁻¹	nonlinear parameter
F	5 and 31	number of channels
K	5 and 31	number of pulses
N	1-16	number of spans
L	100 km	span length
C_f	0	chirp parameter on the pulse in the f th channel, which governs the frequency chirp imposed on the pulse
T_{0f}	7.51 ps	half-width of the pulse in the f th channel at the $1/e$ intensity point
a_{fk}	{0,1}	modulating symbol of the f th channel and the k th pulse
P_f	1-10 mW	launched peak power in the f th channel
A_f	$\sqrt{P_f}$	peak amplitude of the Gaussian pulse in the f th channel
Δ	$2\pi \times 50$ GHz	channel spacing in rads/sec
R_s	40 Gsp/s	symbol rate
T_s	$\frac{1}{R_s}$	symbol period
Φ_{fk}	0	phase of the k th pulse in the f th channel

We compare the filtered output fields for the center channel and the center pulse calculated by our model and obtained by the SSF simulation by using the normalized squared deviation (NSD) as a measure of the difference between the output fields. The NSD between the output

fields after N spans, defined as

$$NSD(N) = \frac{\int_{\frac{K}{2}T_s}^{\frac{K+1}{2}T_s} \left| r_{\frac{F+1}{2}}^{(Model)}(t) - r_{\frac{F+1}{2}}^{(SSF)}(t) \right|^2 dt}{\int_{\frac{K}{2}T_s}^{\frac{K+1}{2}T_s} \left| r_{\frac{F+1}{2}}^{(SSF)}(t) \right|^2 dt}, \quad (3.30)$$

is plotted in Fig. 3.2. The pulse width T_{0f} is chosen so that the full-width half-maximum point is $T_s/2$. The initial phases are set to zeros for all the channels and all the pulses. The power levels are the same for all the channels. The output calculated by the model is in excellent agreement with that from the SSF method, even for high launched power levels.

The NSD can be further reduced if the higher-order Volterra kernels are included. However a higher-order VSTF model entails the simplification of a higher-order integral. For example, the simplification of a quintuple integral is required for a fifth-order VSTF model. Although any higher order integral obtained from the VSTF method can be simplified to a simple integral using the derivations similar to that in the Appendix, the simplification is analytically demanding.

3.2.2 Computational Complexity

The SSF method is a recursive method and its computational complexity for K symbols and F channels is $O(\frac{NL}{h}FKM \log_2 FKM)$, where h is the step size in z , and M is the number of samples per symbol.

The third-order VSTF method is a nonrecursive method in which the computation is a one-shot process involving in general a triple integral. The numerical evaluation of the double integral with respect to ω_1 and ω_2 using a trapezoidal rule dominates the computation with complexity of order of W^2 , where W is the number of frequency steps needed; the evaluation of the simple integral with respect to z is proportional to $\frac{L}{h_t}$, where h_t is the step size used in the trapezoidal rule. Therefore the computational complexity of the third-order VSTF method for a WDM system is $O(\frac{L}{h_t}FK\tilde{F}^2\tilde{K}^2W^2)$, where $\tilde{F} \times \tilde{K}$ is the number of other symbols interacting with any given symbol, i.e., the number of terms needed in the triple

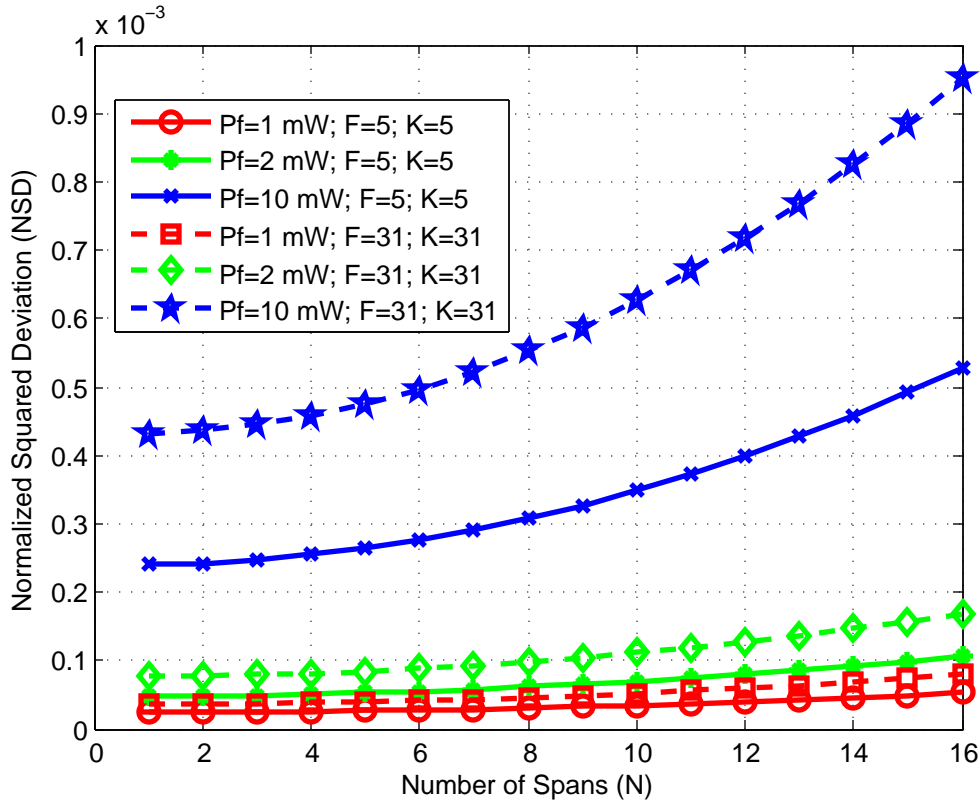


Figure 3.2: Normalized squared deviation of the output fields obtained by our proposed model and the SSF simulation

summations in Eq. (3.23). The values of \tilde{F} and \tilde{K} needed so that all significant physical impairments are included have been determined in [87]: at $R_s = 40$ Gs/s, for IXPM, $\tilde{K} \approx 19$; for IFWM, $\tilde{K} \approx 65$; at $\Delta = 2\pi \times 50$ GHz, for XPM, $\tilde{F} \approx 3$; for FWM, $\tilde{F} \approx 4$. The complexity becomes $O(\frac{L}{h_t} F K W^2)$ since \tilde{F} and \tilde{K} are constants independent of F and K .

In this dissertation, the double integral with respect to ω_1 and ω_2 given by Eq. (A.2) in the Appendix has been solved and its closed-form solution, Eq. (3.9), is a simple fraction easily evaluated. In this way, the need to evaluate numerically the double integral is eliminated and the triple integral is simplified to a simple integral with respect to z . The computational complexity is only $O(\frac{L}{h_t} F K)$.

For a multichannel multipulse multispan system, our model is computationally more efficient than both the VSTF method and the SSF method.

3.3 Summary

This chapter presents the development and validation of a 2D discrete-time model of physical impairments in long-haul DWDM systems. The model development is based on the third-order VSTF model. The model features a simple integral that is easy to evaluate and takes into account multichannel effects, fiber losses, frequency chirp, optical filtering, and photodetection, which are ignored in the current literature. The model has the potential to serve as the foundation of discrete-time signal processing for long-haul DWDM systems. Compared with the third-order VSTF method and the SSF method, the model offers significant computational savings and strong impairment separation capability and analytical capability. Chapter 4 and Chapter 5 present the applications of the model in system analysis and system performance improvement, respectively.

Chapter 4

Model Applications in System Analysis

This chapter presents two applications of the 2D discrete-time model in system analysis. These applications cannot be developed without the model. In Section 4.1, the model is applied to analyze the effect of varying system parameters and pulse shape on individual physical impairments in long-haul DWDM systems. In Section 4.2, the model is applied to determine the range of influence of each individual physical impairment. Section 4.3 concludes this chapter with a summary.

4.1 Effect of System Parameters and Pulse Shape

In this section the 2D discrete-time model is applied to analyze the average impact of varying certain system parameters on the individual physical impairments in a long-haul DWDM system. The two most important system parameters for long-haul DWDM systems are the symbol rate and the channel spacing. For a DWDM system with F channels and K pulses, there are $2^{(FK)}$ possible input matrices. We calculate the impairment characteristic coefficients using the definitions in the Appendix, and substitute these coefficients into the 2D discrete-time model in Tables 3.1 and 3.2 to obtain the various individual physical

impairments for each input matrices. Then we take the average over the input matrix for each individual impairment. In this section, $P_f = 1$ mW. In addition, we analyze the effect of pulse shape on the individual physical impairments.

4.1.1 Effect of Symbol Rate

We choose a 3-channel system with 7 pulses each channel to investigate how the individual physical impairments affecting the symbol located on the center time slot change when the symbol rate changes, by averaging them over the 2^{21} possible input matrices. Figs. 4.1 and 4.2 show the level of the various physical impairments when the system operates at symbol rates of 10 Gb/s and 40 Gb/s for OOK and DBPSK, both for a matched optical filter and a filter set to a channel spacing of 100 GHz. For a 3-channel system, the intrachannel physical impairments, i.e., ISI, signal-ISI beat term, IXPM, and IFWM, vary with the symbol rate. ISI is independent of symbol rate and remains unchanged if using an optical matched filter. At higher symbol rates, a fixed optical filter causes the temporal overlap from neighboring symbols to worsen, thus causing stronger ISI and signal-ISI beat term. The intrachannel nonlinear impairments, i.e., IXPM and IFWM, are generally worsened by the decrease in the symbol period.

4.1.2 Effect of Channel Spacing

Similarly, we choose a 3-pulse WDM system with 7 channels to investigate how the individual physical impairments imposed on the symbol located on the center channel change when the channel spacing changes. Figs. 4.3 and 4.4 show the level of the various physical impairments when the system operates at channel spacings of 100 GHz and 200 GHz for 40 Gb/s OOK and DBPSK, for both optical filter types. For a 3-pulse WDM system, when the channel spacing changes, the interchannel physical impairments change. At larger channel spacings, the impact from neighboring channels weakens for both linear impairments and nonlinear

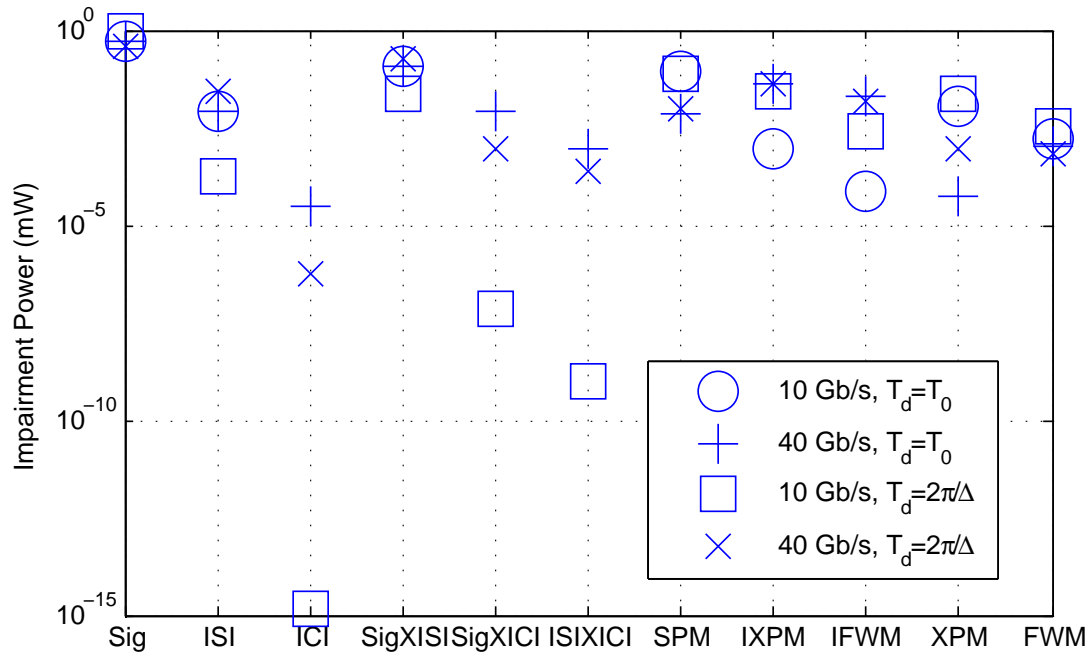


Figure 4.1: Effect of symbol rate on individual physical impairments for OOK ($F=3, K=7$)

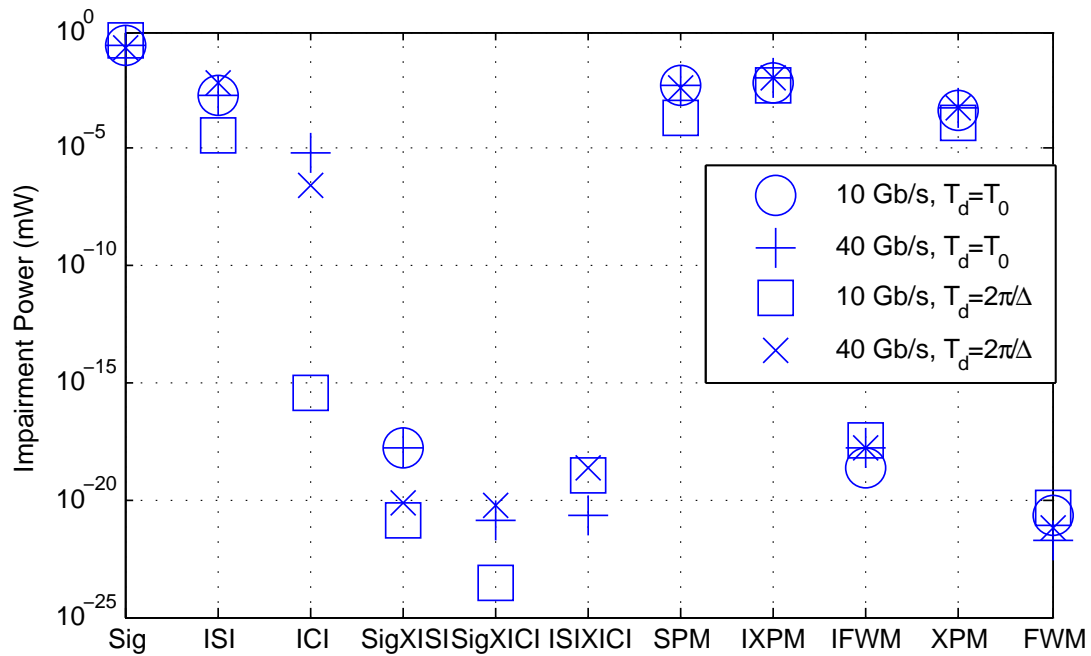


Figure 4.2: Effect of symbol rate on individual physical impairments for DBPSK ($F=3, K=7$)

impairments, i.e., smaller ICI, signal-ICI beat term, XPM and FWM. In general both linear and nonlinear effects are weaker for DBPSK than for OOK.

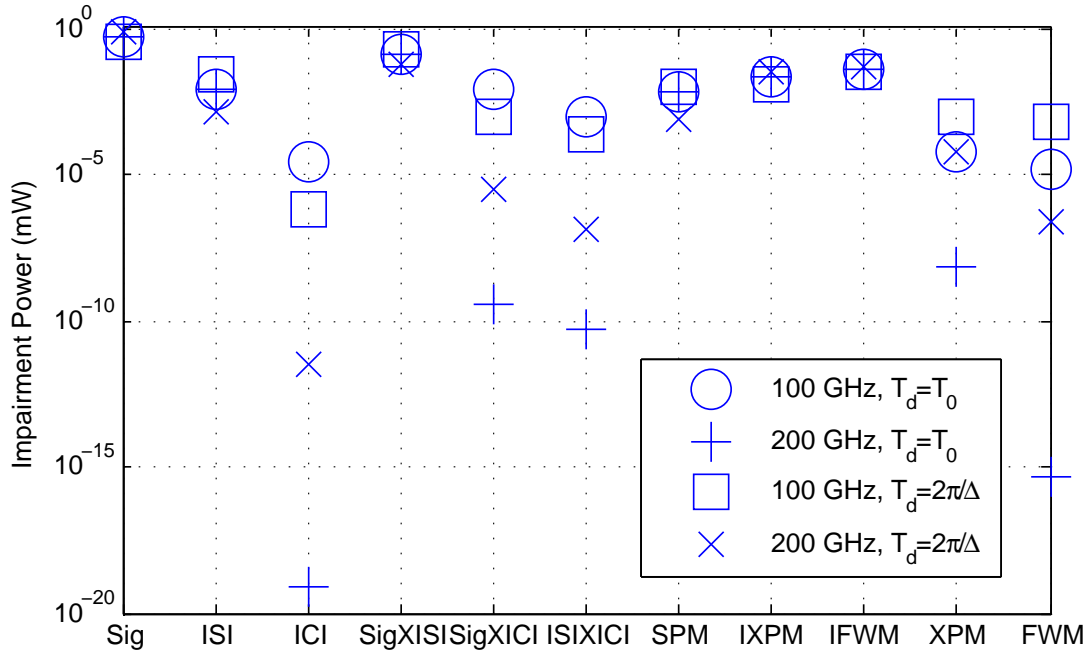


Figure 4.3: Effect of channel spacing on individual physical impairments for OOK ($F=7$, $K=3$)

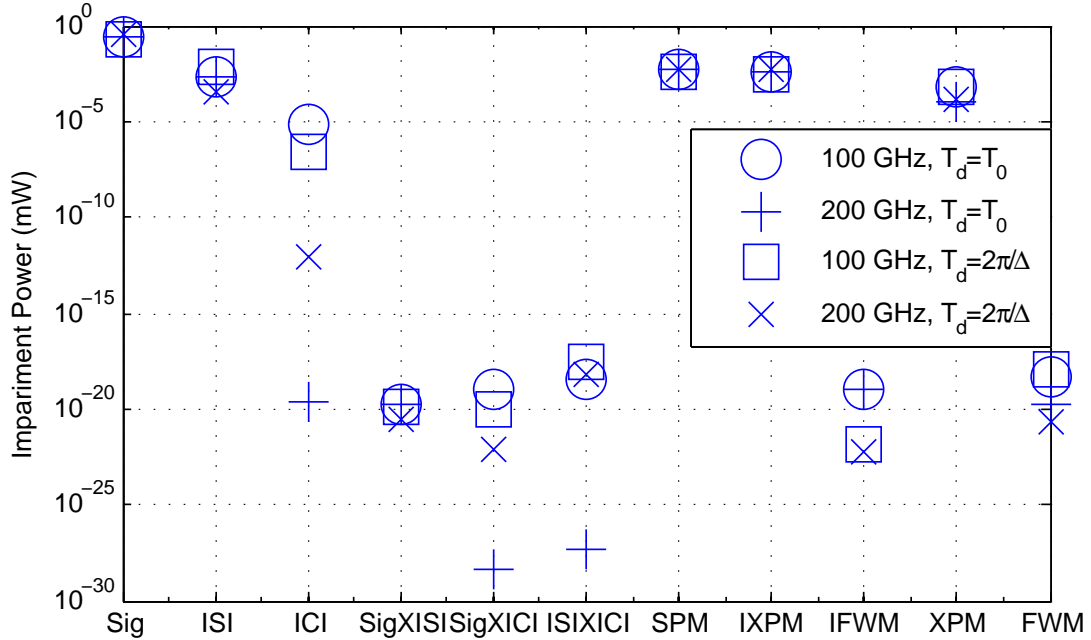


Figure 4.4: Effect of channel spacing on individual physical impairments for DBPSK ($F=7$, $K=3$)

4.1.3 Effect of Pulse Shape

To see the effect that the pulse shape has on individual physical impairments, we compare the individual physical impairments from our analytical model for chirped Gaussian pulses with those from the third-order VSTF method for some non-Gaussian pulse shapes used in fiber-optic communication systems. In this study, non-Gaussian pulse shapes under consideration include the hyperbolic secant pulses and super-Gaussian pulses. The hyperbolic secant pulses are used to model the pulse shape emitted from some mode-locked lasers and optical solitons [2]. Super-Gaussian pulses usually model the effects of steep leading and trailing edges on dispersion-induced pulse broadening [2].

The hyperbolic secant pulses are given as [2]

$$A(0, t) = \operatorname{sech} \left(\frac{t}{T_0} \right) \exp \left(-\frac{iCt^2}{2T_0^2} \right) \quad (4.1)$$

where C is the chirp parameter that controls the initial chirp.

The super-Gaussian pulses are given as [2]

$$A(0, t) = \exp \left[-\frac{1 + iC}{2} \left(\frac{t}{T_0} \right)^{2m} \right] \quad (4.2)$$

where m is the parameter that controls the degree of edge sharpness. For $m=1$, super-Gaussian pulses degenerate to chirped Gaussian pulses. For $m > 1$, super-Gaussian pulses become square shaped with sharper leading and trailing edges.

The evaluation of the third-order VSTF method involves numerical integration of the triple integral, which is computationally intensive. The results for the worst case, i.e., a 7-channel 7-pulse WDM system with input symbols being all ones, are shown in Fig. 4.5. The figure shows that the interchannel effects for all pulse shapes are similar, while the intrachannel effects vary significantly, especially for pulse shapes not resembling a Gaussian pulse.

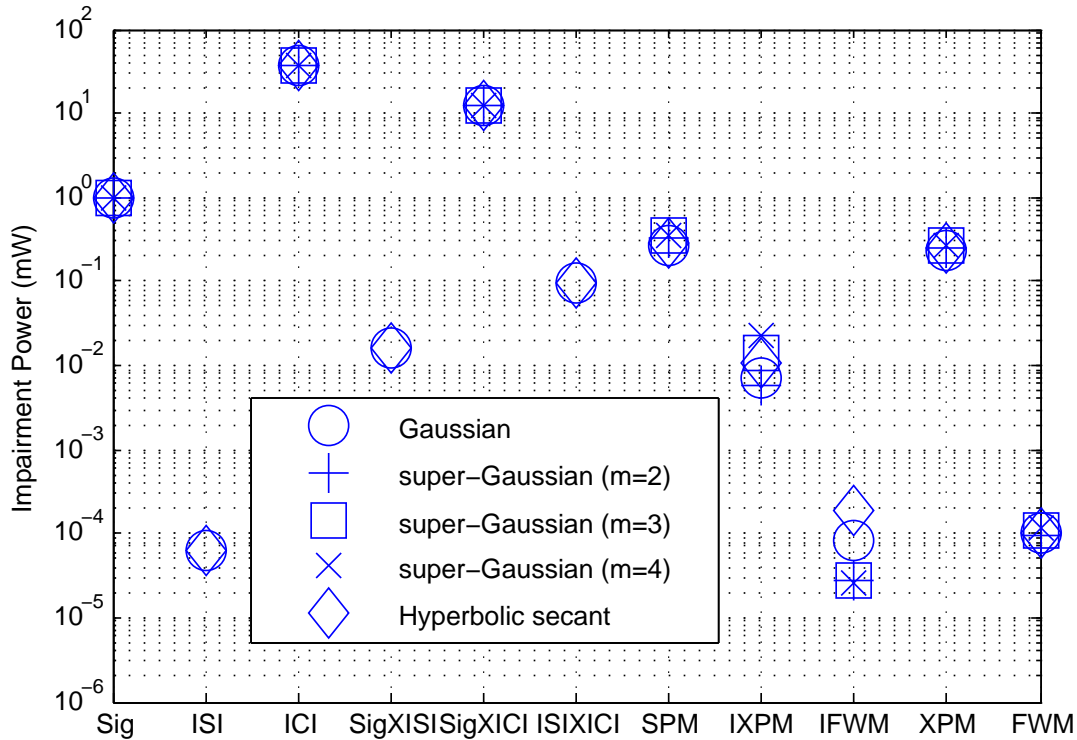


Figure 4.5: Effect of pulse shape on individual physical impairments for OOK ($F=7$, $K=7$, $R_s=10$ Gsps, $\Delta=100$ GHz, m is the edge sharpness parameter of the super-Gaussian pulses [2])

4.2 Range of Influence of Physical Impairments

The physical impairments acting on a symbol in a WDM system are caused by other symbols located in neighboring channels and neighboring time slots. If two symbols are close to each other in time and/or wavelength, there are strong physical impairments imposed on one another. If two symbols are far enough from each other in time and/or wavelength, these impairments all weaken. Therefore, there exists a range of influence (RoI) for physical impairments that must be carefully determined to reduce the complexity of signal processing techniques, such as electrical equalization and constrained coding. This section determines the RoIs for various physical impairments.

To our knowledge, this is the first work to identify the RoI of physical impairments in WDM systems. In addition to point-to-point links, the technique proposed in this dissertation can be used on all-optical networks to predict the crosstalk due to switched lightpaths sharing

a fiber.

To improve the applicability of the RoIs, we seek RoIs independent of modulation formats and type of WDM demultiplexer. These RoIs are determined by assuming only chirped Gaussian pulses at the transmitter, with the assumption of Gaussian optical filters at the receiver removed.

Taking the inverse Fourier transform of Eq. (3.5), i.e., $R(\omega)$, yields the output field of the fiber in the time domain as follows

$$\begin{aligned}
r(t) = & \sum_{f=0}^{F-1} \sum_{k=0}^{K-1} a_{fk} A_f \exp \left[-\frac{(t - kT_s)^2}{2\tilde{T}_f^2} + if\Delta t + i\Phi_{fk} \right] \\
& + iN\gamma \sum_{u=0}^{F-1} \sum_{v=0}^{F-1} \sum_{w=0}^{F-1} \sum_{l=0}^{K-1} \sum_{m=0}^{K-1} \sum_{n=0}^{K-1} a_{ul} a_{vm} a_{wn} A_u A_v A_w \tilde{T}_u \tilde{T}_v \tilde{T}_w \\
& \times \exp[i(\Phi_{ul} - \Phi_{vm} + \Phi_{wn})] E(t) \int_0^L \exp(-\alpha z) J(t, z) dz, \tag{4.3}
\end{aligned}$$

where

$$E(t) = \exp \left[i\Delta T_s (ul - vm + wn) - \frac{(u\Delta)^2 \tilde{T}_u^2}{2} - \frac{(v\Delta)^2 \tilde{T}_v^2}{2} - \frac{(w\Delta)^2 \tilde{T}_w^2}{2} \right], \tag{4.4}$$

and

$$J(t, z) = \frac{\exp \left\{ \frac{\{u\Delta \tilde{T}_u^2 + v\Delta \tilde{T}_v^2 + w\Delta \tilde{T}_w^2 + A_1 + B_1 + i[t - (l - m + n)T]\}^2}{2(\tilde{T}_u^2 + \tilde{T}_v^2 + \tilde{T}_w^2 + 2A_2)} + A_0 + B_0 + C \right\}}{\sqrt{\left[(\tilde{T}_u^2 + \tilde{T}_v^2) (\tilde{T}_v^2 + \tilde{T}_w^2) - (\tilde{T}_v^2 + i\beta_2 z)^2 \right] (\tilde{T}_u^2 + \tilde{T}_v^2 + \tilde{T}_w^2 + 2A_2)}}. \tag{4.5}$$

The definitions of the simplifying functions A_0 , A_1 , A_2 , B_0 , B_1 and C are the same as those in Chapter 3, and are given explicitly in the Appendix.

To quantify the impact of the various impairments on the fiber output, the following impairment characteristic coefficients are introduced, defined somewhat differently than the coefficients presented in Chapter 3, since optical filtering has been omitted:

ISI coefficient:

$$\rho_{k,\hat{k}}^{ISI} = \exp \left[-\frac{(\hat{k} - k)^2 T_s^2}{2\tilde{T}_f^2} \right]. \quad (4.6)$$

SPM, IXPM, and IFWM coefficients:

$$\rho_{f,k,l,m,n}^{\text{intra}} = i\gamma E_{l,m,n}^{\text{intra}} \int_0^L \exp(-\alpha z) J_{l,m,n}^{\text{intra}} dz, \quad \text{intra} \in \{SPM, IXPM, IFWM\} \quad (4.7)$$

where

$$E_{l,m,n}^{\text{intra}} = \exp \left[i\Delta T_s(l - m + n) - \frac{3(f\Delta)^2 \tilde{T}_f^2}{2} \right], \quad (4.8)$$

and

$$J_{l,m,n}^{\text{intra}} = \frac{\exp \left[\frac{(3f\Delta \tilde{T}_f^2 + A_1 + B_1)^2}{2(3\tilde{T}_f^2 + 2A_2)} + A_0 + B_0 + C \right]}{\sqrt{(3\tilde{T}_f^2 + i\beta_2 z) (\tilde{T}_f^2 - i\beta_2 z) (3\tilde{T}_f^2 + 2A_2)}}. \quad (4.9)$$

XPM and FWM coefficients:

$$\rho_{f,k,u,v,w}^{\text{inter}} = i\gamma E_{u,v,w}^{\text{inter}} \int_0^L \exp(-\alpha z) J_{u,v,w}^{\text{inter}} dz, \quad \text{inter} \in \{XPM, FWM\} \quad (4.10)$$

where

$$E_{u,v,w}^{\text{inter}} = \exp \left[i\Delta T_s(u - v + w) - \frac{(u\Delta)^2 \tilde{T}_u^2}{2} - \frac{(v\Delta)^2 \tilde{T}_v^2}{2} - \frac{(w\Delta)^2 \tilde{T}_w^2}{2} \right], \quad (4.11)$$

and

$$J_{u,v,w}^{\text{inter}} = \frac{\exp \left[\frac{(u\Delta\tilde{T}_u^2 + v\Delta\tilde{T}_v^2 + w\Delta\tilde{T}_w^2 + A_1 + B_1)^2}{2(\tilde{T}_u^2 + \tilde{T}_v^2 + \tilde{T}_w^2 + 2A_2)} + A_0 + B_0 + C \right]}{\sqrt{\left[(\tilde{T}_u^2 + \tilde{T}_v^2) (\tilde{T}_v^2 + \tilde{T}_w^2) - (\tilde{T}_v^2 + i\beta_2 z)^2 \right] (\tilde{T}_u^2 + \tilde{T}_v^2 + \tilde{T}_w^2 + 2A_2)}}. \quad (4.12)$$

Note that normally a WDM demultiplexer is required to obtain the output field of the f th channel $r_f(t)$, but it is not necessary for characterizing physical impairments. Without loss of generality, the WDM demultiplexer is not considered in this application for notational simplicity and model generality. With the above coefficients, the output field on the f th channel at discrete times kT_s is given by

$$\begin{aligned} r_f(kT_s) = & a_{fk} A_f e^{(if\Delta kT_s + i\Phi_{fk})} + \sum_{\hat{k}=0; \hat{k} \neq k}^{K-1} a_{f\hat{k}} A_f e^{(if\Delta kT_s + i\Phi_{f\hat{k}})} \rho_{k,\hat{k}}^{ISI} + N a_{fk}^3 A_f^3 \tilde{T}_f^3 e^{(if\Delta kT_s + i\Phi_{fk})} \rho^{SPM} \\ & + N \sum_{l,m,n=0}^{K-1} a_{fl} a_{fm} a_{fn} A_f^3 \tilde{T}_f^3 e^{(if\Delta kT_s)} e^{[i(\Phi_{fl} - \Phi_{fm} + \Phi_{fn})]} [\rho_{f,k,l,m,n}^{IXPM} + \rho_{f,k,l,m,n}^{IFWM}] \\ & + N \sum_{u,v,w=0}^{F-1} a_{uk} a_{vk} a_{wk} A_u A_v A_w \tilde{T}_u \tilde{T}_v \tilde{T}_w e^{(if\Delta kT_s)} e^{[i(\Phi_{uk} - \Phi_{vk} + \Phi_{wk})]} [\rho_{f,k,u,v,w}^{XPM} + \rho_{f,k,u,v,w}^{FWM}] \\ & + \sum_{\hat{f}=0; \hat{f} \neq f}^{F-1} \sum_{\hat{k}=0}^{K-1} a_{f\hat{k}} A_{\hat{f}} e^{(if\Delta kT_s + i\Phi_{f\hat{k}})} e^{-\frac{(\hat{k}-k)^2 T_s^2}{2\tilde{T}_{\hat{f}}^2}} \end{aligned} \quad (4.13)$$

The last term in Eq. (4.13) is due to the overlap of other channels on the channel on interest, f . Once optical filtering is added to the model, the linear adjacent channel interference experienced by the signal could be computed from the last term. Without optical filtering, this interference cannot be isolated, and is therefore removed from the model.

The key to use this discrete-time model is to find the index combinations that meet the requirements for various nonlinear physical impairments, i.e., SPM, IXPM, IFWM, XPM, and FWM, and to calculate the impairment coefficients corresponding to these index combinations.

The index combinations must satisfy the following conditions: for SPM, $u = v = w = f$ and $l = m = n = k$; for IXPM, $l = m \neq n$ or $l \neq m = n$ and $u = v = w = f$; for IFWM, $l \neq m \neq n$ or $l = n \neq m$ and $u = v = w = f$; for XPM, $u = v \neq w$ or $u \neq v = w$ and $l = m = n = k$; for FWM, $u \neq v \neq w$ or $u = w \neq v$ and $l = m = n = k$. In addition, for interchannel effects, i.e., XPM and FWM, the frequency location of the nonlinear interaction satisfies the phase-matching condition: $(u - v + w)\Delta = f\Delta$; for intrachannel effects, i.e., IXPM and IFWM, the time location of the nonlinear interaction satisfies $(l - m + n)T_s = kT_s$.

For example, consider a 3-pulse case ($K = 3$). There are $3^3 = 27$ index triplets $[lmn]$ and 7 possible time locations because $-2 \leq (l - m + n) \leq 4$, e.g., the output field at $t = T_s$ ($k = 1$) is affected by 7 different triplets. The triplet $[111]$ contributes to the SPM impairment. The IXPM impairment is caused by $[001]$, $[221]$, $[100]$, and $[122]$, whereas the triplets for IFWM impairment are $[012]$, and $[210]$. The type and location of the intrachannel nonlinear impairments generated by a pulse triple located at $t = 0$, T_s and $2T_s$ are summarized in Table 4.1. When the following parameters are used: $\alpha = 0.2$ dB/km, $\beta_2 = -20$ ps²/km, $\gamma = 2$ W⁻¹km⁻¹, $L = 100$ km, $T_0 = 7.51$ ps, $T_s = 25$ ps and $C = 0$, the absolute values of the corresponding intrachannel impairment coefficients are summarized in Table 4.2. Due to space limitation, only 5 valid time locations are presented.

Table 4.1: Index Triplets $[lmn]$ for a Triple Pulse Case

Nonlinearity	Time Location $l - m + n$				
	0	1	2	3	4
SPM	000	111	222		
IXPM	011	001	002		
	022	221	112		
	110	100	200		
	220	122	211		
IFWM	121	012	101	102	202
		210		201	
				212	

Table 4.2: Intrachannel Coefficients for a Triple Pulse Case

Nonlinearity	Time Location $l - m + n$				
	0	1	2	3	4
SPM	0.0165	0.0165	0.0165		
IXPM	0.0070	0.0070	0.0036		
	0.0036	0.0070	0.0070		
	0.0070	0.0070	0.0036		
	0.0036	0.0070	0.0070		
IFWM	0.0024	0.0024	0.0024	0.0010	0.0003
		0.0024		0.0010	
				0.0024	

Similarly, consider a 3-channel case ($F = 3$). The type and location of the interchannel nonlinear impairments generated by a channel triple located at $f = 0, 1$, and 2 are summarized in Table 4.3. When $\Delta = 2\pi \times 50$ GHz and other parameters take the same values as above, the absolute values of the corresponding interchannel impairment coefficients are summarized in Table 4.4. Due to space limitation, only 5 valid frequency locations are presented.

Table 4.3: Index Triplets $[uvw]$ for a Triple Channel Case

Nonlinearity	Frequency Location $u - v + w$				
	0	1	2	3	4
XPM	011	001	002		
	022	221	112		
	110	100	200		
	220	122	211		
FWM	121	012	101	102	202
		210		201	
				212	

The definition of the RoI differs for different physical impairments. For ISI, IXPM, and IFWM, the RoI is defined as the number of adjacent symbols causing a significant effect. For XPM and FWM, the RoI is defined as the number of channels causing notable degradation. The concept of RoI is shown schematically in Fig. 4.6.

Table 4.4: Interchannel Coefficients for a Triple Channel Case

Nonlinearity	Frequency Location $u - v + w$				
	0	1	2	3	4
XPM	0.0159	0.0159	0.0144		
	0.0144	0.0159	0.0159		
	0.0159	0.0159	0.0144		
	0.0144	0.0159	0.0159		
FWM	0.0158	0.0150	0.0158	0.0146	0.0139
		0.0150		0.0146	
				0.0158	

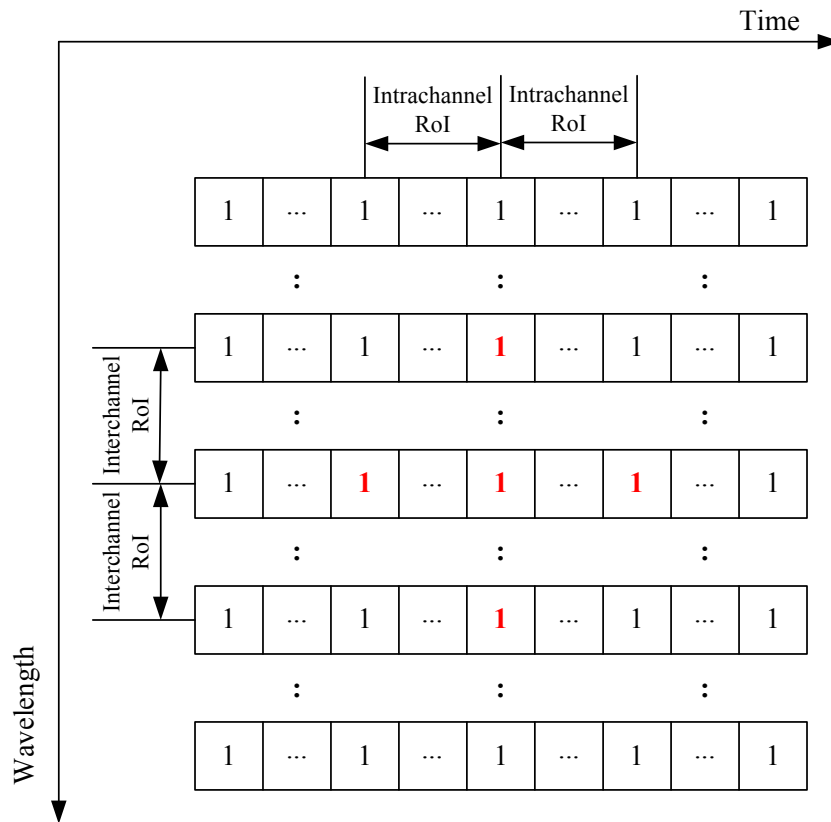


Figure 4.6: Concept of RoI

In this dissertation, for ISI, the RoI is defined as \bar{k} if \bar{k} is the smallest integer such that the worst-case cumulative ISI degradation

$$D^{ISI}(\bar{k}) = \sum_{\hat{k}=k+1}^{k+\bar{k}} \left| \rho_{k,\hat{k}}^{ISI} \right| \quad (4.14)$$

is practically unchanged. In this research, the tolerance level of cumulative impairment degradation is defined as 0.0001%. When the increase in the cumulative degradation is less than the tolerance, we say that the cumulative degradation is practically unchanged. This definition applies to RoIs of all physical impairments.

For IXPM (IFWM), the RoI is \bar{k} if \bar{k} is the smallest integer such that the worst-case cumulative IXPM (IFWM) degradation

$$D^{IXPM(IFWM)}(\bar{k}) = \sum_{l,m,n=k+1}^{k+\bar{k}} \left| \rho_{f,k,l,m,n}^{IXPM(IFWM)} \right| \quad (4.15)$$

is practically unchanged; intrachannel effects depend on the symbol rate R_s but are independent of channel spacing Δ .

For XPM (FWM), the RoI is \bar{f} if \bar{f} is the smallest integer such that the worst-case cumulative XPM (FWM) degradation

$$D^{XPM(FWM)}(\bar{f}) = \sum_{u,v,w=f+1}^{f+\bar{f}} \left| \rho_{f,k,u,v,w}^{XPM(FWM)} \right| \quad (4.16)$$

is practically unchanged; interchannel effects depend on the channel spacing but not the symbol rate.

The SPM coefficient is a constant, unaffected by the symbol rate or the channel spacing. There is no RoI for SPM. For the above parameters, $|\rho^{SPM}| = 0.0165 \text{ mW}^{-1}\text{ps}^{-3}$.

4.2.1 RoI of ISI

The definition of the ISI coefficient ρ^{ISI} in Eq. (4.6) suggests that the severity of ISI is determined by $|\hat{k} - k|$. The cumulative ISI degradation $D^{ISI}(\bar{k})$ as the number of adjacent symbols \bar{k} varies is given in Fig. 4.7. The change in $D^{ISI}(\bar{k})$ remains below the tolerance level of 0.0001% when $\bar{k} \geq 1$; therefore, the RoI of ISI is 1 for both 40 Gs/s and 100 Gs/s.

This result has been verified using the split-step Fourier method by varying the number of pulses and ignoring nonlinearity.

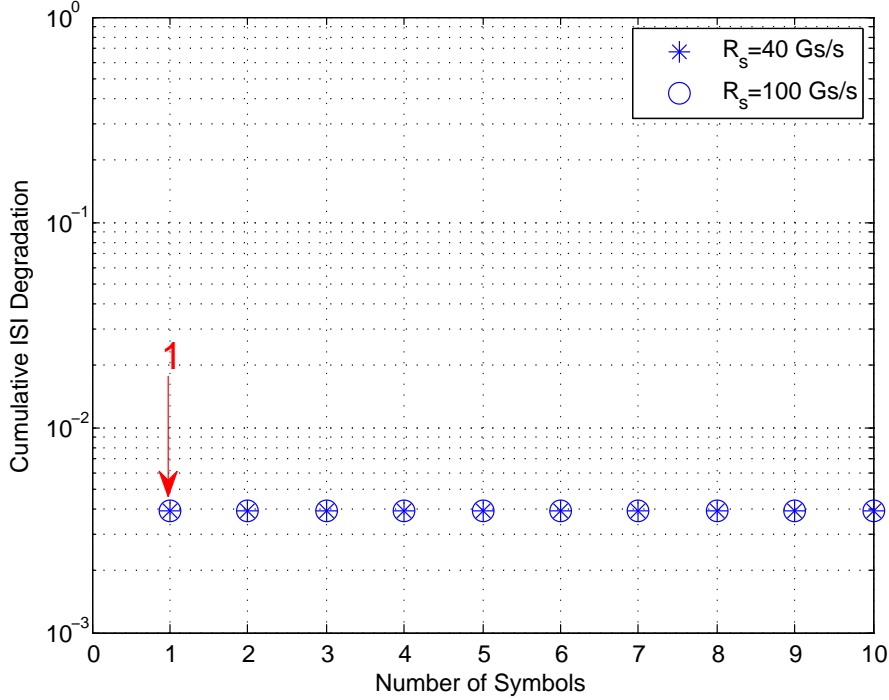


Figure 4.7: Computation of cumulative degradation due to ISI for SMF fiber operating at $1.55 \mu m$ for various symbol rates

4.2.2 RoI of Intrachannel Nonlinear Impairments

The changes in $D^{IXPM}(\bar{k})$ and $D^{IFWM}(\bar{k})$ with varying \bar{k} are given in Figs. 4.8 and 4.9, respectively. From Fig. 4.8, at a symbol rate of 40 Gs/s, the change in $D^{IXPM}(\bar{k})$ remains below the tolerance level of 0.0001% when $\bar{k} \geq 19$; at a symbol rate of 100 Gs/s, $D^{IXPM}(\bar{k})$ remains unchanged when $\bar{k} \geq 185$. Therefore, the RoIs of IXPM are 19 and 185, respectively, for 40 Gs/s and 100 Gs/s. Similarly, from Fig. 4.9, we can verify that the RoIs of IFWM are 65 and around 300, respectively, for 40 Gs/s and 100 Gs/s.

When the symbol rate increases, the symbol interval reduces and the RoIs of IXPM and IFWM increase. Note that the phase term $e^{i(\Phi_{fl}-\Phi_{fm}+\Phi_{fn})}$ is not included in our definition of $\rho_{f,k,l,m,n}^{IFWM}$ in Eq. (4.7). When we take the phase information into account, the IFWM

impairment is significantly reduced on average. The IFWM impairment can be reduced by manipulating the input phases [24].

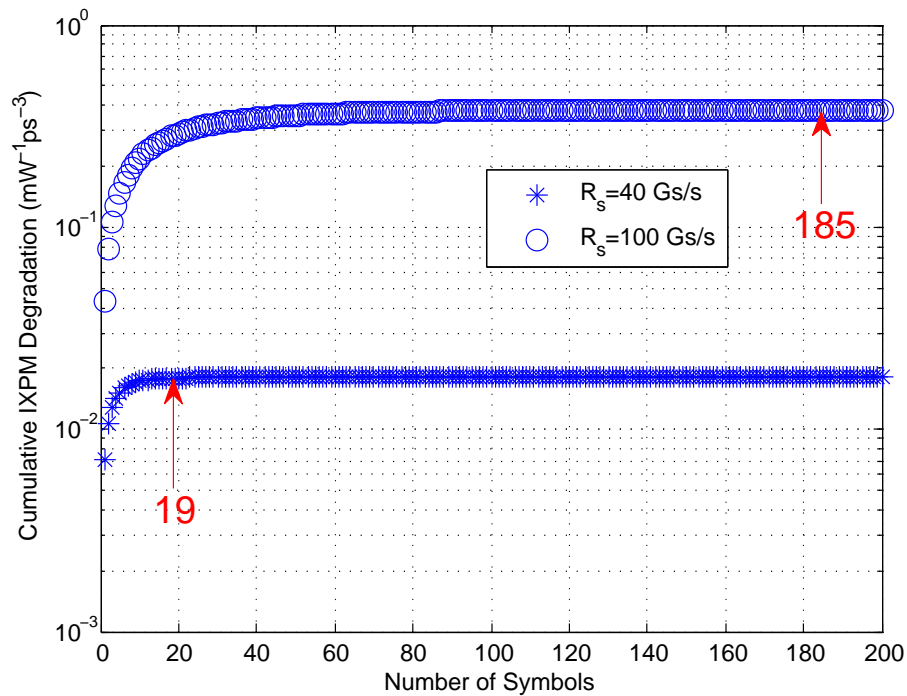


Figure 4.8: Computation of cumulative degradation due to IXPM for SMF fiber operating at $1.55 \mu\text{m}$ for various symbol rates

The RoIs of intrachannel nonlinear impairments, including IXPM and IFWM are large. In practice, we must consider the neighbouring symbols in the time domain that fall in these RoIs. A tradeoff between the accuracy and the complexity of the RoIs is desired. Sometimes we are interested in the RoIs for which a given percent of the worst-case cumulative impairment degradation is achieved. Tables 4.5 and 4.6 give the RoIs of intrachannel nonlinear impairments for three percentages of the total impairment (80%, 90%, and 100%) at 40 and 100 Gs/s, respectively. The RoIs for 100% correspond to the above original definitions of RoIs.

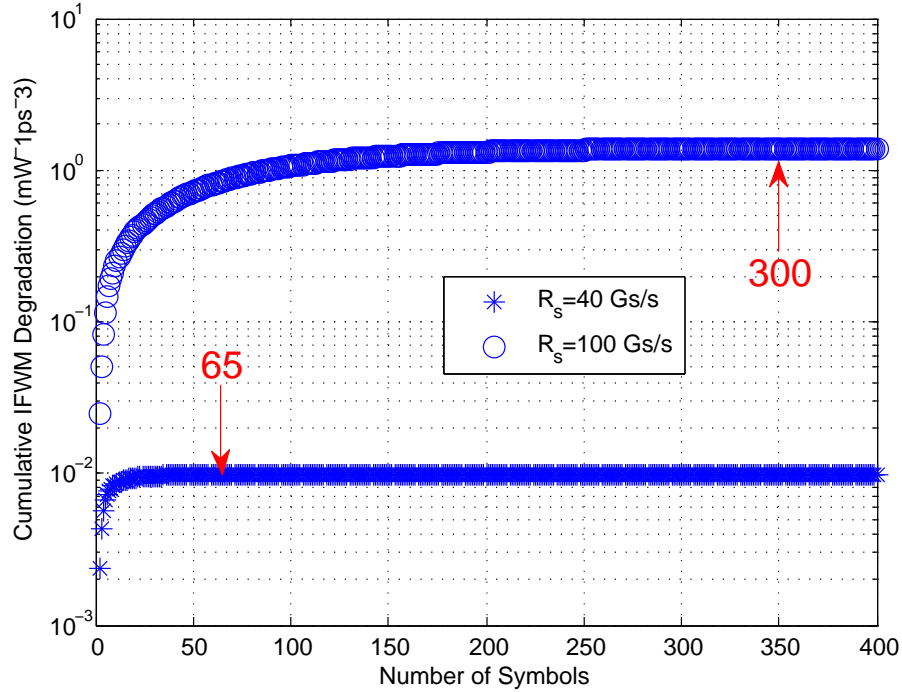


Figure 4.9: Computation of cumulative degradation due to IFWM for SMF fiber operating at $1.55 \mu\text{m}$ for various symbol rates

Table 4.5: RoIs of Intrachannel Nonlinear Impairments at 40 Gs/s

RoI	80%	90%	100%
IXPM	4	7	19
IFWM	8	13	65

Table 4.6: RoIs of Intrachannel Nonlinear Impairments at 100 Gs/s

RoI	80%	90%	100%
IXPM	23	37	185
IFWM	110	155	300

4.2.3 RoI of Interchannel Nonlinear Impairments

The changes in $D^{XPM}(\bar{f})$ and $D^{FWM}(\bar{f})$ with varying number of channels \bar{f} are given in Figs. 4.10 and 4.11, respectively. At a channel spacing of 50 GHz, the change in $D^{XPM}(\bar{f})$ remains below the tolerance level of 0.0001% when $\bar{f} \geq 3$; at a channel spacing of 100 GHz, the

change in $D^{XPM}(\bar{f})$ remains below the tolerance level of 0.0001% when $\bar{f} \geq 2$. Therefore, the RoIs of XPM are 3 and 2, respectively, for 50 GHz and 100 GHz channel spacing. Similarly, from Fig. 4.11, the RoIs of FWM are 4 and 3, respectively, for 50 GHz and 100 GHz. When channel spacing increases, the RoIs of XPM and FWM decrease.

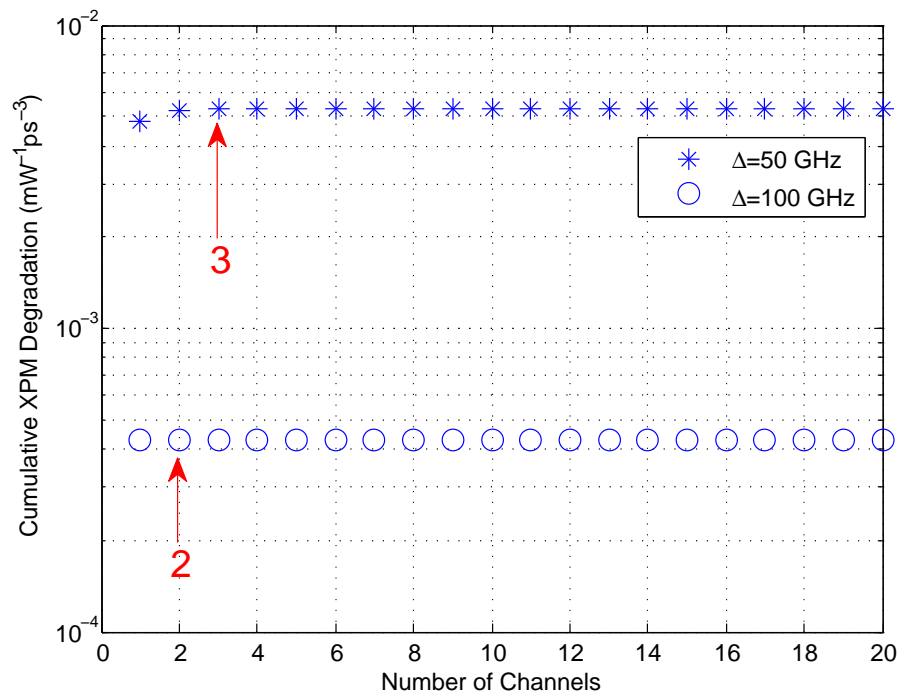


Figure 4.10: Computation of cumulative degradation due to XPM for SMF fiber operating at $1.55 \mu m$ for various channel spacings

4.3 Summary

This chapter presents two applications of the 2D discrete-time model in system analysis. The first application is to analyze the effect of varying system parameters and pulse shape on individual physical impairments in long-haul DWDM systems. The 2D discrete-time model can capture the effect of varying symbol rate on intrachannel effects and the effect of varying channel spacing on interchannel effects. The second application is to determine the RoIs of various individual physical impairments. These RoIs are of great value to the development of

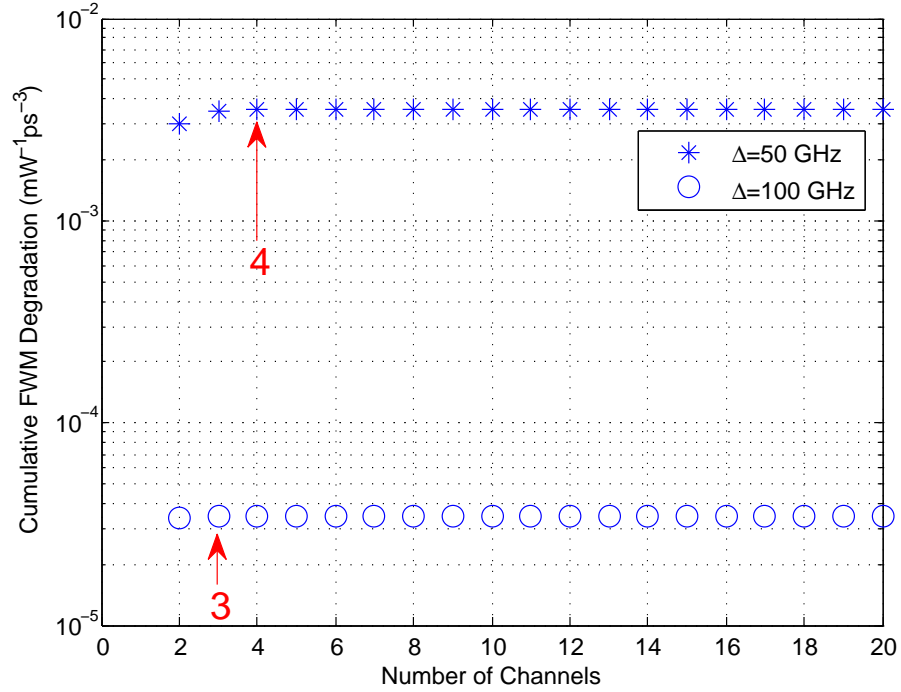


Figure 4.11: Computation of cumulative degradation due to FWM for SMF fiber operating at $1.55 \mu\text{m}$ for various channel spacings

physical impairment mitigation techniques and other signal processing techniques for optical communications.

Chapter 5

Model Applications in System Performance Improvement

This chapter presents two signal processing applications of the 2D discrete-time model in improving system performance. Section 5.1 develops a novel concatenation scheme with the inner code being a constrained code based on Total Impairment Extent Rank (TIER) and the outer code being a low-density parity-check (LDPC) code. Section 5.2 develops a nonlinear equalizer based on third-order inverse Volterra theory. Section 5.3 concludes this chapter with a summary.

5.1 TIER-LDPC Concatenation Scheme

This section develops a novel concatenation scheme with the inner code being a constrained code based on Total Impairment Extent Rank (TIER) and the outer code being a low-density parity-check (LDPC) code for long-haul fiber-optic communication systems [88]. The TIER constrained code is based on a the 2D discrete-time model of physical impairments in long-haul DWDM systems. LDPC codes have attracted great interest due to their remarkable performance under iterative decoding. When properly designed, LDPC codes are capable of closely approaching the fundamental Shannon limit in the presence of channel noise. The

concatenation of TIER and LDPC codes can arguably improve the decoding performance in both ASE and nonlinearity dominant regions.

The extent of the physical impairments depends on the bit patterns, as seen in Section 4.2. For a bit pattern of a given block length, using our 2D discrete-time model, we calculate all the physical impairments imposed on any bit and sum over all bits in the word, resulting in a metric we refer to as the Total Impairment Extent (TIE). Then we rank these bit patterns in increasing order of their TIEs and use this metric to define a code that avoids bit sequences leading to high TIEs. At the receiver, we use a maximum a-posteriori probability (MAP) decoder to produce the soft information required for the LDPC decoder.

The proposed TIER code is superior to current constrained codes [73, 74, 75, 76, 77, 78, 79, 80] because it can not only suppress more physical impairments, including linear effects and nonlinear effects, but it also offers system designers great flexibility in selecting which impairment to suppress, selecting the code rate arbitrarily, and selecting the message length, which determines the complexity of the decoder. Further, it can be easily extended to wavelength-division multiplexed (WDM) systems to mitigate both intrachannel effects and interchannel effects.

We compare the BER performance of the TIER-LDPC concatenation scheme to that of the LDPC code alone. The performance of the TIER-LDPC concatenation scheme is better than the LDPC coding scheme over the entire range of transmitted power levels, particularly for high power levels. Compared with the LDPC alone, which is effective in the suppression of the amplified spontaneous emission (ASE) noise only, the TIER-LDPC concatenation scheme is effective in the suppression of both the nonlinear impairments and the ASE noise because it combines the strength of the TIER code in suppressing severe nonlinear physical impairments effectively and that of LDPC code in correcting memoryless errors due to ASE noise. The TIER-LDPC concatenation scheme overcomes the weakness of the LDPC code, i.e., its vulnerability to nonlinear impairments.

The performance of other constrained coding schemes in the literature was evaluated in

the absence of ASE noise. In this section we evaluate the performance of our TIER-LDPC concatenation coding scheme through split-step Fourier simulation in the presence of ASE noise.

5.1.1 TIER-LDPC Concatenation Scheme

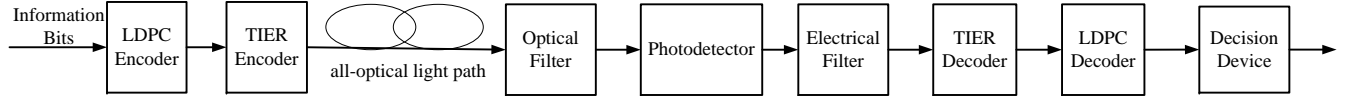


Figure 5.1: Schematic of TIER-LDPC Concatenation Scheme

In this section we propose a novel TIER-LDPC concatenated coding scheme to combat both the physical impairments and the ASE noise in long-haul fiber-optic communication systems. In this scheme, the inner code is a constrained code based on Total Impairment Extent Rank (TIER) and the outer code is a LDPC code, as shown in Fig. 5.1.

Consider a long-haul single-channel fiber-optic communication system. In the absence of ASE noise, the output optical field of the fiber at discrete times kT_s is given as

$$\begin{aligned}
 r(kT_s) = & a_k A_0 e^{(i\Phi_k)} + \sum_{\hat{k}=0; \hat{k} \neq k}^{K-1} a_{\hat{k}} A_f e^{(i\Phi_{\hat{k}})} \rho_{k, \hat{k}}^{ISI} + N_s a_k^3 A_0^3 \tilde{T}^3 e^{(i\Phi_k)} \rho^{SPM} \\
 & + N_s \sum_{l, m, n=0}^{K-1} a_l a_m a_n A_0^3 \tilde{T}^3 e^{[i(\Phi_l - \Phi_m + \Phi_n)]} [\rho_{k, l, m, n}^{IXPM} + \rho_{k, l, m, n}^{IFWM}]
 \end{aligned} \quad (5.1)$$

From Eq. (5.1), we can see that $r(kT_s)$ consists of the contribution of the transmitted bit a_k and all physical impairments imposed on the transmitted bit a_k . These physical impairments include the linear impairment (ISI) and the nonlinear impairments, i.e., SPM, IXPM, and IFWM. In this section, we define the sum of these physical impairments over all bits of a bit pattern of length K as the Total Impairment Extent (TIE):

$$TIE = \sum_{k=0}^{K-1} |r(kT_s) - r^{Sig}(kT_s)| \quad (5.2)$$

where $r^{Sig}(kT_s) = a_k A_0 e^{i\Phi_k}$ is the desired part of $r(kT_s)$. Alternatively, TIE can be defined as

$$TIE = \sum_{k=0}^{K-1} |y(t_k) - y^{Sig}(t_k)| \quad (5.3)$$

or

$$TIE = \min_{k \in [0, K-1]} |y(t_k) - y^{Sig}(t_k)| \quad (5.4)$$

where $y^{Sig}(t_k) = |r^{Sig}(kT_s)|^2$ is the desired part of $y(t_k)$. In our analysis, we use Eq. (5.2). The other two definitions yield quite similar results. The TIE depends on what bit pattern is sent. There are 2^N different bit patterns for a given codeword of block length N .

The idea of the rate- R , $R = \frac{K}{N}$, TIER constrained code is as follows. First, by applying the definition of the TIE above, we calculate the TIEs for all possible bit patterns of length N . Next, we rank these bit patterns and select the best 2^K bit patterns of length N with smallest TIEs out of all 2^N bit patterns. Then we establish a one-to-one mapping between all bit patterns of length K and these best bit patterns of length N . In this way, we have a look-up table to be used at the transmitter that maps the bit patterns of length K to bit patterns of length N . At the receiver, for each given received output sequence of length N , we use a MAP decoder to obtain the a-posteriori probabilities for 0 and 1 of each symbol of the corresponding bit pattern of length K . With these two a-posteriori probabilities for 0 and 1 of each symbol, we calculate the likelihood ratio of each symbol as the input of the LDPC decoder. In this way the TIER-LDPC decoder maps each sequence of length N back to the corresponding bit pattern of length K .

The TIER code is flexible in selecting any physical impairment or any combination of impairments to be mitigated with tiny modification of the definition of TIE. For example, in a single channel long-haul fiber-optic communication system, if the linear impairments are negligible compared with the nonlinear impairments, or if a powerful linear equalizer is to be used, we are interested in suppressing the nonlinear physical impairments only. In this case, we can modify the definition of the model to $TIE_L = \sum_{k=0}^{K-1} |[r(kT_s) - r^{Signal} - r^{ISI}]|$,

where $r^{ISI} = \sum_{\hat{k}=0; \hat{k} \neq k}^{K-1} a_{\hat{k}} A_0 e^{(i\Phi_{\hat{k}})} \rho_{k, \hat{k}}^{ISI}$, which is the linear part of $r(kT_s)$.

5.1.2 Performance Evaluation

In this section we present the BER performance results for four cases: the uncoded case; the TIER-only coding case; the TIER-LDPC concatenated coding case; and the LDPC-only coding case.

We consider 40-Gb/s on-off keyed (OOK) signals transmitting through a single-channel fiber-optic communication system with the number of spans being 40, 50, or 60. In the TIER-LDPC concatenation case, we set $K = 7$ and $N = 8$ for the TIER code and $K=504$ and $N=1008$ for the LDPC code, i.e., the code rate of the concatenated case is $(7/8) * (504/1008) = 7/16$. For comparison purposes, the code rate of the LDPC-only coding case is also $7/16$. Correspondingly the symbol rate becomes $40/(7/16) \text{ Gs/s}$.

Fig. 5.1 presents a schematic of the TIER-LDPC concatenation scheme. If we remove both the TIER encoder and the TIER decoder from Fig. 5.1, we have the schematic of the LDPC-only coding scheme. Similarly, if instead both the LDPC encoder and the LDPC decoder are removed, this becomes the TIER-only coding scheme. All schemes operate at the same bit rate for fair comparison. At the transmitter, information bits are encoded by a LDPC encoder and a TIER encoder and launched into the optical fiber. We use the split-step Fourier method to simulate the propagation of optical waves through the fiber and to obtain the received signal statistics needed for decoding. Periodic dispersion compensation and amplification are assumed.

At the receiver, the output of the fiber passes through an optical filter, a square-law photodetector and an electrical filter. The filtered output vector is denoted by \underline{y} . In the TIER-LDPC concatenation scheme, we use the MAP rule to calculate $P(b_i = 0|y)$ and $P(b_i = 1|y)$ assuming y is a jointly Gaussian vector with its mean based on the split-step Fourier simulation in the absence of ASE noise. The covariance matrix is assumed diagonal and also based on a noiseless SSF simulation. Then we can calculate the log likelihood ratio

(LLR): $LLR((i)) = \log(P(b_i = 0|y)/P(b_i = 1|y))$, which is used by the LDPC decoder. In the LDPC-only coding scheme, in order to be able to calculate the 1st-order statistics of the channel output, we use the Monte-Carlo method to estimate $P(y|0)$ and $P(y|1)$ and calculate the log likelihood ratio (LLR): $LLR(y) = \log(P(y|0)/P(y|1))$, which is used by the LDPC-only coding decoder. In the TIER-only coding scheme, the decoder uses the ML rule based on the above Gaussian vector.

For the rate-1/2 LDPC code, MacKay's (1008, 504) regular $\{3, 6\}$ LDPC code is used. For the rate-7/16 LDPC code we choose all variable nodes (VNs) to have degree 3, then a (1008, 441) code is built using the Progressive Edge-Growth (PEG) algorithm; among 567 check nodes (CNs), 378 have degree 5 and 189 have degree 6.¹ When decoding, the sum-product algorithm [89] is used and the maximum number of iterations is set to 50. Finally, it is worth noting that the optical channel is asymmetric so the all-zero codeword assumption [89] is no longer valid. In the simulation LDPC codewords are randomly generated and decoded. The LLR from the histograms generated through the split-step Fourier simulation is used in decoding. Fig. 5.2 shows the histograms when the launched power is 2 mW.

Figs. 5.3, 5.4 and 5.5 show the BER performance results when the launched power P_0 varies from 0.1 mW to 10 mW for a code rate of 7/16 when the number of spans is 40, 50, and 60, respectively. In this section, the bit rate is held constant and the symbol rate varies as the code rate changes. We can see that the performance of the TIER-LDPC concatenation scheme is much better than the corresponding uncoded case. Nonlinear impairments increase when the launched power becomes large. The performance of the TIER-LDPC concatenation scheme is better than both the LDPC-only coding scheme and the TIER-only coding scheme over the entire range of transmitted power levels. For low power levels where the ASE noise dominates and the nonlinear impairments are small, the LDPC code is effective; for high power levels, the TIER-LDPC scheme works better than the LDPC code because nonlinear impairments dominate and the ASE noise is small compared with the nonlinear impairments

¹We gratefully acknowledge the help of Tingjun Xie who designed both the rate-1/2 LDPC code and the rate-7/16 LDPC code for this dissertation.

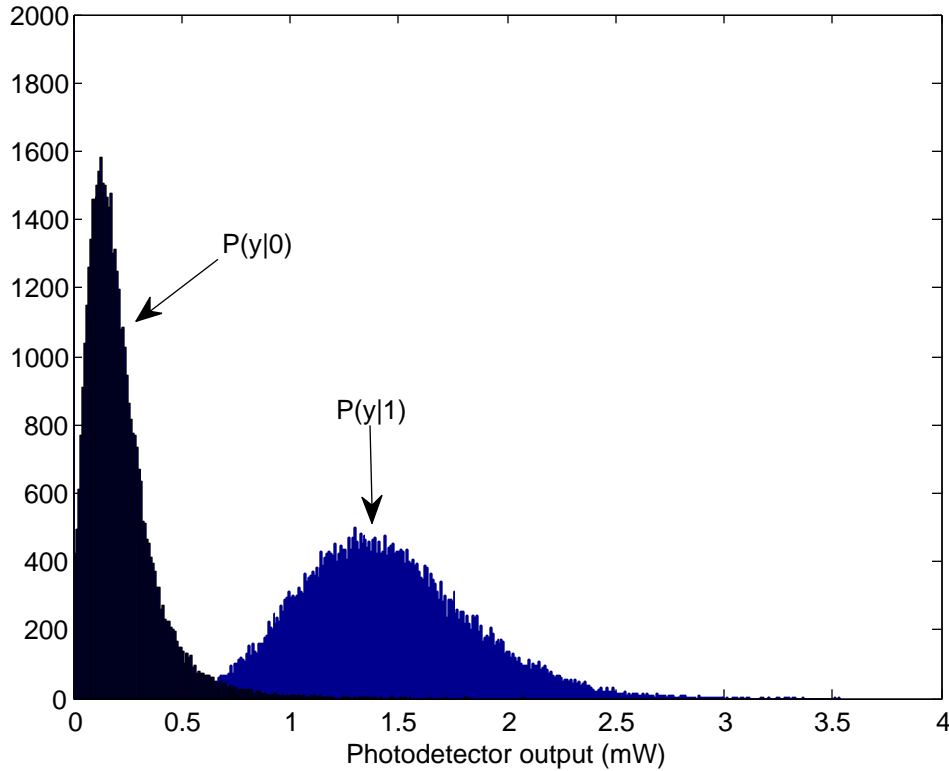


Figure 5.2: Histograms obtained from split-step Fourier simulation ($P_0=2$ mW)

in this region. When the number of spans is 50 or 60, the LDPC-only code almost loses its error correcting capability because the nonlinearity becomes severe with the increase in the number of spans. In this case we have to resort to the TIER code. The TIER-LDPC concatenation scheme combines the strength of the TIER code in correcting errors due to physical impairments and that of the LDPC code in correcting errors due to ASE noise.

For a rate- $\frac{K}{N}$ TIER scheme, its complexity is only $O(2^K)$. So the complexity of the TIER-LDPC concatenation coding scheme is acceptable for small values of K compared with that of the LDPC-only coding scheme. The performance of the TIER-LDPC scheme works best for high power levels where nonlinearity dominates. In fact, the performance of the TIER could be improved further by using longer code words, since the RoIs of physical impairments, determined in Section 4.2 and [87], are much larger than the current length of code words. The above rate-7/16 avoids about 90% of IXPM and less than 80% of IFWM.

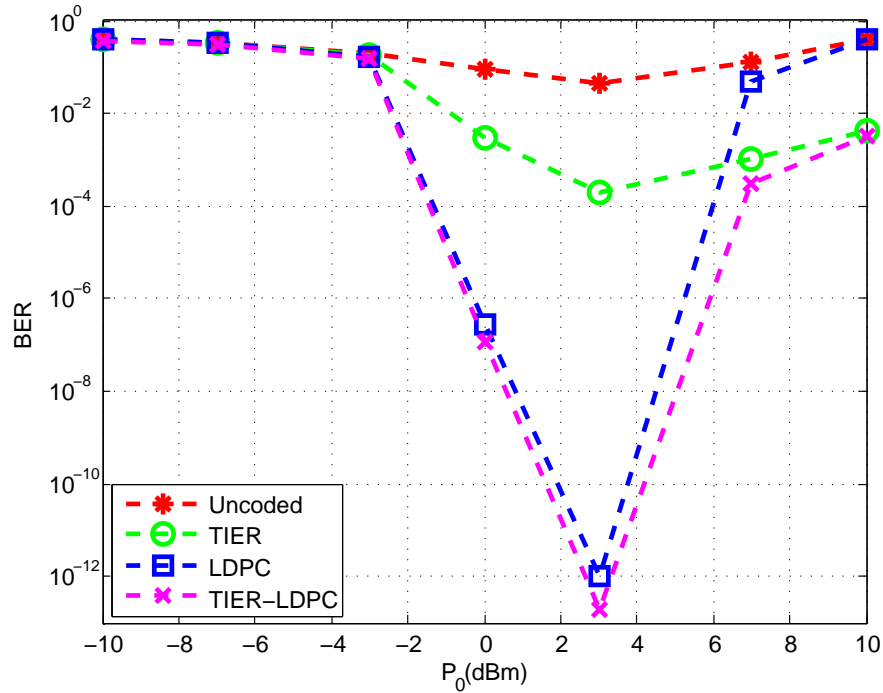


Figure 5.3: Performance evaluation of the TIER-LDPC concatenation scheme, the TIER-only scheme, and the LDPC-only scheme (40 spans)

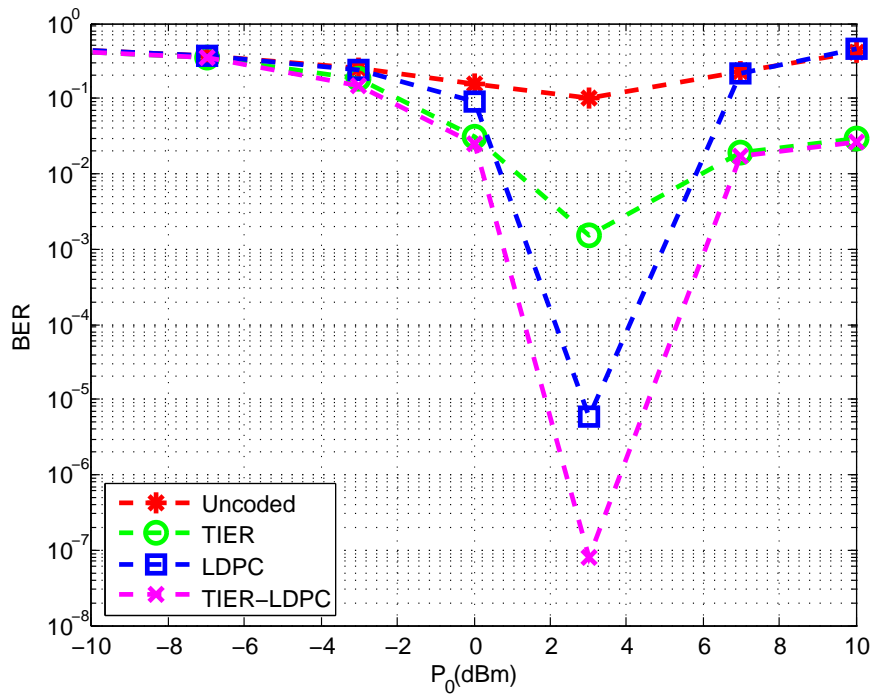


Figure 5.4: Performance evaluation of the TIER-LDPC concatenation scheme, the TIER-only scheme, and the LDPC-only scheme (50 spans)

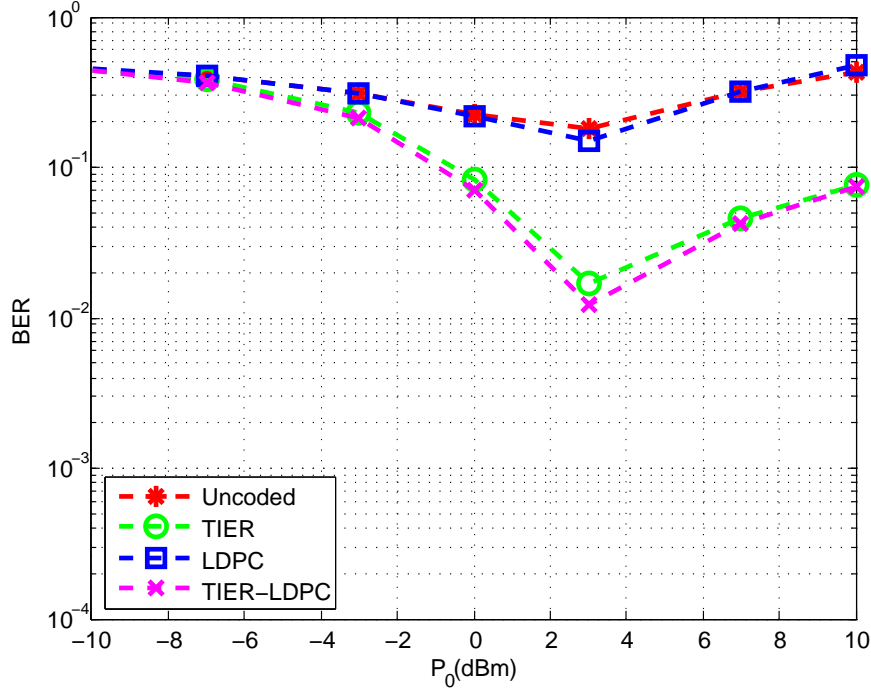


Figure 5.5: Performance evaluation of the TIER-LDPC concatenation scheme, the TIER-only scheme, and the LDPC-only scheme (60 spans)

5.2 Nonlinear Equalization

This section develops a nonlinear equalizer to improve the system performance of long-haul DWDM systems.

According to the p th-order inverse Volterra theory [90], for a nonlinear system expressed as the Volterra series

$$y(t) = H[x(t)] = \sum_{n=1}^{\infty} H_n[x(t)], \quad (5.5)$$

where H is the system operator, and H_n , $n = 1, 2, \dots, \infty$, is the n th-order Volterra operator. If and only if the inverse of the linear operator H_1 is stable and causal, there exists a stable and causal p th-order inverse system, $K_{(p)}$, such that the overall system Z formed by tandem connection of $K_{(p)}$ and H satisfies the conditions given by

$$Z[x(t)] = K_{(p)}[y(t)] = x(t) + \sum_{n=p+1}^{\infty} Z_n[x(t)], \quad (5.6)$$

where Z_n is the n th-order Volterra operator of the system Z . Further, the p th-order pre-inverse of a system H is identical to its p th-order post-inverse.

5.2.1 Nonlinear Equalizer

The schematic of the nonlinear equalization is shown in Fig. 5.6.

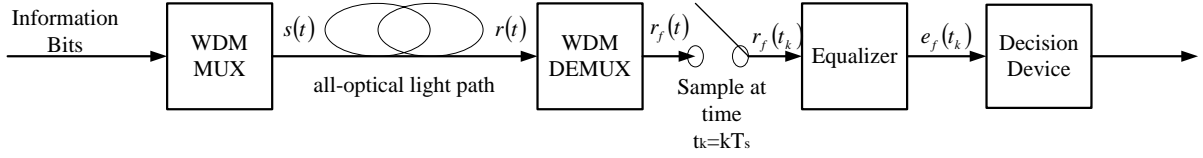


Figure 5.6: Nonlinear Equalization

The 2D discrete-time model developed in Chapter 3 is based on the third-order VSTF method. Let $S(\omega)$ and $R(\omega)$ be the output of the WDM multiplexer and the input of the WDM demultiplexer, the input-output relationship can be expressed as

$$R(\omega) \approx H_1(L, \omega)S(\omega) + \int_{-\infty}^{+\infty} \int_{-\infty}^{+\infty} H_3(L, \omega_1, \omega_2, \omega - \omega_1 + \omega_2)S(\omega_1)S^*(\omega_2)S(\omega - \omega_1 + \omega_2)d\omega_1d\omega_2, \quad (5.7)$$

where

$$H_1(L, \omega) = 1, \quad (5.8)$$

and

$$H_3(L, \omega_1, \omega_2, \omega - \omega_1 + \omega_2) = \frac{iN\gamma}{4\pi^2} H_1(L, \omega) \int_0^L \exp[-\alpha z + i\beta_2 z(\omega_1 - \omega)(\omega_1 - \omega_2)] dz. \quad (5.9)$$

According to the third-order inverse Volterra theory, the nonlinearity in the third-order Volterra system can be compensated up to the third-order by another third-order Volterra system referred to as the third-order inverse system [90]. The nonlinear equalizer based on

the third-order inverse system is

$$E_f(\omega) \approx K_1(L, \omega)R_f(\omega) + \int_{-\infty}^{+\infty} \int_{-\infty}^{+\infty} K_3(L, \omega_1, \omega_2, \omega - \omega_1 + \omega_2)R_f(\omega_1)R_f^*(\omega_2)R_f(\omega - \omega_1 + \omega_2)d\omega_1d\omega_2, \quad (5.10)$$

with the first- and third-order operator of the third-order inverse filter defined as follows [90]:

$$K_1(L, \omega) = H_1(L, \omega)^{-1} = 1, \quad (5.11)$$

and

$$\begin{aligned} K_3(L, \omega_1, \omega_2, \omega - \omega_1 + \omega_2) &= -K_1(L, \omega)H_3(L, \omega_1, \omega_2, \omega - \omega_1 + \omega_2)K_1(L, \omega) \\ &= -\frac{iN\gamma}{4\pi^2} \int_0^L \exp[-\alpha z + i\beta_2 z(\omega_1 - \omega)(\omega_1 - \omega_2)]dz. \end{aligned} \quad (5.12)$$

In practice, for a long-haul DWDM system, an equalizer should be designed to mitigate nonlinearity introduced by the photodetector, in addition to the mitigation of the physical impairments and the ASE noise. The nonlinearity introduced by the photodetector is ignored here to highlight the effectiveness of the nonlinear equalizer based on the inverse Volterra theory in the mitigation of the nonlinear physical impairments due to Kerr effect and the ASE noise. The nonlinearity introduced by the photodetector is hard to suppress and left for future work. In its current form, our nonlinear equalizer is therefore applicable only to coherent detection systems.

Similar to the derivation of the 2D discrete-time model, simplifying Eq. (5.10) to a simple integral and taking its inverse Fourier transform yields the discrete-time output of the

nonlinear equalizer

$$\begin{aligned}
e_f(t_k) \approx & r_f(t_k) - \sum_{\hat{k}=0; \hat{k} \neq k}^{K-1} r_f(t_{\hat{k}}) A_f A_{df} \exp(i\Phi_{f\hat{k}}) \rho_{f,k}^{ISI} \\
& - \sum_{\hat{f}=0; \hat{f} \neq f}^{F-1} \sum_{\hat{k}=0}^{K-1} r_{\hat{f}}(t_{\hat{k}}) A_{\hat{f}} A_{d\hat{f}} \exp(i\Phi_{\hat{f}\hat{k}}) \rho_{f,k}^{ICI} - r_f(t_k)^3 A_f^3 A_{df} \tilde{T}_f^3 \exp(i\Phi_{ul}) \rho_{f,k}^{SPM} \\
& - \sum_{l=0}^{K-1} \sum_{m=0}^{K-1} \sum_{n=0}^{K-1} r_f(t_l) r_f(t_m) r_f(t_n) A_f^3 A_{df} \tilde{T}_f^3 \exp[i(\Phi_{fl} - \Phi_{fm} + \Phi_{fn})] (\rho_{f,k}^{IXPM} + \rho_{f,k}^{IFWM}) \\
& - \sum_{u=0}^{F-1} \sum_{v=0}^{F-1} \sum_{w=0}^{F-1} r_u(t_k) r_v(t_k) r_w(t_k) A_u A_v A_w A_{df} \tilde{T}_u \tilde{T}_v \tilde{T}_w \exp[i(\Phi_{uk} - \Phi_{vk} + \Phi_{wk})] (\rho_{f,k}^{XPM} + \rho_{f,k}^{FWM}).
\end{aligned} \tag{5.13}$$

where the impairment coefficients, $\rho_{f,k}^{Sig}$, $\rho_{f,k}^{ISI}$, $\rho_{f,k}^{ICI}$, $\rho_{f,k}^{IXPM}$, $\rho_{f,k}^{IFWM}$, $\rho_{f,k}^{XPM}$, and $\rho_{f,k}^{FWM}$, are used in Chapter 3 and defined in the Appendix.

Eq. (5.13) is the discrete-time expression of the nonlinear equalizer. If the fifth and higher order terms are ignored, the output of the equalizer $e_f(t_k)$ approximately equals its input $r_f(t_k)$ minus various linear and nonlinear physical impairments. Given F and K , these physical impairments can be easily calculated by using the impairment coefficients and pulse parameters. Therefore the nonlinear equalizer is easy to implement using the most basic DSP device. This advantage is due to the 2D discrete-time model of physical impairments in long-haul DWDM systems. Without the explicit expression of the 2D discrete-time model, it is impossible to design a nonlinear equalizer which is easy to implement using hardware. Although the nonlinear equalizer is similar to backpropagation, the biggest difference between them is that the nonlinear equalizer can be implemented in practice but the backpropagation approach [84][85] is of theoretical significance only.

If we compare Eq. (5.13) with Eq. (3.23), we can find the following relationship between the output of the equalizer $e_f(t_k)$ and the input symbol a_{fk} :

$$e_f(t_k) = a_{fk} A_f A_{df} \exp(i\Phi_{fk}) \rho_{f,k}^{Sig} + H.O.T., \tag{5.14}$$

where the abbreviation H.O.T stands for higher order terms. The output of the equalizer only retains the desired symbol modified by the optical filter. All third order nonlinear physical impairments are mitigated by the nonlinear equalizer.

5.2.2 Performance Evaluation

To evaluate the effectiveness of the above nonlinear equalizer, we present the BER performance results for five cases: the unequalized case; the equalized case; the backpropagation case; the equalized case without ASE noise (i.e., nonlinearity only); the equalized case without nonlinearity (i.e., ASE noise only). We use the SSF method to simulate the propagation of optical waves for the unequalized case and the backpropagation case. For the equalized cases, we use the SSF method to simulate the propagation of optical waves till the WDM demultiplexer and then use the above discrete-time nonlinear equalizer with $K=20$ to obtain the output of the nonlinear equalizer.

We consider 40-Gs/s OOK signals transmitting through a single-channel fiber-optic communication system. Figs. 5.7, 5.8, and 5.9 show the BER performance results when the launched power varies from 0.1 mW to 10 mW for 40, 50, and 60 spans, respectively. The performance of the equalized case is better than the unequalized case, particularly for large launched power levels where nonlinearity dominates. The performance of the equalized case is comparable to the backpropagation case. The fine difference between the equalized case and the backpropagation case is due to the small value of K used and the unequalized fifth and higher order terms. In Section 4.2.2, the RoIs of IXPM and IFWM at a symbol rate of 40 Gs/s are 19 and 65, respectively. The current setting of K corresponds to the suppression of all ISI and IXPM, but only 95.3% of IFWM.

The performance of the equalized case without nonlinearity is better than that of the unequalized case. This demonstrates that the nonlinear equalizer is effective in suppressing ASE noise. The performance of the equalized case without ASE noise is best and the BERs are below the resolution of the split-step simulation. We were unable to determine via

simulation how low the BERs fall for this case, so results are not included in the figures. This demonstrates that the nonlinear equalizer is effective in suppressing nonlinear physical impairments. Therefore the nonlinear equalizer performs well in mitigating both nonlinear physical impairments and ASE noise. Compared with backpropagation, the nonlinear equalizer based on the 2D discrete-time model is easy to implement using the most basic DSP device.

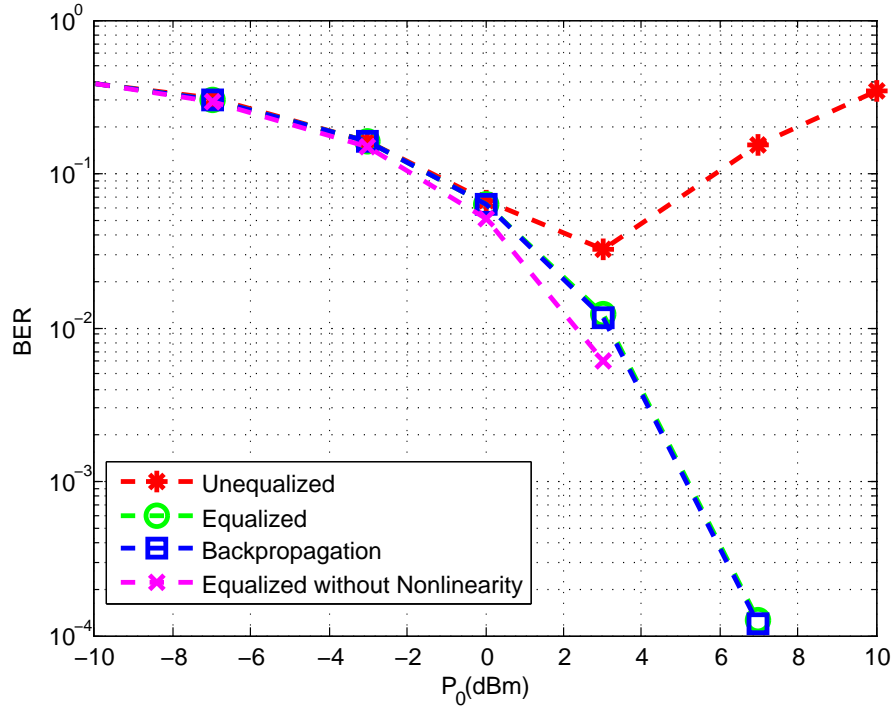


Figure 5.7: BER Performance of the nonlinear equalizer (40 spans)

5.3 Summary

This chapter presents two signal processing applications of the 2D discrete-time model in improving system performance.

The first signal processing application of the model in system performance improvement is the development of a novel TIER (Total Impairment Extent Rank)-LDPC concatenation scheme to combat both the deterministic physical impairments and the ASE noise in long-haul fiber-optic communication systems. The difference between the TIER constrained code

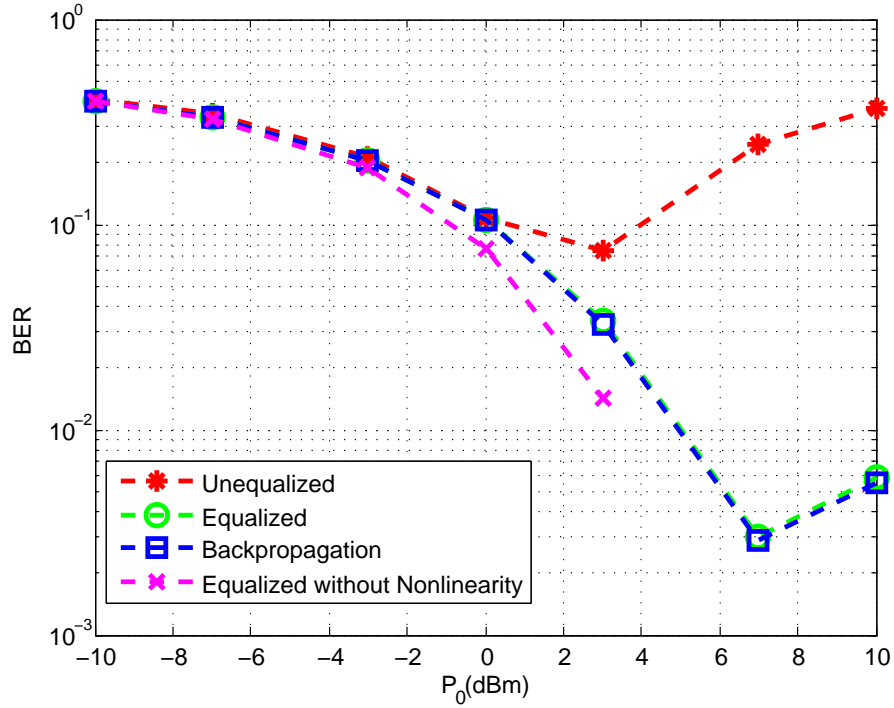


Figure 5.8: BER Performance of the nonlinear equalizer (50 spans)

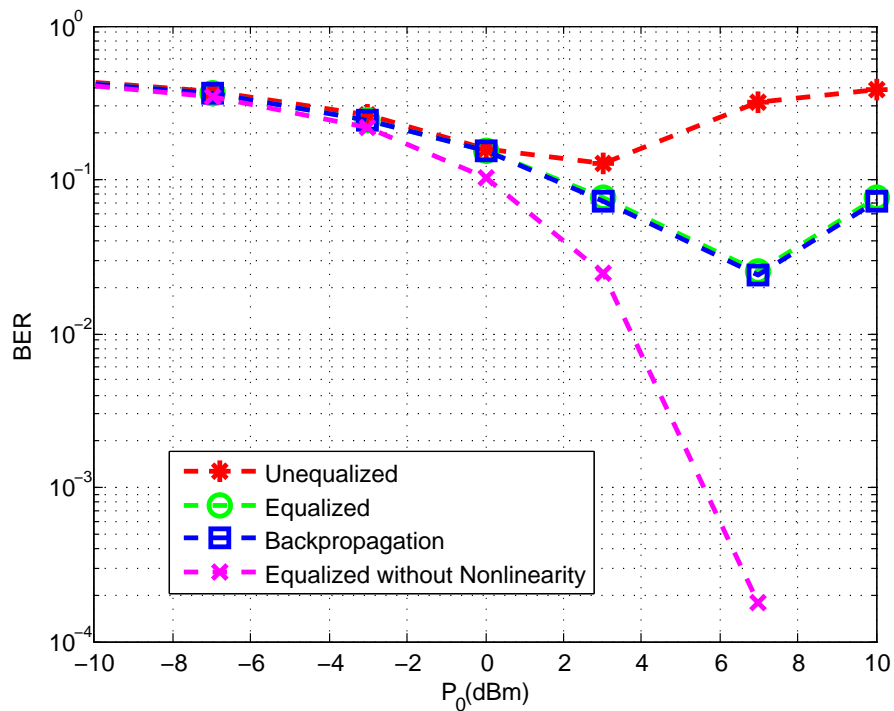


Figure 5.9: BER Performance of the nonlinear equalizer (60 spans)

and the constrained coding schemes in the literature is that it can suppress more physical impairments, including linear effects and nonlinear effects, rather than only intrachannel effects caused by some resonant sequences. With small modifications of the definition of TIE, the TIER code can be used to suppress any physical impairment or any combination of impairments. The TIER code is particularly suitable to the case of severe nonlinearity for which the LDPC code fails. The strength of the TIER code lies in its great flexibility in selecting the code rate arbitrarily, and selecting the message length, which determines the complexity of the decoder. Compared with the LDPC code alone, which fails at high power levels where nonlinearity dominates, the TIER-LDPC concatenation scheme is effective over the entire range of transmitted power levels and link length in suppressing both the physical impairments and the ASE noise in a long-haul fiber-optic communication system.

The second signal processing application of the model in system performance improvement is the development of a nonlinear equalizer based on the third-order inverse Volterra theory. Using the impairment coefficients of the 2D discrete-time model of physical impairments in long-haul DWDM systems, the hardware implementation of the nonlinear equalizer needs only the most basic DSP device. The nonlinear equalizer is effective in the mitigation of linear and nonlinear physical impairments. The performance of the nonlinear equalizer is comparable to the backpropagation algorithm, which is hard to implement in hardware.

Chapter 6

Conclusions and Future Work

This chapter summarizes and concludes the dissertation and proposes future avenues for research.

The performance of long-haul DWDM systems with periodic dispersion compensation and amplification is fundamentally limited by physical impairments due to dispersion and fiber nonlinearity, and by ASE noise. Sophisticated signal processing techniques are needed to mitigate physical impairments and fully exploit the system capacity. These techniques require a mathematical model that describes the input-output relationship of long-haul DWDM systems and characterizes various physical impairments.

This dissertation develops a model-centric approach for discrete-time signal processing for optical communications and addresses the development, validation and applications of a 2D discrete-time model of physical impairments in long-haul DWDM systems with periodic dispersion compensation and amplification.

The model development is based on the third-order Volterra series transfer function (VSTF) method. The model overcomes the well-known triple integral problem inherent in the original VSTF method and simplifies it to a simple integral that is easy to evaluate. The model takes into account multichannel effects, fiber losses, frequency chirp, optical filtering, and photodetection, which are ignored in the current literature. The model is in

discrete-time and facilitates its applications in discrete-time signal processing to improve the system performance of long-haul DWDM systems. The model characterizes each individual physical impairment by introducing the corresponding impairment coefficient. The model offers obvious advantages over the third-order VSTF method and the split-step Fourier (SSF) method. The model is in excellent agreement with results obtained from the SSF method.

The 2D discrete-time model is applied in system analysis and system performance improvement of long-haul DWDM systems. In system analysis, two applications are developed. Using the 2D discrete-time model, the effects of varying system parameters (symbol rate and channel spacing) and pulse shape on individual physical impairments in long-haul DWDM systems are analyzed. The concept of range of influence (RoI) of physical impairments is proposed and the RoI of each individual physical impairment is determined to guide the development of discrete-time signal processing. In system performance improvement, two applications are developed. Using the 2D discrete-time model, a novel constrained code based on the Total Impairment Extent Rank (TIER) is proposed to mitigate the nonlinear physical impairments in long-haul fiber-optic communication systems; a TIER-LDPC concatenation scheme is proposed to combine the strength of the TIER code in suppressing severe nonlinear physical impairments effectively and that of the LDPC code in correcting memoryless errors due to ASE noise. A nonlinear equalizer based on the third-order inverse Volterra theory is also proposed. Different from backpropagation that is hard to implement in hardware, this equalizer features various basic discrete-time signal processing operations. The nonlinear equalizer is effective in suppressing the physical impairments and the ASE noise in a long-haul fiber-optic communication systems, particularly for high launched power levels where fiber nonlinearity dominates.

To fully exploit the potential of applying the 2D discrete-time model in system analysis and system performance improvement of long-haul DWDM systems, and the capacity of fiber-optic communication systems, further research is recommended in the following aspects: First, the model development methodology can be easily extended to polarization-division

multiplexing (PDM) systems and coherent receivers. Second, the joint modeling of physical impairments and ASE noise is the ultimate prerequisite for the most powerful discrete-time signal processing for long-haul DWDM systems. However, determining the statistics of the ASE noise in the highly nonlinear fiber regime remains an open problem. The joint modeling of these two factors that limit the system performance is possible after the statistics of the ASE noise are clearly understood by the fiber-optic communication community. Third, although the 2D discrete-time model is designed for point-to-point long-haul DWDM systems, it is possible for the model development methodology proposed in this dissertation to be applied to multipoint fiber-optic communication systems, such as wide-area and metro-area networks or multi-access WDM networks. If the model can be developed for broader fiber-optic communication networks, discrete-time signal processing applications can be developed for these systems to improve their performance. Fourth, the wider use of the model in discrete-time signal processing for optical communications may require further simplification of the 2D discrete-time model. A tradeoff between the model complexity and the model accuracy is needed, as further simplification of the model may sacrifice its accuracy in capturing the exact propagation of the optical field over the long-haul fiber-optic communication system. Fifth, further enhancements are possible for the nonlinear equalizer. Photodetection is not considered in the current nonlinear equalizer. A nonlinear equalizer using the output of the photodetector as its input is desired. It is desirable to extend the nonlinear equalizer to multichannel equalization and evaluate the performance of the nonlinear equalizer in DWDM systems. Sixth, using the 2D discrete-time model, more applications can be developed to analyze the system and improve the system performance of long-haul DWDM systems. For example, the effect of the frequency chirp on the system can be analyzed and then new prechirping techniques can be developed.

Appendix A

Derivation of 2-D Discrete-Time Model

This appendix presents the derivation of the 2-D discrete-time model of physical impairments in long-haul DWDM systems, as given in Eq. (3.23). The derivations of Eq. (4.13) and Eq. (5.13) are similar to the following derivation.

A.1 Simplification of Triple Integral

Using the third-order VSTF method, the output of the optical filter in long-haul DWDM systems with periodic dispersion compensation and amplification is a triple integral in the frequency domain. This section presents how this triple integral can be simplified to a simple integral for Gaussian shaped pulses and a Gaussian optical filter.

The output of the optical filter can be given by

$$\begin{aligned}
R_f(\omega) &= 2\pi \sum_{\hat{f}=0}^{F-1} \sum_{\hat{k}=0}^{K-1} a_{\hat{f}\hat{k}} A_{\hat{f}} A_{df} \tilde{T}_{\hat{f}} T_{df} \exp \left[-i(\omega - \hat{f}\Delta) \hat{k} T_s \right] \\
&\times \exp \left[-\frac{(\omega - \hat{f}\Delta)^2 \tilde{T}_f^2}{2} - \frac{(\omega - f\Delta)^2 T_{df}^2}{2} + i\Phi_{\hat{f}\hat{k}} \right] \\
&+ iN\gamma \sum_{u=0}^{F-1} \sum_{v=0}^{F-1} \sum_{w=0}^{F-1} \sum_{l=0}^{K-1} \sum_{m=0}^{K-1} \sum_{n=0}^{K-1} a_{ul} a_{vm} a_{wn} \\
&\times A_u A_v A_w A_{df} \tilde{T}_u \tilde{T}_v \tilde{T}_w T_{df} \exp [i(\Phi_{ul} - \Phi_{vm} + \Phi_{wn})] \\
&\times E_{u,v,w,l,m,n}(\omega) \int_0^L \exp(-\alpha z) I(\omega, z) dz, \tag{A.1}
\end{aligned}$$

where

$$\begin{aligned}
I(\omega, z) &= \int_{-\infty}^{+\infty} \int_{-\infty}^{+\infty} \exp(-i\omega_1 \omega_2 \beta_2 z) \\
&\times \exp \left(-\frac{\omega_1^2 \tilde{T}_u^2}{2} - \frac{\omega_1^2 \tilde{T}_v^2}{2} - \frac{\omega_2^2 \tilde{T}_v^2}{2} - \frac{\omega_2^2 \tilde{T}_w^2}{2} \right) \\
&\times \exp[-\omega\omega_1(\tilde{T}_u^2 + \tilde{T}_v^2) - \omega\omega_2(\tilde{T}_v^2 + \tilde{T}_w^2) - \omega_1\omega_2\tilde{T}_v^2] \\
&\times \exp(\omega_1 u \Delta \tilde{T}_u^2 + \omega_1 v \Delta \tilde{T}_v^2 + \omega_2 v \Delta \tilde{T}_v^2 + \omega_2 w \Delta \tilde{T}_w^2) \\
&\times \exp[-i\omega_1(l-m)T_s - i\omega_2(n-m)T_s] d\omega_1 d\omega_2. \tag{A.2}
\end{aligned}$$

By solving the double integral $I(\omega, z)$, the triple integral can be simplified to a simple integral.

We first separate all terms containing ω_1 from $I(\omega, z)$:

$$\begin{aligned}
I(\omega, z) &= \int_{-\infty}^{+\infty} \exp \left[-\frac{(\omega_2^2 + 2\omega\omega_2)(\tilde{T}_v^2 + \tilde{T}_w^2)}{2} \right] \\
&\times \left\{ \int_{-\infty}^{+\infty} \exp \left[-\frac{(\tilde{T}_u^2 + \tilde{T}_v^2)\omega_1^2}{2} + b_1\omega_1 \right] d\omega_1 \right\} \\
&\times \exp \left[\omega_2 \Delta (v\tilde{T}_v^2 + w\tilde{T}_w^2) - i\omega_2(n-m)T_s \right] d\omega_2, \tag{A.3}
\end{aligned}$$

where

$$b_1 = -\omega_2 \tilde{T}_v^2 - \omega(\tilde{T}_u^2 + \tilde{T}_v^2) + \Delta(u\tilde{T}_u^2 + v\tilde{T}_v^2) - i[(l-m)T_s + \omega_2\beta_2]. \quad (\text{A.4})$$

We solve the integral in ω_1 by applying the generalized Gaussian integral formula [35] and $I(\omega, z)$ becomes a simple integral

$$\begin{aligned} I(\omega, z) &= \int_{-\infty}^{+\infty} \exp\left[-\frac{(\omega_2^2 + 2\omega\omega_2)(\tilde{T}_v^2 + \tilde{T}_w^2)}{2}\right] \exp\left[\omega_2\Delta(v\tilde{T}_v^2 + w\tilde{T}_w^2) - i\omega_2(n-m)T_s\right] \\ &\quad \times \sqrt{\frac{2\pi}{\tilde{T}_u^2 + \tilde{T}_v^2}} \exp\left[\frac{b_1^2}{2(\tilde{T}_u^2 + \tilde{T}_v^2)}\right] d\omega_2. \end{aligned} \quad (\text{A.5})$$

We rearrange $I(\omega, z)$ to a generalized Gaussian integral in ω_2 as follows:

$$I(\omega, z) = \sqrt{\frac{2\pi}{\tilde{T}_u^2 + \tilde{T}_v^2}} \times \left[\int_{-\infty}^{+\infty} \exp(-a_2\omega_2^2 + b_2\omega_2) d\omega_2 \right] \exp[P(\omega)]. \quad (\text{A.6})$$

where

$$a_2 = \frac{(\tilde{T}_v^2 + \tilde{T}_w^2)}{2} - \frac{(\tilde{T}_v^2 + i\beta_2 z)^2}{2(\tilde{T}_u^2 + \tilde{T}_v^2)}, \quad (\text{A.7})$$

$$\begin{aligned} b_2 &= -\omega(\tilde{T}_v^2 + \tilde{T}_w^2) + \Delta(v\tilde{T}_v^2 + w\tilde{T}_w^2) - i(n-m)T_s \\ &\quad - \frac{[-\omega(\tilde{T}_u^2 + \tilde{T}_v^2) + \Delta(u\tilde{T}_u^2 + v\tilde{T}_v^2)](\tilde{T}_v^2 + i\beta_2 z)}{\tilde{T}_u^2 + \tilde{T}_v^2} \\ &\quad + \frac{i(l-m)T(\tilde{T}_v^2 + i\beta_2 z)}{\tilde{T}_u^2 + \tilde{T}_v^2}, \end{aligned} \quad (\text{A.8})$$

and

$$P(\omega) = \frac{[-\omega(\tilde{T}_u^2 + \tilde{T}_v^2) + \Delta(u\tilde{T}_u^2 + v\tilde{T}_v^2) - i(l - m)T_s]^2}{2(\tilde{T}_u^2 + \tilde{T}_v^2)}. \quad (\text{A.9})$$

We then solve the integral in ω_2 to obtain

$$I(\omega, z) = \sqrt{\frac{2\pi}{\tilde{T}_u^2 + \tilde{T}_v^2}} \times \sqrt{\frac{\pi}{a_2}} \exp\left(\frac{b_2^2}{4a_2}\right) \times \exp[P(\omega)]. \quad (\text{A.10})$$

In this way, the double integral $I(\omega, z)$ is solved and the triple integral is simplified to a simple integral.

Further, we can transform Eq. (A.10) to a symmetric form given by Eq. (3.9).

A.2 Simplifying Functions Used in Frequency Domain Output

This section gives expressions for A , B and C used in Eq. (3.9):

$$A = \frac{1}{2} \frac{[\tilde{T}_u^2(\omega - u\Delta) + \tilde{T}_v^2(\omega - v\Delta)]^2}{\tilde{T}_u^2 + \tilde{T}_v^2 - \frac{(\tilde{T}_v^2 + i\beta_2 z)^2}{\tilde{T}_v^2 + \tilde{T}_w^2}} + \frac{1}{2} \frac{[\tilde{T}_v^2(\omega - v\Delta) + \tilde{T}_w^2(\omega - w\Delta)]^2}{\tilde{T}_v^2 + \tilde{T}_w^2 - \frac{(\tilde{T}_v^2 + i\beta_2 z)^2}{\tilde{T}_u^2 + \tilde{T}_v^2}} - \frac{[\tilde{T}_u^2(\omega - u\Delta) + \tilde{T}_v^2(\omega - v\Delta)](\tilde{T}_v^2 + i\beta_2 z)}{(\tilde{T}_u^2 + \tilde{T}_v^2)(\tilde{T}_v^2 + \tilde{T}_w^2) - (\tilde{T}_v^2 + i\beta_2 z)^2} [\tilde{T}_v^2(\omega - v\Delta) + \tilde{T}_w^2(\omega - w\Delta)]. \quad (\text{A.11})$$

$$\begin{aligned}
B = & i(l-m)T_s \frac{[\tilde{T}_u^2(\omega - u\Delta) + \tilde{T}_v^2(\omega - v\Delta)](\tilde{T}_w^2 - i\beta_2 z)}{(\tilde{T}_u^2 + \tilde{T}_v^2)(\tilde{T}_v^2 + \tilde{T}_w^2) - (\tilde{T}_v^2 + i\beta_2 z)^2} \\
& + i(n-m)T_s \frac{[\tilde{T}_v^2(\omega - v\Delta) + \tilde{T}_w^2(\omega - w\Delta)](\tilde{T}_u^2 - i\beta_2 z)}{(\tilde{T}_u^2 + \tilde{T}_v^2)(\tilde{T}_v^2 + \tilde{T}_w^2) - (\tilde{T}_v^2 + i\beta_2 z)^2}. \tag{A.12}
\end{aligned}$$

$$C = -\frac{(l-n)^2 T_s^2}{2 \left[\tilde{T}_u^2 + \tilde{T}_v^2 - \frac{(\tilde{T}_v^2 + i\beta_2 z)^2}{\tilde{T}_v^2 + \tilde{T}_w^2} \right]} - \frac{(l-m)(n-m)T_s^2(\tilde{T}_w^2 - i\beta_2 z)}{(\tilde{T}_u^2 + \tilde{T}_v^2)(\tilde{T}_v^2 + \tilde{T}_w^2) - (\tilde{T}_v^2 + i\beta_2 z)^2}. \tag{A.13}$$

A.3 Simplifying Functions Used in Time Domain Output

This section gives expressions for A_0 , A_1 , A_2 , B_0 , and B_1 used in (4.12). C is defined in Section A.2.

$$\begin{aligned}
A_0 = & -\frac{(\tilde{T}_u^2 u\Delta + \tilde{T}_v^2 v\Delta)(\tilde{T}_v^2 v\Delta + \tilde{T}_w^2 w\Delta)(\tilde{T}_v^2 + i\beta_2 z)}{(\tilde{T}_u^2 + \tilde{T}_v^2)(\tilde{T}_v^2 + \tilde{T}_w^2) - (\tilde{T}_v^2 + i\beta_2 z)^2} \\
& + \frac{(\tilde{T}_u^2 u\Delta + \tilde{T}_v^2 v\Delta)^2(\tilde{T}_v^2 + \tilde{T}_w^2)}{2 \left[(\tilde{T}_u^2 + \tilde{T}_v^2)(\tilde{T}_v^2 + \tilde{T}_w^2) - (\tilde{T}_v^2 + i\beta_2 z)^2 \right]}. \\
& + \frac{(\tilde{T}_v^2 v\Delta + \tilde{T}_w^2 w\Delta)^2(\tilde{T}_u^2 + \tilde{T}_v^2)}{2 \left[(\tilde{T}_u^2 + \tilde{T}_v^2)(\tilde{T}_v^2 + \tilde{T}_w^2) - (\tilde{T}_v^2 + i\beta_2 z)^2 \right]}.
\end{aligned}$$

$$\begin{aligned}
A_1 = & -\frac{(\tilde{T}_u^2 + \tilde{T}_v^2)(\tilde{T}_v^2 + \tilde{T}_w^2)(\tilde{T}_u^2 u \Delta + 2\tilde{T}_v^2 v \Delta + \tilde{T}_w^2 w \Delta)}{(\tilde{T}_u^2 + \tilde{T}_v^2)(\tilde{T}_v^2 + \tilde{T}_w^2) - (\tilde{T}_v^2 + i\beta_2 z)^2} \\
& + \frac{(\tilde{T}_u^2 + \tilde{T}_v^2)(\tilde{T}_v^2 v \Delta + \tilde{T}_w^2 w \Delta)(\tilde{T}_v^2 + i\beta_2 z)}{(\tilde{T}_u^2 + \tilde{T}_v^2)(\tilde{T}_v^2 + \tilde{T}_w^2) - (\tilde{T}_v^2 + i\beta_2 z)^2} \\
& + \frac{(\tilde{T}_v^2 + \tilde{T}_w^2)(\tilde{T}_u^2 u \Delta + \tilde{T}_v^2 v \Delta)(\tilde{T}_v^2 + i\beta_2 z)}{(\tilde{T}_u^2 + \tilde{T}_v^2)(\tilde{T}_v^2 + \tilde{T}_w^2) - (\tilde{T}_v^2 + i\beta_2 z)^2}.
\end{aligned}$$

$$\begin{aligned}
A_2 = & -\frac{(\tilde{T}_u^2 + \tilde{T}_v^2)^2(\tilde{T}_v^2 + \tilde{T}_w^2) + (\tilde{T}_v^2 + \tilde{T}_w^2)^2(\tilde{T}_u^2 + \tilde{T}_v^2)}{2 \left[(\tilde{T}_u^2 + \tilde{T}_v^2)(\tilde{T}_v^2 + \tilde{T}_w^2) - (\tilde{T}_v^2 + i\beta_2 z)^2 \right]} \\
& + \frac{(\tilde{T}_u^2 + \tilde{T}_v^2)(\tilde{T}_v^2 + \tilde{T}_w^2)(\tilde{T}_v^2 + i\beta_2 z)}{(\tilde{T}_u^2 + \tilde{T}_v^2)(\tilde{T}_v^2 + \tilde{T}_w^2) - (\tilde{T}_v^2 + i\beta_2 z)^2}.
\end{aligned}$$

$$\begin{aligned}
B_0 = & -i(l-m)T_s \frac{(\tilde{T}_u^2 u \Delta + \tilde{T}_v^2 v \Delta)(\tilde{T}_w^2 - i\beta_2 z)}{(\tilde{T}_u^2 + \tilde{T}_v^2)(\tilde{T}_v^2 + \tilde{T}_w^2) - (\tilde{T}_v^2 + i\beta_2 z)^2} \\
& - i(n-m)T_s \frac{(\tilde{T}_v^2 v \Delta + \tilde{T}_w^2 w \Delta)(\tilde{T}_u^2 - i\beta_2 z)}{(\tilde{T}_u^2 + \tilde{T}_v^2)(\tilde{T}_v^2 + \tilde{T}_w^2) - (\tilde{T}_v^2 + i\beta_2 z)^2}.
\end{aligned}$$

$$\begin{aligned}
B_1 = & i(l-m)T_s \frac{(\tilde{T}_u^2 + \tilde{T}_v^2)(\tilde{T}_w^2 - i\beta_2 z)}{(\tilde{T}_u^2 + \tilde{T}_v^2)(\tilde{T}_v^2 + \tilde{T}_w^2) - (\tilde{T}_v^2 + i\beta_2 z)^2} \\
& + i(n-m)T_s \frac{(\tilde{T}_v^2 + \tilde{T}_w^2)(\tilde{T}_u^2 - i\beta_2 z)}{(\tilde{T}_u^2 + \tilde{T}_v^2)(\tilde{T}_v^2 + \tilde{T}_w^2) - (\tilde{T}_v^2 + i\beta_2 z)^2}.
\end{aligned}$$

A.4 Simplifying Functions and Coefficients Used in PD Output for DBPSK

If $\rho_{f,k}^{Sig}$, $\rho_{f,k}^{ISI}$, $\rho_{f,k}^{ICI}$, $\rho_{f,k}^{SPM}$, $\rho_{f,k}^{IXPM}$, $\rho_{f,k}^{IFWM}$, $\rho_{f,k}^{XPM}$, $\rho_{f,k}^{FWM}$, $\rho_{f,k}^L$, and $\rho_{f,k}^{NL}$, in Chapter 3, are replaced by $\rho_{f,k}^{Sig\pm}$, $\rho_{f,k}^{ISI\pm}$, $\rho_{f,k}^{ICI\pm}$, $\rho_{f,k}^{SPM\pm}$, $\rho_{f,k}^{IXPM\pm}$, $\rho_{f,k}^{IFWM\pm}$, $\rho_{f,k}^{XPM\pm}$, $\rho_{f,k}^{FWM\pm}$, $\rho_{f,k}^{L\pm}$, and $\rho_{f,k}^{NL\pm}$, respectively, we have the definitions of the following simplifying functions used in the photodetector output for DBPSK modulation: $r^{Sig\pm}(f, k)$, $r^{ISI\pm}(f, k)$, $r^{ICI\pm}(f, k)$, and $r^{NL\pm}(f, k)$. The indicator functions I^{SPM} , I^{IXPM} , I^{IFWM} , I^{XPM} , and I^{FWM} are defined in Section 3.1.

For DBPSK, $\rho_{f,k}^{L\pm}$ and $\rho_{f,k}^{NL\pm}$ are defined as

$$\rho_{f,k}^{L\pm} = \rho_{f,\hat{k}}^L \pm \rho_{f,\hat{k}}^L \exp \left[\frac{\left[\frac{(1-2k)T_s^2}{T_{df}^4} - \frac{2\hat{k}T_s^2}{\hat{T}_f^2 T_{df}^2} - \frac{i2T_s(\hat{f}-f)\Delta}{T_{df}^2} \right]}{2\left(\frac{1}{\hat{T}_f^2} + \frac{1}{T_{df}^2}\right)} \right] \exp \left[\frac{(2k-1)T_s^2}{2T_{df}^2} - if\Delta T_s \right],$$

$$\rho_{f,k}^{NL\pm} = U(kT_s) \pm U[(k-1)T_s].$$

where

$$U(t) = i\gamma\sqrt{2\pi}E_{u,v,w,l,m,n}(t) \int_0^L \exp(-\alpha z) J_{u,v,w,l,m,n}(t, z) dz.$$

A.5 Simplifying Functions and Coefficients Used in PD Quadrature Output of DQPSK

If $\rho_{f,k}^{Sig\pm}$, $\rho_{f,k}^{ISI\pm}$, $\rho_{f,k}^{ICI\pm}$, $\rho_{f,k}^{SPM\pm}$, $\rho_{f,k}^{IXPM\pm}$, $\rho_{f,k}^{IFWM\pm}$, $\rho_{f,k}^{XPM\pm}$, $\rho_{f,k}^{FWM\pm}$, $\rho_{f,k}^{L\pm}$, and $\rho_{f,k}^{NL\pm}$, in Section A.4, are replaced by $\rho_{f,k}^{QSig\pm}$, $\rho_{f,k}^{QISI\pm}$, $\rho_{f,k}^{QICI\pm}$, $\rho_{f,k}^{QSPM\pm}$, $\rho_{f,k}^{QIXPM\pm}$, $\rho_{f,k}^{QIFWM\pm}$, $\rho_{f,k}^{QXPM\pm}$, $\rho_{f,k}^{QFWM\pm}$, $\rho_{f,k}^{QL\pm}$, and $\rho_{f,k}^{QNL\pm}$, respectively, we have the definitions of the following simplifying

functions used in the photodetector output for DQPSK modulation: $r_Q^{Sig^\pm}(f, k)$, $r_Q^{ISI^\pm}(f, k)$, $r_Q^{ICI^\pm}(f, k)$, and $r_Q^{NL^\pm}(f, k)$.

For DQPSK, $\rho_{f,k}^{QL^\pm}$ and $\rho_{f,k}^{QNL^\pm}$ are defined as

$$\rho_{\hat{f},\hat{k}}^{QL^\pm} = i\rho_{\hat{f},\hat{k}}^L \pm \rho_{\hat{f},\hat{k}}^L \exp \left[\frac{\frac{(1-2k)T_s^2}{T_{df}^4} - \frac{2kT_s^2}{T_f^2 T_{df}^2} - \frac{i2T_s(\hat{f}-f)\Delta}{T_{df}^2}}{2\left(\frac{1}{T_f^2} + \frac{1}{T_{df}^2}\right)} \right] \exp \left[\frac{(2k-1)T_s^2}{2T_{df}^2} - if\Delta T_s \right],$$

$$\rho_{f,k}^{QNL^\pm} = iU(kT_s) \pm U[(k-1)T_s].$$

Bibliography

- [1] Govind P. Agrawal. *Fiber-Optic Communication Systems*. Wiley, fourth edition, 2010.
- [2] Govind P. Agrawal. *Nonlinear Fiber Optics*. Academic Press, fourth edition, 2006.
- [3] Simon Haykin. *Communication Systems*. Wiley, fifth edition, 2009.
- [4] K.C. Kao and G.A. Hockham. Dielectric-fibre surface waveguides for optical frequencies. *Proceedings of the Institution of Electrical Engineers*, 113(7):1151–1158, Jul 1966.
- [5] T. Welsh, R. Smith, H. Azami, and R. Chrisner. The FLAG cable system. *IEEE Commun. Lett.*, 34(2):30–35, Feb 1996.
- [6] W.C. Marra and J. Schesser. Africa one: the Africa optical network. *IEEE Communications Magazine*, 34(2):50–57, Feb 1996.
- [7] Rene-Jean Essiambre, Gregory Raybon, and Benny Mikkelsen. Pseudo-linear transmission of high-speed TDM signals: 40 and 160 Gb/s. In Ivan P. Kaminow and Tingye Li, editors, *Optical Fiber Telecommunications IV-B: Systems and Impairments*. Academic Press, 2002.
- [8] A. Sano, H. Masuda, and T. Kobayashi. 69.1-Tb/s (432*171-Gb/s) C- and extended L-band transmission over 240 km using PDM-16-QAM modulation and digital coherent detection. In *Optical Fiber Communication Conference 2010*, Mar 2010.
- [9] John Zyskind, Rick Barry, Graeme Pendock, Michael Cahill, and Jinendra Ranka. High-capacity, ultra-long-haul networks. In Ivan Kaminow and Tingye Li, editors, *Optical Fiber Telecommunications IV B: Systems and Impairments*, pages 198–231. Academic Press, 2002.
- [10] Kazuro Kikuchi. Coherent optical communication systems. In Ivan Kaminow, Tingye Li, and Alan E. Willner, editors, *Optical Fiber Telecommunications V B: Systems and Networks*, pages 95–130. Academic Press, 2008.
- [11] Xiang Liu, Sethumadhavan Chandrasekhar, and Andreas Leven. Self-coherent optical transport systems. In Ivan Kaminow, Tingye Li, and Alan E. Willner, editors, *Optical Fiber Telecommunications V B: Systems and Networks*, pages 131–178. Academic Press, 2008.

- [12] E. Basch, R. Egorov, S. Gringeri, and S. Elby. Architectural tradeoffs for reconfigurable dense wavelength-division multiplexing systems. *IEEE J. Sel. Topics Quantum Electron.*, 12(4):615–626, Jul-Aug 2006.
- [13] A. Gnauck, R. Tkach, A. Chraplyvy, and T. Li. High-capacity optical transmission systems. *J. Lightw. Technol.*, 26(9):1032–1045, May 2008.
- [14] M. Wu and W. Way. Fiber nonlinearity limitations in ultra-dense WDM systems. *J. Lightw. Technol.*, 22(6):1483–1498, Jun 2004.
- [15] M. Taghavi, G. Papen, and P. Siegel. On the multiuser capacity of WDM in a nonlinear optical fiber: Coherent communication. *IEEE Trans. Inf. Theory*, 52(11):5008–5022, Nov 2006.
- [16] V. E. Zakharov and A. B. Shabat. Exact theory of two-dimensional self-focusing and one-dimensional self-modulation of waves in nonlinear media. *Sov. Phys*, 34(3):62–69, Jan 1972.
- [17] S. Novikov, S.V. Manakov, L.P. Pitaevskii, and V.E. Zakharov. *Theory of Solitons: The Inverse Scattering Method*. Springer, 1984.
- [18] V.N. Serkin and A. Hasegawa. Exactly integrable nonlinear Schrödinger equation models with varying dispersion, nonlinearity and gain: application for soliton dispersion. *IEEE J. Sel. Topics Quantum Electron.*, 8(3):418–431, May/June 2002.
- [19] K. Peddanarappagari and M. Brandt-Pearce. Volterra series transfer function of single-mode fibers. *J. Lightw. Technol.*, 15(12):2232–2241, Dec 1997.
- [20] Mark J. Ablowitz and Gino Biondini. Multiscale pulse dynamics in communication systems with strong dispersion management. *Opt. Lett.*, 23(21):1668–1670, 1998.
- [21] Martin Schetzen. *The Volterra and Wiener Theories of Nonlinear Systems*. Krieger Publishing Co., Inc., Melbourne, FL, USA, 2006.
- [22] K. Peddanarappagari and M. Brandt-Pearce. Volterra series approach for optimizing fiber-optic communication system designs. *J. Lightw. Technol.*, 16(11):2046–2055, Nov 1998.
- [23] B. Xu and M. Brandt-Pearce. Modified Volterra series transfer function method. *IEEE Photon. Technol. Lett.*, 14(1):47–49, Jan 2002.
- [24] B. Xu and M. Brandt-Pearce. Comparison of FWM- and XPM-induced crosstalk using the Volterra series transfer function method. *J. Lightw. Technol.*, 21(1):40–53, Jan 2003.
- [25] Jacklyn D. Reis and António L. Teixeira. Unveiling nonlinear effects in dense coherent optical WDM systems with Volterra series. *Opt. Express*, 18(8):8660–8670, 2010.

- [26] Jacklyn D. Reis, Liliana N. Costa, and António L. Teixeira. Nonlinear effects prediction in ultra-dense WDM systems using Volterra series. In *Optical Fiber Communication Conference*. Optical Society of America, 2010.
- [27] J. Tang. The Shannon channel capacity of dispersion-free nonlinear optical fiber transmission. *J. Lightw. Technol.*, 19(8):1104–1109, Aug 2001.
- [28] J. Tang. The multispan effects of Kerr nonlinearity and amplifier noises on Shannon channel capacity of a dispersion-free nonlinear optical fiber. *J. Lightw. Technol.*, 19(8):1110–1115, Aug 2001.
- [29] J. Tang. The channel capacity of a multispan DWDM system employing dispersive nonlinear optical fibers and an ideal coherent optical receiver. *J. Lightw. Technol.*, 20(7):1095–1101, Jul 2002.
- [30] J. Tang. A comparison study of the Shannon channel capacity of various nonlinear optical fibers. *J. Lightw. Technol.*, 24(5):2070–2075, May 2006.
- [31] A. Rostami and A. Andalib. A principal investigation of the group velocity dispersion (GVD) profile for optimum dispersion compensation in optical fibers: a theoretical study. *Progress In Electromagnetics Research*, 75:209–224, 2007.
- [32] A. Andalib, A. Rostami, and N. Granpayeh. Analytical investigation and evaluation of pulse broadening factor propagating through nonlinear optical fibers (traditional and optimum dispersion compensated fibers). *Progress In Electromagnetics Research*, 79:119–136, 2008.
- [33] M. Nazarathy, B. Livshitz, Y. Atzmon, M. Secondini, and E. Forestieri. Optically amplified direct detection with pre- and postfiltering: A Volterra series approach. *J. Lightw. Technol.*, 26(22):3677–3693, Nov 2008.
- [34] Le Nguyen Binh. Linear and nonlinear transfer functions of single mode fiber for optical transmission systems. *J. Opt. Soc. Am. A*, 26(7):1564–1575, 2009.
- [35] Daniel Zwillinger. *Handbook of Differential Equations*. Academic Press, third edition, 1997.
- [36] A. Mecozzi, C.B. Clausen, and M. Shtaif. Analysis of intrachannel nonlinear effects in highly dispersed optical pulse transmission. *IEEE Photon. Technol. Lett.*, 12(4):392–394, Apr 2000.
- [37] A. Vannucci, P. Serena, and A. Bononi. The RP method: a new tool for the iterative solution of the nonlinear Schrödinger equation. *J. Lightw. Technol.*, 20(7):1102–1112, Jul 2002.
- [38] Evgenii E. Narimanov and Partha Mitra. The channel capacity of a fiber optics communication system: Perturbation theory. *J. Lightw. Technol.*, 20(3):530–537, 2002.

- [39] A. Mecozzi, C.B. Clausen, M. Shtaif, Sang-Gyu Park, and A.H. Gnauck. Cancellation of timing and amplitude jitter in symmetric links using highly dispersed pulses. *IEEE Photon. Technol. Lett.*, 13(5):445–447, May 2001.
- [40] Xing Wei and Xiang Liu. Analysis of intrachannel four-wave mixing in differential phase-shift keying transmission with large dispersion. *Opt. Lett.*, 28(23):2300–2302, 2003.
- [41] Xing Wei. Power-weighted dispersion distribution function for characterizing nonlinear properties of long-haul optical transmission links. *Opt. Lett.*, 31(17):2544–2546, 2006.
- [42] James W. Cooley and John W. Tukey. An algorithm for the machine calculation of complex Fourier series. *Mathematics of Computation*, 19(90):297–301, 1965.
- [43] H. Louchet, A. Hodzic, K. Petermann, A. Robinson, and R. Epworth. Simple criterion for the characterization of nonlinear impairments in dispersion-managed optical transmission systems. *IEEE Photon. Technol. Lett.*, 17(10):2089–2091, Oct 2005.
- [44] Mark J. Ablowitz and Toshihiko Hirooka. Managing nonlinearity in strongly dispersion-managed optical pulse transmission. *J. Opt. Soc. Am. B*, 19(3):425–439, 2002.
- [45] J.K. Fischer, C.-A. Bunge, and K. Petermann. Equivalent single-span model for dispersion-managed fiber-optic transmission systems. *J. Lightw. Technol.*, 27(16):3425–3432, Aug 2009.
- [46] Alberto Bononi, Paolo Serena, and Alessandra Orlandini. A unified design framework for single-channel dispersion-managed terrestrial systems. *J. Lightw. Technol.*, 26(22):3617–3631, 2008.
- [47] Alberto Bononi, Paolo Serena, and Marco Bertolini. Unified analysis of weakly-nonlinear dispersion-managed optical transmission systems using a perturbative approach. *Comptes Rendus Physique*, 9(9-10):947–962, 2008.
- [48] E. Ciaramella and E. Forestieri. Analytical approximation of nonlinear distortions. *IEEE Photon. Technol. Lett.*, 17(1):91–93, Jan 2005.
- [49] Enrico Forestieri and Marco Secondini. Solving the nonlinear Schrödinger equation. In Enrico Forestieri, editor, *Optical Communication Theory and Techniques*, pages 3–11. Springer US, 2005.
- [50] Mark Ablowitz and Barbara Prinari. Nonlinear Schrodinger systems: continuous and discrete. *Scholarpedia*, 3(8):5561, 2008.
- [51] V.L. Ginzburg and L.D. Landau. On the theory of superconductivity. *Soviet Physics - JETP*, 20:1064–1082, 1950.
- [52] V.L. Ginzburg. Some remarks concerning the macroscopic theory of superconductivity. *Soviet Physics - JETP*, 2:589–600, 1956.

- [53] V.L. Ginzburg and L.P. Pitaevskii. On the theory of superfluidity. *Soviet Physics - JETP*, 7:858–861, 1958.
- [54] R. Y. Chiao, E. Garmire, and C. H. Townes. Self-trapping of optical beams. *Phys. Rev. Lett.*, 13:479–482, Oct 1964.
- [55] V.I. Talanov. Self-focusing of electromagnetic waves in nonlinear media. *Radiophysics*, 8:254–257, 1964.
- [56] H. S. Eisenberg, Y. Silberberg, R. Morandotti, A. R. Boyd, and J. S. Aitchison. Discrete spatial optical solitons in waveguide arrays. *Phys. Rev. Lett.*, 81:3383–3386, Oct 1998.
- [57] Nikolaos K. Efremidis, Jared Hudock, Demetrios N. Christodoulides, Jason W. Fleischer, Oren Cohen, and Mordechai Segev. Two-dimensional optical lattice solitons. *Phys. Rev. Lett.*, 91:213906, Nov 2003.
- [58] C. J. Pethick and H. Smith. *Bose-Einstein Condensation in Dilute Gases*. Cambridge University Press, 2nd edition, 2008.
- [59] V. E. Zakharov. Collapse of Langmuir waves. *Soviet Physics - JETP*, 35:908–914, 1972.
- [60] D. J. Benney and A. C. Newell. Nonlinear wave envelopes. *J. Math. Phys.*, 46:133–139, 1967.
- [61] Mark J. Ablowitz and Harvey Segur. *Solitons and the Inverse Scattering Transform*. SIAM, first edition, 1981.
- [62] A.K. Zvezdin and A.F. Popkov. Contribution to the nonlinear theory of magnetostatic spin waves. *Soviet Physics - JETP*, 57:350–355, 1983.
- [63] Ming Chen, Mincho A. Tsankov, Jon M. Nash, and Carl E. Patton. Backward-volume-wave microwave-envelope solitons in yttrium iron garnet films. *Phys. Rev. B*, 49:12773–12790, May 1994.
- [64] Akira Hasegawa and Frederick Tappert. Transmission of stationary nonlinear optical pulses in dispersive dielectric fibers. i. anomalous dispersion. *Applied Physics Letters*, 23(3):142–144, 1973.
- [65] Akira Hasegawa and Frederick Tappert. Transmission of stationary nonlinear optical pulses in dispersive dielectric fibers. ii. normal dispersion. *Applied Physics Letters*, 23(4):171–172, 1973.
- [66] Akira Hasegawa and Yuji Kodama. *Solitons in Optical Communications*. Oxford University Press, 1995.
- [67] F. D. Tappert and R. H. Hardin. Applications of the split-step Fourier method to the numerical solution of nonlinear and variable coefficient wave equations. *SIAM Rev.*, 15:423–434, 1973.

- [68] Polina Bayvel and Robert Killey. Nonlinear optical effects in WDM transmission. In Ivan P. Kaminow and Tingye Li, editors, *Optical Fiber Telecommunications IV-B: Systems and Impairments*. Academic Press, 2002.
- [69] Thomas Schneider. *Nonlinear Optics in Telecommunications*. Springer Berlin Heidelberg, 2010.
- [70] A. Agata, K. Tanaka, and N. Edagawa. Study on the optimum Reed-Solomon-based FEC codes for 40-Gb/s-based ultralong-distance wdm transmission. *J. Lightw. Technol.*, 20(12):2189 – 2195, Dec 2002.
- [71] T. Mizuochi. Recent progress in forward error correction and its interplay with transmission impairments. *IEEE J. Quantum Electron.*, 12(4):544 –554, Jul-Aug 2006.
- [72] Douglas Lind and Brian Marcus. *An Introduction to Symbolic Dynamics and Coding*. Cambridge University Press, 1995.
- [73] N. Kashyap, P.H. Siegel, and A. Vardy. Coding for the optical channel: the ghost-pulse constraint. *IEEE Trans. Inf. Theory*, 52(1):64–77, Jan 2006.
- [74] B. Vasic, V.S. Rao, I.B. Djordjevic, R.K. Kostuk, and I. Gabitov. Ghost-pulse reduction in 40-Gb/s systems using line coding. *IEEE Photonics Technol. Lett.*, 16(7):1784–1786, Jul 2004.
- [75] I. B. Djordjevic, Bane Vasic, Milos Ivkovic, and Ildar Gabitov. Achievable information rates for high-speed long-haul optical transmission. *J. Lightw. Technol.*, 23(11):3755, 2005.
- [76] Navin Kashyap, Paul H. Siegel, and Alexander Vardy. An application of Ramsey theory to coding for the optical channel. *SIAM J. Discret. Math.*, 19(4):921–937, 2005.
- [77] I.B. Djordjevic, S.K. Chilappagari, and B. Vasic. Suppression of intrachannel nonlinear effects using pseudoternary constrained codes. *J. Lightw. Technol.*, 24(2):769–774, Feb 2006.
- [78] S. Sankaranarayanan, I.B. Djordjevic, and B. Vasic. Iteratively decodable codes on m flats for WDM high-speed long-haul transmission. *J. Lightw. Technol.*, 23(11):3696–3701, Nov 2005.
- [79] H. G. Batshon, I. B. Djordjevic, and B. V. Vasic. An improved technique for suppression of intrachannel four-wave mixing in 40-Gb/s optical transmission systems. *IEEE Photonics Technol. Lett.*, 19(2):67–69, Jan 2007.
- [80] I. B. Djordjevic and Bane Vasic. Constrained coding techniques for the suppression of intrachannel nonlinear effects in high-speed optical transmission. *J. Lightw. Technol.*, 24(1):411, 2006.
- [81] Anantha Raman Krishnan and Shiva K. Planjery. Constrained coding for optical communication. In Ivan Djordjevic, William Ryan, and Bane Vasic, editors, *Coding for Optical Channels*, pages 285–309. Springer, 2010.

- [82] Ioannis Papagiannakis, G. Bosco, Daniel Fonseca, Dimitrios Klonidis, P. Poggiolini, Werner Rosenkranz, Antonio Teixeira, Ioannis Tomkos, and Chunmin Xia. Electronic channel equalization techniques. In Ioannis Tomkos, Maria Spyropoulou, Karin Ennser, Martin Khn, and Branko Mikac, editors, *Towards Digital Optical Networks*, volume 5412 of *Lecture Notes in Computer Science*, pages 23–47. Springer Berlin / Heidelberg, 2009.
- [83] Ezra Ip and Joseph M. Kahn. Optical fiber new developments. chapter Nonlinear Impairment Compensation Using Backpropagation, pages 467–494. InTech, www.intechopen.com, 2009.
- [84] Ezra Ip and Joseph M. Kahn. Compensation of dispersion and nonlinear impairments using digital backpropagation. *J. Lightwave Technol.*, 26(20):3416–3425, Oct 2008.
- [85] Eduardo Mateo, Likai Zhu, and Guifang Li. Impact of XPM and FWM on the digital implementation of impairment compensation for wdm transmission using backward propagation. *Opt. Express*, 16(20):16124–16137, Sep 2008.
- [86] Houbing Song and Maite Brandt-Pearce. A 2-D discrete-time model of physical impairments in wavelength-division multiplexing systems. *J. Lightw. Technol.*, 30(5):713–726, Mar 2012.
- [87] Houbing Song and Maite Brandt-Pearce. Range of influence of physical impairments in wavelength-division multiplexed systems. In *Proc. IEEE Global Communications Conference (GLOBECOM 2011)*, pages 1–6, Houston, USA, Dec 2011.
- [88] Houbing Song, Maite Brandt-Pearce, Tingjun Xie, and Stephen G. Wilson. Combined constrained code and LDPC code for long-haul fiber-optic communication systems. In *Proc. IEEE Global Communications Conference (GLOBECOM 2012)*, pages 1–6, Anaheim, USA, Dec 2012.
- [89] T.J. Richardson, M.A. Shokrollahi, and R.L. Urbanke. Design of capacity-approaching irregular low-density parity-check codes. *IEEE Trans. Inf. Theory*, 47(2):619–637, Feb 2001.
- [90] M. Schetzen. Theory of pth-order inverses of nonlinear systems. *Circuits and Systems, IEEE Transactions on*, 23(5):285 – 291, May 1976.
- [91] Houbing Song and Maite Brandt-Pearce. A discrete-time polynomial model of single channel long-haul fiber-optic communication systems. In *Proc. IEEE International Conference on Communications (ICC'2011)*, pages 1–6, Kyoto, Japan, Jun 2011.
- [92] P. J. Winzer and R.-J. Essiambre. Advanced modulation formats for high-capacity optical transport networks. *J. Lightw. Technol.*, 24(12):4711–4728, Dec 2006.
- [93] H. Louchet, A. Hodzic, K. Petermann, A. Robinson, and R. Epworth. Analytical model for the design of multispan DWDM transmission systems. *IEEE Photon. Technol. Lett.*, 17(1):247–249, Jan 2005.

- [94] I. B. Djordjevic, A. Stavdas, C. Skoufis, S. Sygletos, and C. Matrakidis. Analytical modelling of fibre nonlinearities in amplified dispersion compensated WDM systems. *International Journal of Modeling and Simulation*, 23(4):226–233, 2003.
- [95] V. Zakharov and S. Manakov. On propagation of short pulses in strong dispersion managed optical lines. *JETP Letters*, 70:578–582, 1999.
- [96] G. Raybon, B. Mikkelsen, and R.-J. Essiambre. High speed, 40 to 100 Gbit/s OTDM transmission over nonzero dispersion fiber. In *Lasers and Electro-Optics Society 1999 12th Annual Meeting. LEOS '99. IEEE*, volume 1, pages 341–342, 1999.
- [97] Govind P. Agrawal. *Lightwave Technology: Telecommunication Systems*. Wiley-Interscience, 2005.
- [98] Y. Kodama and S. Wabnitz. Analytical theory of guiding-center nonreturn-to-zero and return-to-zero signal transmission in normally dispersive nonlinear optical fibers. *Opt. Lett.*, 20(22):2291–2293, 1995.
- [99] I.B. Djordjevic and B. Vasic. Noise-predictive BCJR equalization for suppression of intrachannel nonlinearities. *IEEE Photonics Technol. Lett.*, 18(12):1317–1319, Jun 2006.
- [100] R. Storn and K. Price. Differential evolution - a simple and efficient heuristic for global optimization over continuous spaces. *J. Global Optimization*, 11.
- [101] G. Kramer A. Ashikmin and S. ten Brink. Extrinsic information transfer functions: Model and erasure channel property. *IEEE Trans. Inform. Theory*, 50(11):2657–2673, Nov 2004.
- [102] X. Hu, E. Eleftheriou, and D. M. Arnold. Progressive edge-growth Tanner graphs. In *Proc. IEEE Global Communications Conference (GLOBECOM)*, pages 995–1001, San Antonio, Texas, USA, Nov 2001.
- [103] Shiva Kumar and Dong Yang. Optical backpropagation for fiber-optic communications using highly nonlinear fibers. *Opt. Lett.*, 36(7):1038–1040, Apr 2011.
- [104] Jie Pan and Chi-Hao Cheng. Wiener-Hammerstein model based electrical equalizer for optical communication systems. *J. Lightw. Technol.*, 29(16):2454–2459, Aug 2011.
- [105] Jie Pan and Chi-Hao Cheng. Nonlinear electrical predistortion and equalization for the coherent optical communication system. *J. Lightw. Technol.*, 29(18):2785–2789, Sep 2011.
- [106] Jie Pan and Chi-Hao Cheng. Nonlinear electrical compensation for the coherent optical OFDM system. *J. Lightw. Technol.*, 29(2):215–221, Jan 2011.